Structural Studies of RNF146-Mediated PARylation-Dependent Ubiquitylation

Paul A. Da Rosa

A dissertation

submitted in partial fulfillment of the

requirements for the degree of

Doctor of Philosophy

University of Washington

2017

Reading Committee:

Rachel E. Klevit (Chair)

Wenqing Xu

Ning Zheng

Program Authorized to Offer Degree:

Department of Biochemistry

University of Washington

Abstract

Structural Studies of RNF146-Mediated PARylation-Dependent Ubiquitylation

Paul A. Da Rosa

Chair of the Supervisory Committee:

Professor Rachel E. Klevit

Department of Biochemistry

The ubiquitylation of proteins is involved in nearly every cellular process. Hence, precise control of the ligases that facilitate the attachment ubiquitin (Ub) to target substrates is of the utmost importance to eukaryotic biology. My thesis work on the RING E3 ubiquitin ligase RNF146 has defined a new mechanism by which a ligase can be allosterically activated. I have provided the first example of a RING domain (E3 domain) that has a conformational change, with my discovery that RNF146 is conformationally "switched on" by binding the post translational modification poly(ADP-ribose) (PAR). My work on RNF146 (and other proteins) builds on a growing theme of RING E3 ligase regulation, upending the notion that all single subunit RING E3 domains are constitutively able to bind and activate an E2~Ub conjugate to transfer ubiquitin to substrates.

Protein poly(ADP-ribosyl)ation (PARylation) is involved in many cellular processes including DNA repair, cell division, and cell death. It was recently shown that PARylation catalyzed by the PARPs tankyrase-1 and -2 can mark proteins for ubiquitylation and subsequent degradation via the proteasome. The E3 ubiquitin ligase RNF146 (a.k.a. Iduna) is the only E3 identified thus far that participates in PARylation-dependent ubiquitylation (PARdU) with

tankyrases (TNKSs). Through PARdU, RNF146 controls the levels of important regulatory proteins including Axin and 3BP2. We provide a structural basis for the role of RNF146 in PARdU and how RNF146 achieves substrate specificity. First, we show that the smallest internal poly(ADP-ribose) (PAR) structural unit, *iso*-ADPr, binds between the WWE and RING domains of RNF146 acting as an allosteric signal to switch the RING domain from an auto-inhibited conformation to an active one. In the absence of PAR/*iso*-ADPr, RNF146 only weakly binds an E2 and cannot activate it for ubiquitin transfer. In this unliganded state, a loop of the RING domain blocks the E2-E3 interaction. PAR binding causes the incorporation of this loop into the main helix of the RING domain, generating a productive RING E3 ligase. Second, we demonstrate that RNF146 forms a complex with tankyrases via its disordered c-terminus. This complex appears to be mediated by at least four elongated tankyrase-binding motifs (TBMs). We have solved a structure of one of these motifs in complex with a fragment of tankyrase-1 confirming that these non-canonical TBMs are bona fide binding motifs. Mutants that disrupt either the allosteric activation of the RING domain or the RNF146-TNKS interaction inhibit Axin turnover *in vivo*. Third, we show through structural modeling that tankyrases oligomerize through their sterile alpha motif domains in a head-to-tail manner. We can disrupt this interaction with site-directed mutagenesis and oligomerization-deficient mutants cannot promote tankyrase-mediated Wnt signaling enhancement. Hence, we show that RNF146 represents a new class of E3 ligases in which binding of ligands causes conformational changes in the RING domain, that PARdU substrate specificity is likely facilitated by the TNKS-substrate interaction, and that tankyrases oligomerize via a head-to-tail SAM-SAM interaction which likely affects the tankyrase-substrate interaction and the role tankyrases play in Wnt signaling.

TABLE OF CONTENTS

Chapter 1: An introduction **8**
An Introduction *8*
The ubiquitin cascade 8
Complexity of the ubiquitin code 9
Types of eukaryotic E3 ubiquitin ligases 11
RING E3 ligases and their regulation 13
Poly(ADP-ribose) and PARP enzymes 18
Tankyrase 19
PARylation-dependent ubiquitylation and the ubiquitin E3 ligase 21
Figures *22*
References *25*
Chapter 2: Allosteric activation of the RNF146 ubiquitin ligase by a poly(ADP-ribosyl)ation signal 30
Abstract *30*
Main Text *31*
Figures *38*
References *41*
Materials and Methods *44*
Extended/Supplementary Figures *52*
Chapter 3: Structural basis for tankyrase-RNF146 interaction reveals extended tankyrase-binding motifs 62
Abstract *62*
Introduction *63*
Results and Conclusions *65*
RNF146 binds to tankyrases via its flexible C-terminal tail 65
The RNF146-TNKS interaction is mediated by at least 4 motifs in the RNF146 C-terminus 66
RNF146 Exhibits multivalent binding to tankyrase 67
RNF146 motif 1 can bind to TNKS similarly to canonical TBMs 68
Discussion *71*
Figures *73*
References *77*
Materials and Methods *81*
Supplemental Figures *86*
Chapter 4: Structural insights into SAM domain-mediated tankyrase oligomerization 92
Abstract *92*
Introduction *94*
Results *95*
Discussion *100*
Figures *101*
Materials and Methods *105*
References *109*
Supplemental Figures *114*
Chapter 4 Addendum 120
Figures *123*
Materials and Methods *124*
References *125*
Appendix 126
Contributions to UHRF1 Biophysical Studies *126*
Copyright Permissions 127

LIST OF FIGURES

1.1 Figure 1: Ubiquitin conjugation 22
1.2 Figure 2: E2~Ub activation by RING E3 ligases 23
1.3 Figure 3: The PAR polymer and tankyrase 24

2.1 Figure 1: Binding of iso-ADPr or PAR activates RNF146 E3 ubiquitin ligase activity 38
2.2 Figure 2: Crystal structure of the RNF146(RING-WWE)/UbcH5a/iso-ADPr complex 39
2.3 Figure 3: Mechanism of RNF146 PAR-mediated RING activation 40
2.4 Figure 4: RNF146 and TNKS form a tight complex critical to PARdU in vivo 41
2.S1 Extended Data Figure 1: Multiple sequence alignment of RNF146 orthologs 52
2.S2 Extended Data Figure 2: Both PAR and iso-ADPr can activate RNF146 E3 ligase activity 53
2.S3 Extended Data Figure 3: Both RNF146 RING and WWE domains contribute to iso-ADPr binding 54
2.S4 Extended Data Figure 4: ^{1}H-^{15}N HSQC-TROSY spectra of RNF146 reveal a conformational change in the RING domain upon iso-ADPr binding 55
2.S5 Extended Data Figure 5: Comparison of ligand binding in the RNF146(RING-WWE)/UbcH5a/iso-ADPr complex and in the WWE-only structure 56
2.S6 Extended Data Figure 6: Rotation and crystal packing at the E2-E3 binding interface of the RNF146(RING-WWE)/UbcH5a/iso-ADPr complex 57
2.S7 Extended Data Figure 7: RNF146/iso-ADPr binding allows the RING domain to bind and activate a ubiquitin conjugating enzyme (E2) 58
2.S8 Extended Data Figure 8: Stabilizing Helix 1 of RNF146 activates the RING domain 59
2.S9 Extended Data Figure 9: RNF146 directly interacts with TNKS. 60

3.1 Figure 1: Domain architecture of RNF146 and tankyrase-1/2 73
3.2 Figure 2: RNF146 binds to tankyrase via 4 motifs in its flexible C-terminus 74
3.3 Figure 3: Non-canonical RNF146 motif 1 binds ARC2 with an affinity similar to other TBM-TNKS interactions 75
3.4 Figure 4: Structure of the RNF146(motif 1)-TNKS(ARC2-3) interaction 76
3.S1 Supplemental Figure S1: Sequence conservation of the tankyrase ARC binding groove 86
3.S2 Supplemental Figure S2: TBM-like motifs in the disordered RNF146 C-terminus 87
3.S3 Supplemental Figure S3: RNF146 displays tight binding to tankyrase but is competed off by Axin 88
3.S4 Supplemental Figure S4: Comparison of the two peptide binding sites in the asymmetric unit 89

4.1 Figure 1: Modeling tankyrase SAM domain oligomerization 101
4.2 Figure 2: SAM mutants retain a folded structure 102
4.3 Figure 3: Tankyrase 1/2 SAM form strong homo and hetero-oligomers 103
4.3 Figure 4: NMR mapping of the oligomeric interface supports model 104
4.S1 Supporting Information Figure S1: Sequence alignment of hTNKS1/2 SAM domains and orthologues 114
4.S2 Supporting Information Figure S2: Mutant, but not wild-type TNKS2 can be purified from Escherichia Coli 115

4.A1 Chapter 4 Addendum Figure 1: Comparison of tankyrase SAM crystal structures with computational model 123
4.A2 Chapter 4 Addendum Figure 2: Overexpression of tankyrase SAM mutants do not promote Wnt signaling 124

LIST OF TABLES

2.ST1 Extended Data Table 1: Data collection, phasing and refinement statistics *61*

3.T1 Table 1: Data collection, phasing and refinement statistics *77*
3.ST1 Supplemental Table 1: Search results of TBMs from TNKS interacting proteins *90*

4.ST1 Supporting Information Table 1: SAM mutant (DAVK) unbound assignments *116*
4.ST2 Supporting Information Table 2: SAM mutant (DAVK) bound assignments *118*

CHAPTER 1

An Introduction

The ubiquitin cascade

Ubiquitin (Ub) is a highly stable 76-residue protein that can be covalently attached to lysine residues of proteins through its C-terminal glycine via an isopeptide bond (Figure 1A). Modifications of proteins with Ub is therefore known as ubiquitylation (or ubiquitination). The history of protein ubiquitylation is inexorably tied to the degradation or turnover of proteins in cells. Until the late 70's and early 80's it was overwhelmingly thought that protein degradation was driven by the lysozomal pathway mediating the degradation of cytosolic material. In early 1977, however, Etlinger and Goldberg reported a soluble and ATP-dependent proteolytic system with an optimum pH of 7.8 in rabbit reticulocytes, immature blood cells that lack lysosomal vacuoles.[1] In the same year, separate studies found the existence of histone H2A modification by a small protein called ubiquitin (previously reported by Goldstein *et al.*[2]) by virtue of a version of H2A containing two N-termini, but only one C-terminus.[3,4] These works sparked a cascade of papers between 1978 and 1983 from Aaron Ciechanover, Avram Hershko, Irwin Rose and others that laid out the fundamental principles of the ubiquitin proteasome system. Through fractionation of reticulocyte extracts Ciechanover et al.[5] very quickly discovered the existence of a heat-stable component of ATP-dependent proteolysis, which was termed APF-1 (active principle of fraction I; a.k.a. ATP-dependent proteolysis factor 1),[6,7] and a larger ATP dependent component that were both required for proteolysis of ^{125}I-albumin.[6] Shortly thereafter, the APF-1 protein was shown to be directly conjugated to proteolytic substrates and that APF-1 was

actually ubiquitin.[7–9] These findings were followed by the further fractionation of the reticulocyte proteolysis system, resulting in what is known today as the ubiquitin cascade, including the protein components termed E1, E2, and E3 that catalyze the conjugation of Ub to substrates for degradation.[10,11] The discovery of an ATP dependent protease (the 26S proteasome)[12] and subsequent studies in the 1990s on the proteasome completed the general scheme of the ubiquitin proteasome system. Therefore, through classical purification techniques, clever affinity capture techniques of the E1 enzyme, and exemplary chemical intuition, Ciechanover, Hershko, Rose and colleagues laid out the basis for the ubiquitin field. The study of ubiquitin biology has grown explosively since. Indeed, the ubiquitin field is likely much more complex and nuanced than Ciechanover, Hershko, and Rose could have predicted.

As established by Hershko *et al.*,[11] the ubiquitin cascade is mediated by three enzyme types: First, a ubiquitin-activating enzyme (E1) binds the ubiquitin and adenylates its C-terminus in a reaction dependent on ATP and magnesium. Upon adenylation there is a large conformational change in the E1 enzyme that transfers ubiquitin to a cysteine residue of the E1, releasing AMP and generating thioester between the C-terminus of ubiquitin and a cysteine residue of the E1. Second, the activated ubiquitin is transferred to the active site cysteine residue of a ubiquitin conjugating enzyme (E2) in a transthiolation reaction. Lastly, the generated E2~Ub conjugate is utilized by an E3 ubiquitin ligase, which transfers ubiquitin to a lysine residue of a substrate protein, completing the ubiquitin cascade. Since the discovery of these fundamental steps in ubiquitylation, it has been revealed that there are 2 E1s, up to 40 E2s, and an estimated excess of 600 E3 ubiquitin ligases in the human genome.

Complexity of the ubiquitin code

Substrate ubiquitylation can be in the form of monoubiquitylation, multi-monoubiquitylation, and polyubiquitylation (modified by chains of ubiquitin). Interestingly, ubiquitylation can occur on specific lysines, such as in the case of H2A ubiquitylation of K119, which is targeted for monoubuiquitylation,[13] or occur on multiple (or groups/clusters) of lysine residues on target proteins. The monoubiquitylation of specific lysine residues seems to be common thread in protein recruitment to the site of modification, especially in chromatin remodeling during DNA repair and replication. This is exemplified by the ubiquitylation of PCNA at lysine-164 with a single ubiquitin moiety, which acts as a recruitment for Y family polymerases in translesion synthesis.[14] The recruitment of the DNA methyltransferase DNMT1 also appears to be dependent on the ubiquitylation of histone H3 N-termini, that is monoubiquitylated at K23 and K18 in a process that is important for the maintenance of 5-methyl-cytosine sites following DNA replication.[15,16]

While monoubiquitylation is common, ubiquitin itself can act as a substrate for ubiquitylation at each of its seven lysine residues (K6, K11, K27, K29, K33, K48, and K63) or its N-terminal methionine (M1) (see Figure 1A). Chains of ubiquitin can be formed with single, mixed, and/or branched linkage types, all of which have been observed in cells. This complexity extends the diversity of the ubiquitin signal, establishing what some refer to as "the ubiquitin code".[17] The most well-studied homotypic linkages are that of M1, K11, K48, and K63 chains. Lysine-48 (and K11) linkages are typically associated with efficient protein degradation by the 26S proteasome, but, interestingly, are not always signals for protein destruction. Lysine-63 and M1 chains are implicated in NF-κB signaling where these ubiquitin chain types act as protein recruitment scaffolds.[18,19] In response to the varied linkage types of ubiquitin chains, evolution has provided eukaryotes with a host of ubiquitin binding domains and modules that can

distinguish chain types (allowing for the aforementioned scaffolding and recruitment roles of ubiquitin) as well as large families of deubiquitinase enzymes.[17,20,21] In addition to specific chain linkages, chains can also be highly heterogeneous (heterotypic chains) in their lysine connectivity, resulting in mixed and branched ubiquitin chains. While specific roles of branched or mixed chains have not been defined, heterogeneous polyubiquitin chains are likely associated with proteasomal degradation. Adding complexity to our view of ubiquitylation is the presence of other post-translational modifications on ubiquitin itself, including ubiquitin acetylation and phosphorylation at multiple sites, and even modification with the ubiquitin-like modifiers SUMO and NEDD8 (reviewed in ref. 21). The complexity of the ubiquitin code promises a rich scientific future for the study of ubiquitin and its ever-expanding role in biological pathways.

Types of Eukaryotic E3 ubiquitin ligases

Chain types (monoubiquitylation or polyubiquitylation, and linkage types) are determined by the E3 and/or the E2 enzyme that carry out the reaction. There are at least three types of eukaryotic E3 ubiquitin ligases: RING (really interesting new genes)-type (including RING and U-box E3 ligases), HECT (homologous to E6AP carboxy terminus), and RING-between-RING (RBR, or RING-HECT hybrids) E3 ubiquitin ligases (Figure 1B). RINGs constitute the largest class of ubiquitin ligases with greater than 300 RING domains in the human genome.[22,23] There are currently ~28 known HECTs and 14 known RBRs. The actual number of E3s can be hard to estimate given that E3 ligase proteins can form complexes with different substrate binding proteins. The best such examples are the Cullin-RING-E3 ligases (CRLs), which form the largest subclass of RING-E3 ligases. With CRLs and other RING complexes, the number of human RING E3 ubiquitin ligases is estimated to be over 600.[23]

The three E3 classes differ in their mechanism of substrate ubiquitylation, which has important consequences on the type of ubiquitin modifications observed. While HECT and RBRs are structurally unrelated, a thioester intermediate between the E3 and ubiquitin is required prior to ubiquitin transfer to a substrate lysine. In such cases the E3 is thought to dictate chains specificity independently of the E2 enzyme. RING E3 ligases (and U-box proteins) differ in that they work in conjunction with an E2~Ub conjugate to transfer ubiquitin from the E2 active site directly to a substrate lysine. Hence, the role of the RING E3 ligases is to recruit the E2~Ub conjugate and the substrate to facilitate ubiquitin transfer and the E2 likely dictates chain specificity.

Because RING E3s use E2 active sites to transfer ubiquitin to substrates, a single RING E3 can in principle use different E2s to provide different levels of reactivity for lysines or other nucleophiles (i.e. Ser/Thr, Cys, etc.). For example, in *in vitro* autoubiquitylation experiments, BRCA1/BARD1 can use the E2 Ube2D3 (UbcH5c) to build polyubiquitin chains. However, when supplied with the E2 Ube2W, BRCA1/BARD1 will only ligate a single ubiquitin to itself. This phenomenon arises from the Ube2W's unique ability to only target α-amino groups of disordered N-termini.[24–26] Because RING E3s depends on the chemistry catalyzed by the E2 active sites, biology requires a large diversity of E2s. Reciprocally, in response to this diversity of E2s, it is often required of RING E3s to be selective in E2 recruitment and/or have ways of wrangling E2s to produce an intended ubiquitin-conjugate product. An example of this type of control over E2s is seen for the polycomb group proteins with the promiscuous Ube2D family of E2s. The Ube2D family of E2s contains four canonical members that display activity with, it seems, most RING E3s. With RINGs, Ube2D family members catalyze the formation of a variety of mixed chain linkages.[27] However, when a set of RING E3s known as the polycomb

group proteins modify histones, the result is a monoubiquitylated histone H2A at K119,[13] not mixed polyubiquitin chains. This is achieved through interactions of the RING E3 with the E2 and with the substrate histone (within a nucleosome core particle) in such a ways as to only transfer a single ubiquitin.[28] Therefore, unlike other E3 ubiquitin ligases, RING E3s often take part in complex interplays with E2 enzymes and substrates to dictate a wide range of ubiquitin products, making RING E3s the most mechanistically diverse of the ubiquitin ligases.

RING E3 ligases and their regulation

RING domains are small globular domains of about 40 - 120 amino acids that are cross-braced with two Zn^{2+} ions using eight zinc-coordinating residues. Generally the RING motif is of the form: Cys-X_2-Cys-$X_{(9-39)}$-Cys-$X_{(1-3)}$-His-$X_{(2-3)}$-Cys-X_2-Cys-$X_{(4-48)}$-Cys-X_2-Cys, but replacements of some of the conserved cysteine residues with other zinc-binding groups is common (i.e. a His or Asp can replace the Zn^{2+}-binding Cys residues) (reviewed in Deshaies *et al.*).[29] U-box proteins have a similar fold, but lack the Zn^{2+}-binding residues. Instead, a hydrophobic core stabilizes the U-box domain. The sequence length and variability in RING domains can make finding common structural motifs within RING domains difficult. For instance, while some residues might be important for E2 binding and Ub transfer in one RING, they may not be in another. A complete analysis of the co-evolution of residues within the RINGs might be informative to assess the importance of RING residues for activity with specific E2s. Current structural work has assigned catalytic functionality to some conserved RING residues (see below).

Three papers on the mechanism of how RING/U-box domains allosterically activate E2~Ub conjugates were published in 2012.[30–32] In the absence of the E3, the E2~Ub species is

conformationally flexible; Ub adopts a spectrum of conformations relative to the E2 (ref. 33) (Figure 2A). However, when a RING E3 engages the conjugate, ubiquitin favors a "closed conformation" (Figure 2B) in which ubiquitin is in simultaneous contact with the E2 and the E3 enzymes.[30,31,34] This conformation exposes the reactive thioester linkage at the E2 active site. It is thought that the conformation of ubiquitin's C-terminus provides the means to stabilize an oxyanion intermediate. It is unclear if RING E3s induce other allosteric effects on the E2 active site not observed in crystal structures of E3/E2-Ub complexes. [30,34–36] In NMR experiments, E3s cause chemical shifts perturbations near the E2 active site in the absence of a ubiquitin conjugated to the E2 (Klevit lab observation). In each of the three 2012 papers noted above, an allosteric Arg/Lys following the last chelating cysteine in RING domains was identified to be important for the closed conformation. This Arg/Lys forms hydrogen bonds with a backbone carbonyl of the E2 and the C-terminal tail of ubiquitin in the E2~Ub conjugate (Figure 2C). Furthermore, the zinc-binding His (fourth metal binding residue), has important contacts with Ub in the activated E3/E2-Ub ternary complexes structurally characterize to date (Figure 2C). How RING E3s such as TRAF6 that do not have an allosteric Arg/Lys compensate for lacking this important residue is currently unclear.

While RING E3 ligases can exist as monomers, more often they are present in complexes or as dimers. These complexes have important implications for RING function and regulation. As mentioned above, CRLs are important examples of RING E3 ligase complexes. Each CRL is composed of a scaffold protein (one of seven cullins), a separate RING subunit bound to the C-terminal end of the cullin scaffold, and an adaptor and/or substrate receptor. The most well characterized substrate receptors are composed of the Skp-1 adaptor and an F-box receptor. The Skp-1/Cullin-1/F-box (SCF) complexes are extremely diverse in their specificity because there

are over 69 unique human F-box proteins (reviewed in Wang *et al.*[37]). One F-box protein can target many substrates (generally) by recognizing a sequence motif (known as a degron). A degron can be an unmodified protein sequence or can be controlled through post-translation modification. For example, the F-box protein, β-TrCP, recognizes a doubly phosphorylated motif, DpSGXX(X)pS, and therefore may target hundreds of phosphorylated proteins.[38] Another example of modified degron recognition by CRLs occurs for the transcription factor, HIF-1α. Under hypoxic conditions HIF-1α acts a transcription factor to promote the expression of genes that adapt cells to low oxygen conditions. However, in normoxia, HIF-1α is hydroxylated and subsequently degraded by a CRL composed of cullin-2, Rbx-1, elongin B and C, and VHL (VHL box substrate receptor), which specifically recognizes a hydroxylated proline in the HIF-1α degron.[39–41] Post-translational modification is therefore a theme in the regulation of CRL-mediated degradation at the substrate level. However, there are other methods for CRL regulation at the ligase level. For instance, CRL complexes are neddylated (modified with the Ub-like protein NEDD8) on a position near the RING subunit on the cullin scaffold.[42] Neddylation dramatically increases the ubiquitylation activity of the complex[43] by inducing a conformational change in the cullin scaffold itself and increasing the dynamics of the associated Rbx1 RING module.[44] Denedylation of the cullin by the COP9 signalosome and CAND1-mediated substrate receptor exchange are other regulatory mechanisms.

RING E3 ligases that are not part of CRL complexes have less generalizable modes of regulation. However, dimerization has emerged as an important strategy utilized by RING domains to affect E3 activity. RINGs can form hetero- or homo-dimers. Many RING domains are known to be inactive as monomers, but active as dimers.[45] Some RING-RING dimers form tight complex and therefore appear to be obligate dimers (e.g. BRCA1/BARD1, Mdm4/MdmX)

while others may be explicitly regulated by their dimerization. Interestingly, the polycomb group proteins also form obligate dimers composed of an active RING E3 (RING1a/RING1b) and an inactive RING (one of the six PCGF proteins). In these complexes the RING domains form direct RING-RING contacts and flanking residues on the N and C-terminal side of the RING domains form a helical bundle. The dimerization partner in polycomb proteins can dramatically change the intrinsic E3 ligase activity of the RING pair.[46] Higher intrinsic activities in these complexes has been attributed to additional contacts from the non-catalytic RING partner with ubiquitin in the activated E2~Ub conjugate. Hence, modulation of polycomb E3 activity may be determined by the presence or availability of its binding partner. However, the significance of these dimer variations for actual substrate modification is unclear as differences in substrate recognition can partially compensate for low intrinsic E3 activity.[46] Still, the polycomb proteins illustrate an important point regarding dimeric RING E3 activity: additional contacts with the E2~Ub conjugate outside the primary E2-binding RING domain can serve to elicit the closed conformation and modulate E3 activity.

For some RING E3 ligases dimerization plays a more explicit role in E3 activation. For example RNF4 is only active as a homo-dimer, but has a weak affinity for itself at its RING-RING interface.[47] RNF4 recognizes the ubiquitin-like protein SUMO via SUMO-interacting motifs capable of binding SUMO chains. Upon SUMOylation of proteins or the formation of free SUMO2/3 chains, RNF4 becomes a SUMO-directed E3. Binding of SUMO chains increases the local concentration of RNF4 on the SUMO chains. The high local concentration induces dimerization of the RING domains, thereby activating the E3 ligase.[47] The RN4 dimer forms via a β-sheet in the RING domain opposite the E2 binding surface. Importantly, the C-terminus of one copy of RNF4 crosses from one RING toward the E2 binding surface of the second copy,

providing extra contacts for the activated ubiquitin of the bound E2~Ub conjugate.[34] Hence dimerization activates RNF4 for SUMO chain ubiquitylation. The cellular inhibitor of apoptosis (cIAP) proteins demonstrate a still more intricate mechanism of activation. The cIAP proteins (cIAP1 and cIAP2) must also form dimers to be fully active. Active cIAPs bind and inhibit caspase proteins from commencing cell death through binding to caspases via baculovirus IAP repeat (BIR) domains in cIAP. The proteins SMAC and DIABLO inhibit cIAPs interaction with caspases, by binding to the same BIR domain. Interestingly, recent structural work from Dueber et al.[48] show how SMAC and DIABLO cause the activation of cIAP E3 ligase activity causing the autoubiquitylation (self ubiquitylation) of cIAPs, further enhancing the effect of SMAC/DIABLO and their small molecule mimics. In the resting state of cIAP1, the RING domain is sequestered in an autoinhibited state as an inactive monomer. When cIAP antagonists bind to the BIR domain, the RING is released and is able to form an active homo-dimer leading to the autoubiquitylation of the cIAP enzymes and their subsequent degradation.[48,49] The dimer formed by cIAP RING domains is likely activated in an analogous mechanism seen in RNF4 in which the C-terminus of one RING copy helps to promote the closed conformation of the E2~Ub bound to the neighboring RING.

Another example of RING E3 activation is exemplified by the RING E3 ligase c-Cbl (in the Cbl family including c-Cbl, Cbl-C, and Cbl-B) which catalyze the formation of receptor and non-receptor tyrosine kinase ubiquitin conjugates.[50] Rather than dimerization leading to an activation of c-Cbl, this E3 is regulated by phosphorylation of a conserved tyrosine residue in a mechanism likely shared in the Cbl family.[51–53] The Cbl family shares a common architecture including a tyrosine kinase-binding domain (TKBD) that recognizes substrate phosphotyrosine sites, a linker helix region (LHR) harboring a critical tyrosine residue (Y371 in c-Cbl) that is

itself phosphorylated, and a RING domain. In the inactive state, c-Cbl can still bind E2 (albeit weakly) and substrate, but the RING domain is held in a position partially occluded by the TKBD and LHR such that substrate-binding site is inaccessible to the RING.[54] When c-Cbl Y371 is phosphorylated a large rearrangement of the domains occurs in which the RING domain is repositioned to a site near substrate.[54] Interesting, this rearrangement also has the effect of increasing the intrinsic activity of the RING by two secondary mechanisms. First the E2 binding surface, partially blocked in the inactive state is, is free to bind E2 producing a ~10 fold increase in E2 affinity.[54] Second, in the active state the LHR containing the phosphotyrosine is positioned to act as an addition contact for ubiquitin in the bound E2~Ub conjugate, helping the complex induce the closed conformation of the E2~Ub species.[35]

While examples of single subunit (non-CRL) RING E3 regulation are currently limited, growing evidence of other E3 regulatory mechanisms (especially for RBR and HECT E3s; reviewed by Zheng and Shabek[55]) likely suggests that single subunit RING E3s are also likely to be commonly regulated. In my doctoral research I have studied two RING E3s that are each regulated by novel mechanisms. In Chapter 2 of this document we provide a novel example of RING regulation driven by the binding of poly(ADP-ribose) (see below). I continue to work on the regulatory mechanism of the RING E3 ligase UHRF1, which is activated by binding hemi-methylated DNA.[56]

Poly(ADP-ribose) and PARP enzymes

Poly(ADP-ribosyl)ation (PARylation) is a common post-translational modification involved in many cellular processes including transcriptional regulation, DNA-damage response, cell death, signaling, and mitosis.[57–62] PARylation is catalyzed by a subset of enzymes in the

diptheria toxin-like ADP-ribosyltransferase (ARTD) family. The ARTD family is composed of 17 human enzymes that modify proteins via addition of ADP-ribose (ADPr) to Asp, Glu, and Lys residues on the surface of substrate proteins. There are (at least) two classifications of ARTDs: (1) mono-ADP-ribosyltransferases, that catalyze the addition of one ADPr moiety to a substrate, and (2) poly-ADP-ribosyltransferases (a.k.a. poly(ADP-ribose) polymerases or PARPs), that modify proteins with ADPr polymers (known as poly(ADP-ribose) or PAR) (Figure 3A). These two classes of ARTDs differ by triad motif at the active site that either exhibit PARylation activity or not.[58] In both cases, NAD^+ is used as a donor of ADPr, and the catalytic mechanism is presumed to be similar. Still other ARTD family members are purportedly inactive.

Of the 17 ARTDs, only 6 are confirmed PARPs. PAR is generated when ADPr units are added to ADPr itself, forming an α(1→2) O-glycosidic bond between the nicotinamide ribose of NAD^+ and the adenosine ribose of the growing PAR chain. Nicotinamide is released as a leaving group. PAR polymers can range from just a few ADPr units to hundreds of units long.[63] Interestingly, at least some PARPs (PARP1 and PARP2) catalyze the formation of branched chains where the adjoining ribose moiety is a substrate for chain elongation (see Figure 3A).

Tankyrase

The tankyrase (TNKS) proteins (tankyrase 1 and 2; referred to collectively as tankyrase or TNKS) comprise two highly homologous members of the bona fide PARPs that are distinct from their other poly-ADP-ribosyltransferase counterparts. The tankyrases have a unique domain architecture with 5 ankyrin repeat clusters (ARCs) followed by a sterile alpha motif (SAM) domain closely spaced to the catalytic PARP domain at its C-terminus (Figure 3B). Intriguingly,

the SAM domains in TNKS take the place of the regulatory domains in other PARPs. These regulatory domains in PARP1, and PARP2 inhibit the PARP domains activity until PARP1/2 binds to DNA lesions. Currently it is known that the SAM domain likely mediates oligomerization of TNKS, and that this may be reversed by PARylation.[64,65] The SAM domain was suggested to affect inhibitor binding at the TNKS catalytic cite.[66] While the fold of the PARP domain is similar between PARP members and the tankyrases, there are notable differences, including a Zn^{2+}-binding motif near the active site. The five ARCs of TNKS recruit substrates and binding partners, which, to date, always contain at least one tankyrase binding motif (TBM). TBMs are of the form RXXΦDG, where X is any amino acid and Φ is a small hydrophobic, and can bind to four of the five ARCs (ARC 1, 2, 4, and 5) found in tankyrases. The binding site in ARCs 2 and 4 have been structurally characterized[67–69] and the residues involved in these interactions are conserved for the remaining TBM binding ARCs (e.i. ARCs 1 and 5).

As the simplicity of the TBM would imply, TNKS proteins have many targets (potentially hundreds), including well-studied proteins involved in centriole formation, telomere length regulation, proteasome assembly, and Wnt signaling.[70] Curiously, not all TNKS binding partners seem to be PARylated and may actually act as regulators of TNKS PARylation activity.[71] Unfortunately the specificity of the TNKS catalytic domain is not known. Hence, we cannot currently predict whether or not a protein will be PARylated by TNKS upon binding to the ARCs. Furthermore, TNKS appears to regulate the degradation of proteins by PARylation (see below), in which PARylation acts as a signal for proteasomal degradation. It is also unclear how many proteins that are PARylated by TNKS are also ubiquitylated.

PARylation-dependent ubiquitylation and the ubiquitin E3 ligase RNF146

Recently, modification by PAR was shown to be a signal for protein degradation by the ubiquitin proteasome system,[72,73] in a process we have termed PARylation-dependent ubiquitylation (PARdU). PARdU occurs in two steps: (1) a protein is PARylated by a PARP, and (2) the PARylated protein is ubiquitylated by an E3 that recognizes the PAR signal.

The PARP tankyrase-1/2 (TNKS) in conjunction with the RING E3 ligase, RNF146 (also known as Iduna) are known proteins responsible for PARdU.[72–78] There have been a number of reports that TNKS can regulate the levels of several proteins including TRF1,[79,80] 3BP2,[68,74,81] Axin-1 and 2, BLZF1, CASC3,[72,73,81] CPAP,[82] the proteasomal regulator PI31,[83] PTEN,[75] and most recently the Angiomotin family of proteins.[76–78] BLF1, CASC3, and the disease-related proteins 3BP2, PTEN, Axin, and the Angiomotins are confirmed substrates of RNF146. However, the stability of some TNKS substrates appear to be regulated by PARylation including TRF1, and CPAP. RNF146 may regulate these proteins as well.

RNF146 contains two domains, a RING domain near its N-terminus and a WWE domain coupled to the RING by a short linker. RNF146 was previously shown to selectively bind to *iso*-ADPr, the internal structural unit of the PAR polymer via its WWE domain (K_d = 372 nM) (see Figure 3A).[84] It was also observed that addition of free PAR polymers enhancement the autoubiquitylation of RNF146.[73,85] This was presumed to be an effect of RNF146 clustering on PAR polymers. The possibility that RNF146 is allosterically regulated by PAR was not explored. Furthermore, the question of how RNF146 can ubiquitylate specific substrates and not all PARylated proteins was not explained. The following chapters in this document seek to address these and other fundamental holes in our understanding of PARdU.

Figures

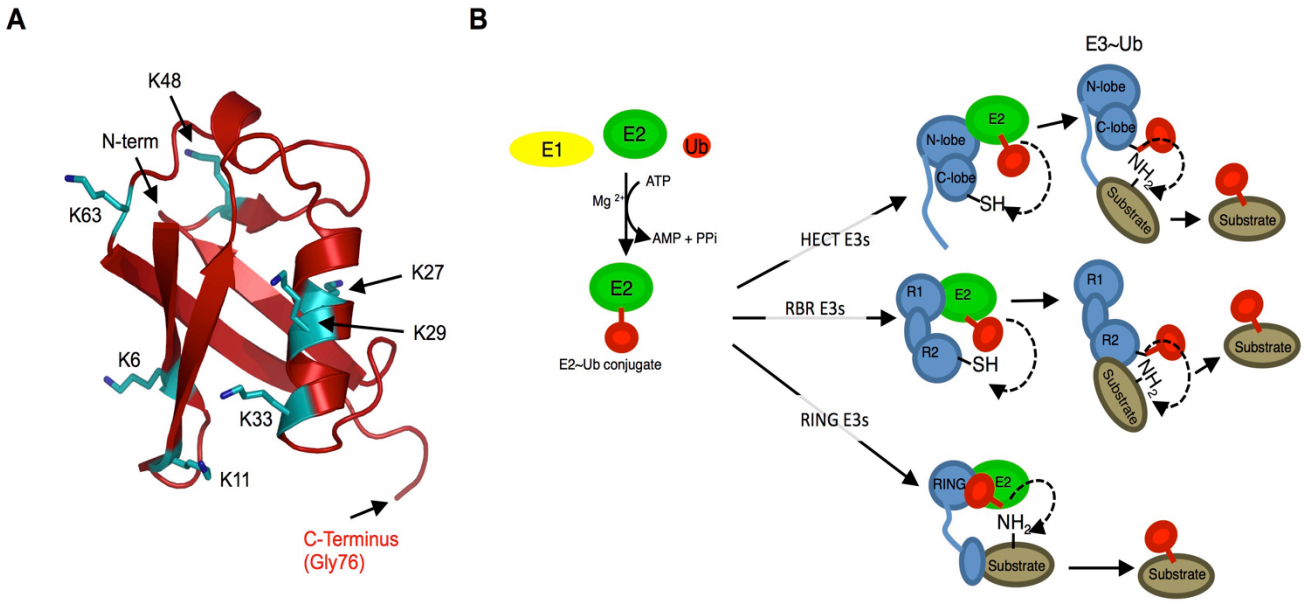

Figure 1 | Ubiquitin conjugation
(A) Cartoon representation of ubiquitin (Ub; PDB 1UBQ)[86] showing positions of Ub modifications (M1, K6, K11, K27, K29, K33, K48, and K63). Lysines are shown in cyan with visible side-chains. **(B)** The Ub cascade shown for HECT, RBR, and RING E3 ubiquitin ligases. HECT domains reside on the C-terminus and are composed of an N and C lob connected by a relatively flexible linker. E2 binds to the N-lobe of HECTs, but the active site cysteine resides on the C-lobe. RBRs contain RING1 (R1) (similar to canonical RING domains), an In-between-RING (IBR), and RING2 (R2) motifs. The active site cysteine resides on the R2 of RBRs. Both HECTs and RBRs form an obligate E3~Ub conjugate prior to transferring Ub to substrate lysine residues. RING E3 ligases facilitate the transfer of Ub directly to substrate lysines. In all cases, depending on the E3 and/or E2, substrate may be polyubiquitylated.

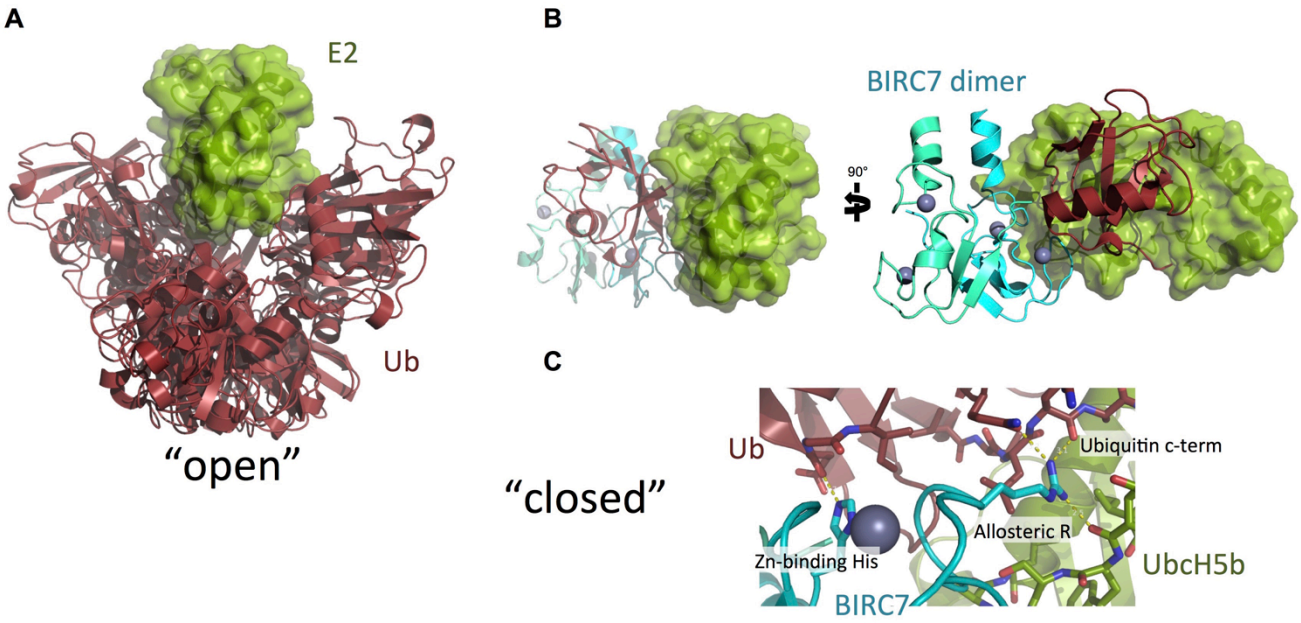

Figure 2 | E2~Ub activation by RING E3 ligases
(A) Model of an E2~Ub conjugate (Ube2D3-O-Ub; formed via an oxyester linkage) generated based on SAX data by Pruneda *et al*.[33] Ubiquitin at the active site of the Ube2D (UbcH5) family of E2s is highly dynamic in the absence of an E3. **(B)** X-ray crystal structure of the homo-dimer of the RING E3, BIRC7 bound to Ube2D2-Ub conjugate (PDB 4AUQ).[30] RING E3s appear to share common mechanism of E2~Ub activation moving the ubiquitin from an "open" conformation seen (A) to the "closed" conformation trapped in (B and C). **(C)** Close-up showing important interactions between the RING domain and Ub and the E2 in the E2~Ub species. RING domains not only bind to a surface of the E2 shown in (B), but also contact Ub, including interactions from a Zn^{2+} binding histidine, and an allosteric Arg/Lys (lynchpin) residue. The allosteric Arg/Lys forms hydrogen-bonding interactions with both the backbone of the E2 and, simultaneously, residues in the C-terminus of ubiquitin, helping to promote the closed conformation.

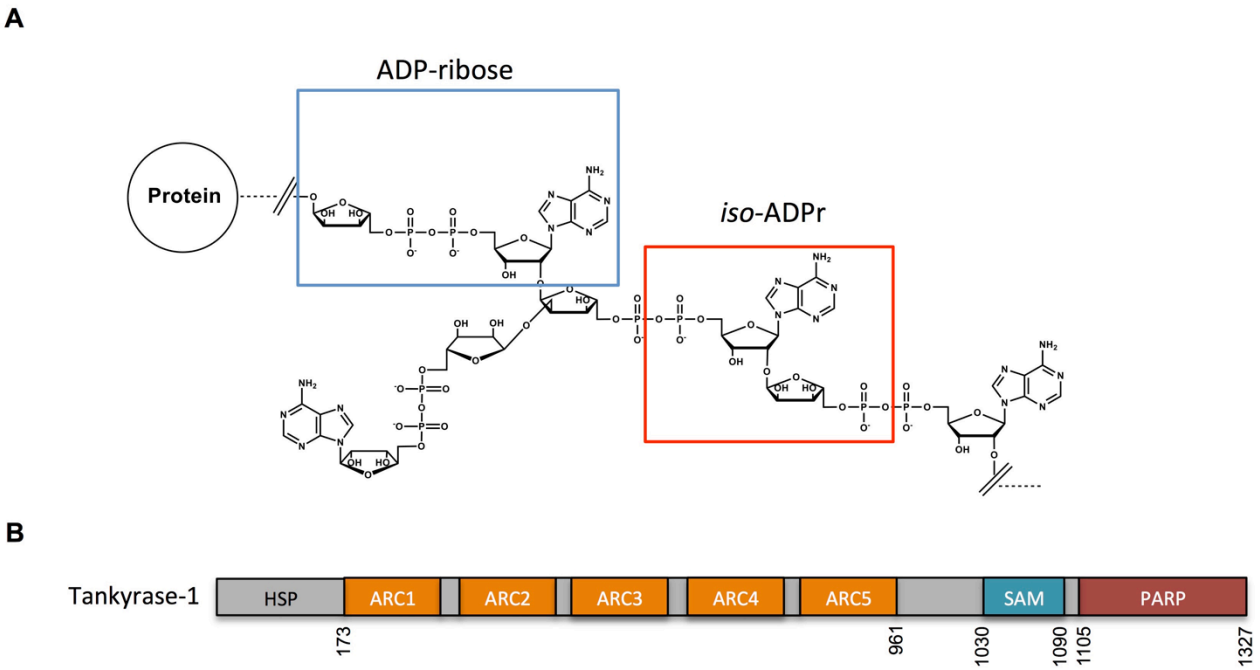

Figure 3 | The PAR polymer and tankyrase
(A) PAR polymer shown as a post-translational modification on a protein. The ADP-ribose (ADPr) unit is indicated showing the structural unit of the PAR polymer. *Iso*-ADPr represents the smallest repeating internal fragment of the PAR polymer and serves as the recognition site for WWE domain PAR-binding. Branched chains can form by ADP-robosylation of a hydroxyl neighboring an existing glycosidic linkage shown above on the second ADP-ribose unit. Branched chains have not been observed for polymers generated by the tankyrase proteins. **(B)** Linear schematic of the PARP tankyrase-1. Numbers indicate approximate sequence positions in tankyrase 1. Tankyrase-2 is highly homologous, but lacks the N-terminal HSP region. HSP, histidine, serine, proline rich sequence; ARC, ankyrin repeat cluster; SAM, sterile alpha motif; PARP, poly-ADP-ribose polymerase.

References

1. Etlinger, J. D. & Goldberg, A. L. A soluble ATP-dependent proteolytic system responsible for the degradation of abnormal proteins in reticulocytes. *Proc. Natl. Acad. Sci. U. S. A.* **74,** 54–58 (1977).
2. Goldstein, G. *et al.* Isolation of a polypeptide that has lymphocyte-differentiating properties and is probably represented universally in living cells. *Proc. Natl. Acad. Sci. U. S. A.* **72,** 11–15 (1975).
3. Goldknopf, I. L. & Busch, H. Isopeptide linkage between nonhistone and histone 2A polypeptides of chromosomal conjugate-protein A24. *Proc. Natl. Acad. Sci. U. S. A.* **74,** 864–868 (1977).
4. Hunt, L. T. & Dayhoff, M. O. Amino-terminal sequence identity of ubiquitin and the nonhistone component of nuclear protein A24. *Biochem. Biophys. Res. Commun.* **74,** 650–655 (1977).
5. Ciechanover, A., Hod, Y. & Hershko, A. A heat-stable polypeptide component of an ATP-dependent proteolytic system from reticulocytes. *Biochem. Biophys. Res. Commun.* **81,** 1100–1105 (1978).
6. Hershko, A., Ciechanover, A. & Rose, I. A. Resolution of the ATP-dependent proteolytic system from reticulocytes: a component that interacts with ATP. *Proc. Natl. Acad. Sci. U. S. A.* **76,** 3107–3110 (1979).
7. Ciechanover, A., Heller, H., Elias, S., Haas, A. L. & Hershko, A. ATP-dependent conjugation of reticulocyte proteins with the polypeptide required for protein degradation. *Proc. Natl. Acad. Sci. U. S. A.* **77,** 1365–1368 (1980).
8. Wilkinson, K. D., Urban, M. K. & Haas, A. L. Ubiquitin is the ATP-dependent proteolysis factor I of rabbit reticulocytes. *J. Biol. Chem.* **255,** 7529–7532 (1980).
9. Hershko, A., Ciechanover, A., Heller, H., Haas, A. L. & Rose, I. A. Proposed role of ATP in protein breakdown: conjugation of protein with multiple chains of the polypeptide of ATP-dependent proteolysis. *Proc. Natl. Acad. Sci. U. S. A.* **77,** 1783–1786 (1980).
10. Ciechanover, A., Elias, S., Heller, H. & Hershko, A. 'Covalent affinity' purification of ubiquitin-activating enzyme. *J. Biol. Chem.* **257,** 2537–2542 (1982).
11. Hershko, A., Heller, H., Elias, S. & Ciechanover, A. Components of ubiquitin-protein ligase system. Resolution, affinity purification, and role in protein breakdown. *J. Biol. Chem.* **258,** 8206–8214 (1983).
12. Hough, R., Pratt, G. & Rechsteiner, M. Ubiquitin-lysozyme conjugates. Identification and characterization of an ATP-dependent protease from rabbit reticulocyte lysates. *J. Biol. Chem.* **261,** 2400–2408 (1986).
13. Wang, H. *et al.* Role of histone H2A ubiquitination in Polycomb silencing. *Nature* **431,** 873–878 (2004).
14. Bienko, M. *et al.* Ubiquitin-Binding Domains in Y-Family Polymerases Regulate Translesion Synthesis. *Science* . **310,** 1821 LP-1824 (2005).
15. Nishiyama, A. *et al.* Uhrf1-dependent H3K23 ubiquitylation couples maintenance DNA methylation and replication. *Nature* **502,** 249–253 (2013).
16. Qin, W. *et al.* DNA methylation requires a DNMT1 ubiquitin interacting motif (UIM) and histone ubiquitination. *Cell Res* **25,** 911–929 (2015).
17. Komander, D. & Rape, M. The ubiquitin code. *Annu. Rev. Biochem.* **81,** 203–229 (2012).
18. Chen, J. & Chen, Z. J. Regulation of NF-κB by ubiquitination. *Curr. Opin. Immunol.* **25,**

4–12 (2013).
19. Wertz, I. E. & Dixit, V. M. Signaling to NF-κB: Regulation by Ubiquitination. *Cold Spring Harb. Perspect. Biol.* **2,** a003350 (2010).
20. Komander, D., Clague, M. J. & Urbe, S. Breaking the chains: structure and function of the deubiquitinases. *Nat Rev Mol Cell Biol* **10,** 550–563 (2009).
21. Swatek, K. N. & Komander, D. Ubiquitin modifications. *Cell Res.* **26,** 399–422 (2016).
22. Smit, J. J. & Sixma, T. K. "Ubiquitylation: mechanism and functions" Review series: RBR E3-ligases at work. *EMBO Rep.* **15,** 142–154 (2014).
23. Li, W. *et al.* Genome-Wide and Functional Annotation of Human E3 Ubiquitin Ligases Identifies MULAN, a Mitochondrial E3 that Regulates the Organelle's Dynamics and Signaling. *PLoS One* **3,** e1487 (2008).
24. Tatham, M. H., Plechanovova, A., Jaffray, E. G., Salmen, H. & Hay, R. T. Ube2W conjugates ubiquitin to alpha-amino groups of protein N-termini. *Biochem. J.* **453,** 137–145 (2013).
25. Scaglione, K. M. *et al.* The ubiquitin conjugating enzyme (E2) Ube2w ubiquitinates the N-terminus of substrates. *J. Biol. Chem.* (2013). doi:10.1074/jbc.C113.477596
26. Vittal, V. *et al.* Intrinsic disorder drives N-terminal ubiquitination by Ube2w. *Nat Chem Biol* **11,** 83–89 (2015).
27. Brzovic, P. S. & Klevit, R. E. Ubiquitin Transfer from the E2 Perspective: Why is UbcH5 So Promiscuous? *Cell Cycle* **5,** 2867–2873 (2006).
28. McGinty, R. K., Henrici, R. C. & Tan, S. Crystal structure of the PRC1 ubiquitylation module bound to the nucleosome. *Nature* **514,** 591–596 (2014).
29. Deshaies, R. J. & Joazeiro, C. A. P. RING domain E3 ubiquitin ligases. *Annu. Rev. Biochem.* **78,** 399–434 (2009).
30. Dou, H., Buetow, L., Sibbet, G. J., Cameron, K. & Huang, D. T. Structure of BIRC7–E2 ubiquitin conjugate reveals the mechanism of ubiquitin transfer by a RING dimer. *Nat. Struct. Mol. Biol.* **19,** 10.1038/nsmb.2379 (2012).
31. Pruneda, J. N. *et al.* Structure of an E3:E2~Ub complex reveals an allosteric mechanism shared among RING/U-box ligases. *Mol. Cell* **47,** 933–942 (2012).
32. Plechanovová, A., Jaffray, E., Tatham, M. H., Naismith, J. H. & Hay, R. T. Structure of a RING E3 ligase and ubiquitin-loaded E2 primed for catalysis. *Nature* **489,** 115–120 (2012).
33. Pruneda, J. N., Stoll, K. E., Bolton, L. J., Brzovic, P. S. & Klevit, R. E. Ubiquitin in Motion: Structural studies of the E2~Ub conjugate. *Biochemistry* **50,** 1624–1633 (2011).
34. Plechanovova, A., Jaffray, E. G., Tatham, M. H., Naismith, J. H. & Hay, R. T. Structure of a RING E3 ligase and ubiquitin-loaded E2 primed for catalysis. *Nature* **489,** 115–120 (2012).
35. Dou, H., Buetow, L., Sibbet, G. J., Cameron, K. & Huang, D. T. Essentiality of a non-RING element in priming donor ubiquitin for catalysis by a monomeric E3. *Nat. Struct. Mol. Biol.* **20,** 982–986 (2013).
36. Buetow, L. *et al.* Activation of a primed RING E3-E2-ubiquitin complex by non-covalent ubiquitin. *Mol. Cell* **58,** 297–310 (2015).
37. Wang, Z., Liu, P., Inuzuka, H. & Wei, W. Roles of F-box proteins in cancer. *Nat. Rev. Cancer* **14,** 233–247 (2014).
38. Low, T. Y. *et al.* A systems-wide screen identifies substrates of the SCFbetaTrCP ubiquitin ligase. *Sci. Signal.* **7,** rs8 (2014).

39. Jaakkola, P. *et al.* Targeting of HIF-alpha to the von Hippel-Lindau ubiquitylation complex by O2-regulated prolyl hydroxylation. *Science* . **292,** 468–472 (2001).
40. Ivan, M. *et al.* HIFalpha targeted for VHL-mediated destruction by proline hydroxylation: implications for O2 sensing. *Science* . **292,** 464–468 (2001).
41. Hon, W.-C. *et al.* Structural basis for the recognition of hydroxyproline in HIF-1 alpha by pVHL. *Nature* **417,** 975–978 (2002).
42. Hori, T. *et al.* Covalent modification of all members of human cullin family proteins by NEDD8. *Oncogene* **18,** 6829–6834 (1999).
43. Read, M. A. *et al.* Nedd8 Modification of Cul-1 Activates SCF(β(TrCP))-Dependent Ubiquitination of IκBα. *Mol. Cell. Biol.* **20,** 2326–2333 (2000).
44. Duda, D. M. *et al.* Structural Insights into NEDD8 Activation of Cullin-RING Ligases: Conformational Control of Conjugation. *Cell* **134,** 995–1006 (2008).
45. Metzger, M. B., Pruneda, J. N., Klevit, R. E. & Weissman, A. M. RING-type E3 ligases: Master manipulators of E2 ubiquitin-conjugating enzymes and ubiquitination. *Biochim. Biophys. Acta* **1843,** 47–60 (2014).
46. Taherbhoy, A. M., Huang, O. W. & Cochran, A. G. BMI1-RING1B is an autoinhibited RING E3 ubiquitin ligase. *Nat. Commun.* **6,** 7621 (2015).
47. Rojas-Fernandez, A. *et al.* SUMO chain-induced dimerization activates RNF4. *Mol. Cell* **53,** 880–892 (2014).
48. Dueber, E. C. *et al.* Antagonists Induce a Conformational Change in cIAP1 That Promotes Autoubiquitination. *Science* . **334,** 376–380 (2011).
49. Varfolomeev, E. *et al.* IAP Antagonists Induce Autoubiquitination of c-IAPs, NF-KappaB Activation, and TNFalpha-Dependent Apoptosis. *Cell* **131,** 669–681 (2017).
50. Mohapatra, B. *et al.* Protein tyrosine kinase regulation by ubiquitination: Critical roles of Cbl-family ubiquitin ligases. *Biochim. Biophys. Acta* **1833,** 122–139 (2013).
51. Levkowitz, G. *et al.* Ubiquitin ligase activity and tyrosine phosphorylation underlie suppression of growth factor signaling by c-Cbl/Sli-1. *Mol. Cell* **4,** 1029–1040 (1999).
52. Kassenbrock, C. K. & Anderson, S. M. Regulation of ubiquitin protein ligase activity in c-Cbl by phosphorylation-induced conformational change and constitutive activation by tyrosine to glutamate point mutations. *J. Biol. Chem.* **279,** 28017–28027 (2004).
53. Ryan, P. E., Sivadasan-Nair, N., Nau, M. M., Nicholas, S. & Lipkowitz, S. The N Terminus of Cbl-c Regulates Ubiquitin Ligase Activity by Modulating Affinity for the Ubiquitin-conjugating Enzyme. *J. Biol. Chem.* **285,** 23687–23698 (2010).
54. Dou, H. *et al.* Structural basis for autoinhibition and phosphorylation-dependent activation of c-Cbl. *Nat Struct Mol Biol* **19,** 184–192 (2012).
55. Zheng, N. & Shabek, N. Ubiquitin Ligases: Structure, Function, and Regulation. *Annu. Rev. Biochem.* **86,** 14.1-14 (2017).
56. Harrison, J. S. *et al.* Hemi-methylated DNA regulates DNA methylation inheritance through allosteric activation of H3 ubiquitylation by UHRF1. *Elife* **5,** e17101 (2016).
57. Gibson, B. A. & Kraus, W. L. New insights into the molecular and cellular functions of poly(ADP-ribose) and PARPs. *Nat Rev Mol Cell Biol* **13,** 411–424 (2012).
58. Hottiger, M. O., Hassa, P. O., Luscher, B., Schuler, H. & Koch-Nolte, F. Toward a unified nomenclature for mammalian ADP-ribosyltransferases. *Trends Biochem. Sci.* **35,** 208–219 (2010).
59. Luo, X. & Kraus, W. L. On PAR with PARP: cellular stress signaling through poly(ADP-ribose) and PARP-1. *Genes Dev.* **26,** 417–432 (2012).

60. Wang, Y., Dawson, V. L. & Dawson, T. M. Poly(ADP-ribose) Signals to Mitochondrial AIF: A Key Event in Parthanatos. *Exp. Neurol.* **218,** 193–202 (2009).
61. Virag, L. 50 Years of poly(ADP-ribosyl)ation. *Mol. Aspects Med.* **34,** 1043–1045 (2013).
62. Hsiao, S. J. & Smith, S. Tankyrase function at telomeres, spindle poles, and beyond. *Biochimie* **90,** 83–92 (2008).
63. Kiehlbauch, C. C., Aboul-Ela, N., Jacobson, E. L., Ringer, D. P. & Jacobson, M. K. High resolution fractionation and characterization of ADP-ribose polymers. *Anal. Biochem.* **208,** 26–34 (1993).
64. De Rycker, M. & Price, C. M. Tankyrase polymerization is controlled by its sterile alpha motif and poly(ADP-ribose) polymerase domains. *Mol. Cell. Biol.* **24,** 9802–12 (2004).
65. De Rycker, M., Venkatesan, R. N., Wei, C. & Price, C. M. Vertebrate tankyrase domain structure and sterile alpha motif (SAM)-mediated multimerization. *Biochem. J.* **372,** 87–96 (2003).
66. Narwal, M., Haikarainen, T., Fallarero, A., Vuorela, P. M. & Lehtiö, L. Screening and structural analysis of flavones inhibiting tankyrases. *J. Med. Chem.* **56,** 3507–3517 (2013).
67. Morrone, S., Cheng, Z., Moon, R. T., Cong, F. & Xu, W. Crystal structure of a Tankyrase-Axin complex and its implications for Axin turnover and Tankyrase substrate recruitment. *Proc. Natl. Acad. Sci.* **109,** 1500–1505 (2012).
68. Guettler, S. *et al.* Structural Basis and Sequence Rules for Substrate Recognition by Tankyrase Explain the Basis for Cherubism Disease. *Cell* **147,** 1340–1354 (2011).
69. Li, B. *et al.* Crystal structure of a tankyrase 1 – telomere repeat factor 1 complex research communications. **2,** 320–327 (2016).
70. Haikarainen, T., Krauss, S. & Lehtio, L. Tankyrases: structure, function and therapeutic implications in cancer. *Curr. Pharm. Des.* **20,** 6472–88 (2014).
71. Bisht, K. K. *et al.* GDP-Mannose-4,6-Dehydratase Is a Cytosolic Partner of Tankyrase 1 That Inhibits Its Poly(ADP-Ribose) Polymerase Activity. *Mol. Cell. Biol.* **32,** 3044–3053 (2012).
72. Callow, M. G. *et al.* Ubiquitin ligase RNF146 regulates tankyrase and Axin to promote Wnt signaling. *PLoS One* **6,** (2011).
73. Zhang, Y. *et al.* RNF146 is a poly(ADP-ribose)-directed E3 ligase that regulates axin degradation and Wnt signalling. *Nat. Cell Biol.* **13,** 623–9 (2011).
74. Levaot, N. *et al.* Loss of Tankyrase-mediated destruction of 3BP2 is the underlying pathogenic mechanism of cherubism. *Cell* **147,** 1324–1339 (2011).
75. Li, N. *et al.* Poly-ADP ribosylation of PTEN by tankyrases promotes PTEN degradation and tumor growth. *Genes Dev.* **29,** 157–170 (2015).
76. Campbell, C. I. *et al.* The RNF146 and tankyrase pathway maintains the junctional Crumbs complex through regulation of angiomotin. *J. Cell Sci.* **129,** 3396 LP-3411 (2016).
77. Wang, H. *et al.* Tankyrase Inhibitor Sensitizes Lung Cancer Cells to Endothelial Growth Factor Receptor (EGFR) Inhibition via Stabilizing Angiomotins and Inhibiting YAP Signaling. *J. Biol. Chem.* **291,** 15256–15266 (2016).
78. Wang, W. *et al.* Tankyrase Inhibitors Target YAP by Stabilizing Angiomotin Family Proteins. *Cell Rep.* **13,** 524–532 (2015).
79. Chang, W., Dynek, J. N. & Smith, S. TRF1 is degraded by ubiquitin-mediated proteolysis after release from telomeres. *Genes Dev.* **17,** 1328–1333 (2003).
80. Smith, S., Giriat, I., Schmitt, A. & de Lange, T. Tankyrase, a Poly(ADP-Ribose)

Polymerase at Human Telomeres. *Science* . **282,** 1484 LP-1487 (1998).
81. Matsumoto, Y. *et al.* RANKL coordinates multiple osteoclastogenic pathways by regulating expression of ubiquitin ligase RNF146. *J. Clin. Invest.* **127,** (2017).
82. Kim, M. K., Dudognon, C. & Smith, S. Tankyrase 1 regulates centrosome function by controlling CPAP stability. *EMBO Rep.* **13,** 724–732 (2012).
83. Cho-Park, P. F. & Steller, H. Proteasome regulation by ADP-ribosylation. *Cell* **153,** 614–627 (2013).
84. Wang, Z. *et al.* Recognition of the iso-ADP-ribose moiety in poly(ADP-ribose) by WWE domains suggests a general mechanism for poly(ADP-ribosyl)ation-dependent ubiquitination. *Genes Dev.* **26,** 235–240 (2012).
85. Kang, H. C. *et al.* Iduna is a poly(ADP-ribose) (PAR)-dependent E3 ubiquitin ligase that regulates DNA damage. *Proc. Natl. Acad. Sci. U. S. A.* **108,** 14103–14108 (2011).
86. Vijay-Kumar, S., Bugg, C. E. & Cook, W. J. Structure of ubiquitin refined at 1.8 A resolution. *J. Mol. Biol.* **194,** 531–544 (1987).

CHAPTER 2

Adapted from:

Allosteric Activation of the RNF146 Ubiquitin Ligase by a Poly(ADP-ribosyl)ation Signal

Paul A. DaRosa[1,2]*, Zhizhi Wang[2]*, Xiaomo Jiang[3], Jonathan N. Pruneda[1,4], Feng Cong[3], Rachel E. Klevit[1], Wenqing Xu[2]

[1] Department of Biochemistry, University of Washington, Seattle, WA 98195
[2] Department of Biological Structure, University of Washington, Seattle, WA 98195
[3] Novartis Institutes for Biomedical Research, Cambridge, MA 02139
[4] Present address: Medical Research Council Laboratory of Molecular Biology, Cambridge CB2 0QH, UK
* These authors contributed equally.

Published in the journal Nature.

Abstract

Protein poly(ADP-ribosyl)ation (PARylation) plays a role in diverse cellular processes such as DNA repair, transcription, Wnt signaling, and cell death[1-6]. Recent studies have shown that PARylation can serve as a signal for the polyubiquitination and degradation of several critical regulatory proteins, including Axin and 3BP2 (refs 7-9). The RING-type E3 ubiquitin ligase RNF146 (a.k.a. Iduna) is responsible for PARylation-dependent ubiquitination (PARdU)[10-12] . Here we provide a structural basis for RNF146 catalyzed PARdU and how PARdU specificity is achieved. First, we show that *iso*-ADPr, the smallest internal poly(ADP-ribose) (PAR) structural unit, binds between the WWE and RING domains of RNF146 and functions as an allosteric signal that switches the RING domain from a catalytically inactive state to an active one. In the absence of PAR, the RING domain is unable to efficiently bind and activate an E2. Binding of PAR/*iso*-ADPr induces a major conformational change that creates a functional RING structure. Thus RNF146 represents a new mechanistic class of RING E3 ligases whose activities are

regulated by non-covalent ligand binding, which may provide a template for designing inducible protein-degradation systems. Second, we found that RNF146 directly interacts with the PAR polymerase tankyrase (TNKS). Disruption of the RNF146/TNKS interaction inhibits turnover of the substrate Axin in cells. Thus, both substrate PARylation and PARdU are catalyzed by enzymes within the same protein complex, and PARdU substrate specificity may be primarily determined by the substrate-TNKS interaction. We propose that maintenance of unliganded RNF146 in an inactive state may serve to maintain the stability of the RNF146-TNKS complex, which in turn regulates the homeostasis of PARdU activity in the cell.

Main Text

Two domains can be identified within the 358-residue sequence of RNF146: an N-terminal RING domain followed by a WWE domain that binds *iso*-ADPr[13] (Fig. 1a and Extended Data Fig. 1). RING E3 ligases activate a ubiquitin-conjugating enzyme (E2) to transfer ubiquitin directly from the E2 active site to a lysine residue of a substrate. The intrinsic ability of RING E3s to stimulate Ub transfer can be assayed by following Ub transfer from E2~Ub to free amino acid lysine[14]. Unexpectedly, neither purified RNF146 RING domain nor full-length RNF146 significantly enhance the rate of Ub transfer from UbcH5~Ub to lysine (Fig. 1b and Extended Data Fig. 2a). However, addition of the WWE ligands *iso*-ADPr or PAR to the full-length RNF146 or a fragment containing the RING and WWE domains (RING-WWE), but not a RING-only construct, results in robust activation (Fig. 1 and Extended Data Fig. 2), consistent with reports that RNF146 is a PARylation-dependent E3 (refs 10-12). Isothermal titration calorimetry (ITC) analysis shows that *iso*-ADPr binds to RNF146(RING-WWE) ten times

tighter than to the WWE domain alone (K_d 39 nM and 372 nM, respectively; Extended Data Fig. 3a, b), suggesting that the presence of the RING domain contributes to ligand binding. Furthermore, RNF146(RING-WWE) is sensitive to subtilisin digestion in the absence of *iso*-ADPr, but is more resistant to proteolysis in the presence of *iso*-ADPr (Extended Data Fig. 3c), and NMR experiments indicate structural changes within the RING domain of the RING-WWE fragment upon *iso*-ADPr binding (Extended Data Fig. 4). Altogether, the data indicate that both the RING and WWE domains are involved in *iso*-ADPr binding and that ligand binding affects the conformation and/or stability of the RING domain, leading to increased E3 ligase activity.

The structural basis of RNF146 activation by *iso*-ADPr/PAR is evident in a 1.9Å crystal structure of a RNF146(RING-WWE)/UbcH5a/*iso*-ADPr complex (Fig. 2 and Extended Data Table 1). The RING domain structure is largely similar to other structurally characterized RINGs (see below), and the RNF146 WWE domain structure is almost identical to an existing crystal structure[13] (Extended Data Fig. 5a). The most notable feature is the location of *iso*-ADPr, which contacts both the RING and WWE domains (Fig. 2b and Extended Data Fig. 5b, c). Contacts between the WWE domain and *iso*-ADPr are similar to those previously described[13]. Lys 61 from the RING is within hydrogen-bond distance to hydroxyl groups on both ribose moieties of *iso*-ADPr and to a water molecule that can mediate a hydrogen bond with the adenine ring. In addition, RING residue Trp 65 forms a hydrogen bond with a main chain carbonyl in the WWE domain and has van der Waals contacts with the ligand. Although *iso*-ADPr is buried in a valley between the RING and WWE domains, the phosphate groups on either end of *iso*-ADPr are exposed. Thus, the observed ligand orientation is consistent with the notion that RNF146 binds an internal unit of a PAR polymer.

In the crystal, the E2, UbcH5a, binds to the RING domain at the canonical E2-E3 interface, away from the *iso*-ADPr binding site (Fig. 2a). Similar to other RING E3-E2 complex structures[15-24], two Zn^{2+}-binding loops and the central helix of the RING bind E2 Loops 4 and 7. A slight difference in the orientation of the RING and E2 relative to other E2-E3 complex structures is likely due to crystal packing (Extended Data Fig. 6), as the E2/E3 interactions observed in solution by NMR are similar to other well-characterized systems (see below).

Insight into the conformational changes that accompany *iso*-ADPr binding is provided by comparison to an NMR structure of the unliganded RNF146 RING domain (PDB 2D8T; RIKEN Structural Genomics/Proteomics Initiative). In the unliganded RING domain the central helix is one turn shorter, with residues 62-66 instead forming a loop that protrudes into the E2-E3 binding interface (Fig. 3a and Extended Data Fig. 7a). Trp 65 makes hydrophobic interactions with Ile 36, Leu 66, and Ala 71 and is in a position to block E2 binding. Residues 62-66 adopt the helical structure associated with active RING domains in the *iso*-ADPr-bound structure. Thus, the RNF146 RING can adopt two different conformations and binding of *iso*-ADPr stabilizes an active structure with a functional E2-binding surface.

The proposed model is supported by NMR binding experiments. Addition of unliganded RNF146(RING-WWE) resulted in very minor perturbations to the NMR spectrum of ^{15}N-UbcH5c while extensive perturbations occurred when *iso*-ADPr was also present (Fig. 3b; Extended Data Fig. 7b). Furthermore, the observed perturbations are highly similar to those observed with other RING-type E3s binding to UbcH5 and to UbcH5~Ub[21,25] (Fig. 3b and Extended Data Fig. 7c, d).

Mutational analysis was performed to understand the function of key residues in the *iso*-ADPr-induced conformational switch. Mutation of RING Lys 61, which makes multiple contacts with *iso*-ADPr, to Ala or Asp increased the K_d for *iso*-ADPr to values comparable to that of the WWE domain alone (K_d of 214 nM (K61A-RING-WWE) or 457 nM (K61D-RING-WWE) vs. 372 nM (WWE); Extended Data Fig. 3a, b). Although the K61D mutant can still bind ligand, it is not activated by *iso*-ADPr (Fig. 3c and Extended Data Fig. 8a). Thus, Lys 61 serves to couple ligand binding to the activation of the RING domain. RING Gly 62 may serve to maintain the inactive RING conformation by disrupting the central helix (Extended Data Fig. 8b). Mutation of Gly 62 to Ala in the context of both the RNF146(RING) and RNF146(RING-WWE) constructs was performed. In the absence of ligand, the mutants promote E2~Ub lysine reactivity (Fig. 3c and Extended Data Fig. 8c). RNF146(RING)-G62A also shows increased E2 binding in NMR experiments (Extended Data Fig. 8d). Thus, Gly 62 may play a key role in the conformational transition of the central helix. Likewise, a W65A mutation in RNF146(RING-WWE) to disrupt Trp 65 interactions in the inactive state also increased basal E3 activity (Fig. 3c). The double mutant G62A/W65A of RNF146(RING-WWE) exhibits still greater activity than either of the single mutants (Fig. 3c). The mutational results are consistent with our model in which extension of the RING central helix and repositioning of Trp 65 from the E2-E3 binding site to the RING/*iso*-ADPr interface constitute the allosteric switch triggered by ligand binding.

Essentially all known proteins regulated by PARdU, including Axin and 3BP2, are PARylated by TNKS[8,10-12]. We sought to understand the specificity of RNF146 by testing for a direct interaction between RNF146 and TNKS. Both GST pull-down assays and co-migration on size-exclusion chromatography (SEC) showed that full-length RNF146 forms a stable complex with the five ankyrin repeat clusters (ARCs) of TNKS (TNKS(5ARC), residues 173-961) (Fig.

4a and Extended Data Fig. 9a). Co-IP and pull-down assays using full-length TNKS further support the direct RNF146-TNKS interaction in cells (Extended Data Fig. 9b, c).

The ARCs of TNKS recognize a consensus motif of RXXGDG[6,9], although our recent work suggested that deviations may be tolerated in some circumstances[26]. As RNF146 contains no consensus motifs, we used molecular modeling to identify potential TNKS-binding sequences. Five potential motifs reside in the C-terminal region of RNF146 (motif I to V; Fig. 1a and Extended Data Fig. 1); motif I (residues 193-199) is the most conserved. A C-terminal truncation (RNF146(1-183)) could not bind to the ARCs of TNKS, but a construct that includes motif I (RNF146(1-205)) bound TNKS(5ARC) detectably (Fig. 4a). In the context of full-length RNF146, mutations in either motif I (G199V) or motif IV (G337V/G338V) reduced but did not abrogate the observed binding to TNKS(5ARC), with the motif I mutation having a stronger effect (Fig. 4a).

Knockdown of RNF146 in cells by siRNA leads to increased steady-state levels of Axin, and this effect is reversed by expression of RNF146 (refs 7,11) (Fig. 4b). In contrast, expression of the allosteric-switch mutant RNF146-K61D resulted in Axin levels similar to the no-RNF146 control. Disruption of the RNF146/TNKS complex via expression of RNF146-G199V/G337V/G338V mutant also led to increased Axin levels (Fig. 4b). Thus, coupling of PAR binding to the stimulation of E3 activity, and the ability to form an RNF146/TNKS complex are both critical to cellular PARdU regulation and turnover of Axin.

In summary, we propose that RNF146 and TNKS exist as a complex in which the RING domain is predominantly in an inactive state (Fig. 4c). TNKS is responsible for substrate selection and PARylation. Subsequent ubiquitination of the PARylated substrate requires that an

internal PAR moiety binds to RNF146 to trigger the allosteric switch to the RING E3-active state. PARylated substrate is likely held in the RNF146-TNKS complex via its interaction with TNKS, as the RNF146-TNKS interaction is required for ubiquitination of substrate in cells. Thus, our studies have revealed specific insights into the regulatory and substrate-recruitment mechanism of PARdU and have defined the molecular mechanism by which the RNF146 RING domain is allosterically switched by non-covalent small molecule binding. These insights may aid in the design of RNF146 inhibitors that may be useful for cancer treatment, as RNF146 overexpression is associated with lung cancer[27]. Furthermore, data presented herein may provide insight into studies of PAR-dependent cell death (PARthanatos), in which RNF146 was identified to be important in protecting cells from PARthanatos[12,28].

Acknowledgements

We thank Drs. Peter Brzovic and Ning Zheng for helpful discussions and editorial comments. We are grateful to the staff at ALS beamlines BL 8.2.1 and 8.2.2 for assistance with synchrotron data collection. This work was supported by NIH grant R01 GM099766 to W.X. and R.E.K. and NIH T32 GM07270 to P.A.D.

Author Contributions

P.A.D and Z.W. performed experiments. X. J. performed cell-based assays. F.C. and J.P. provided critical insight. P.A.D., Z.W., R.E.K and W.X. wrote the paper. All authors provided editorial comments.

Deposition information

The atomic coordinates and structure factors of the RNF146/UbcH5a/*iso*-ADPr complex are deposited in the Protein Data Bank (PDB) with the accession code 4QPL.

.

Figures

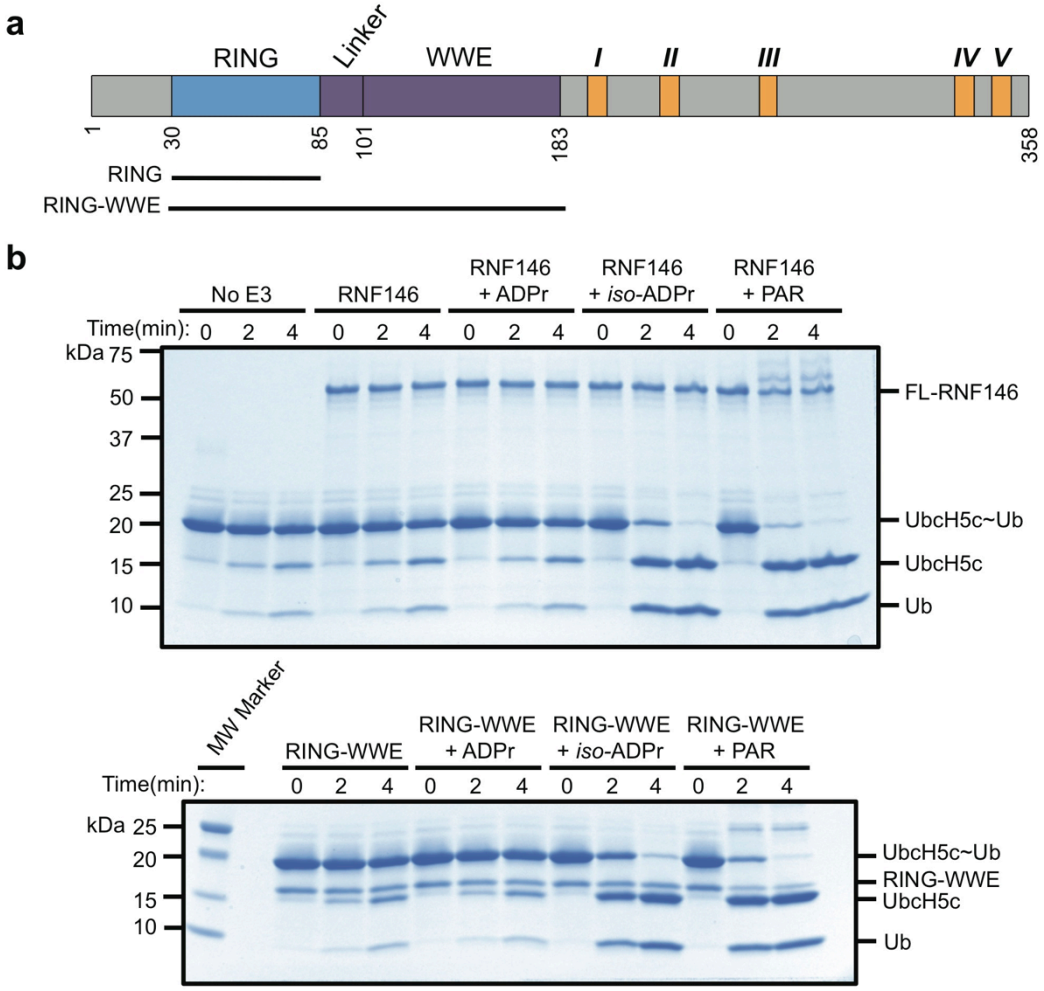

Figure 1 | Binding of *iso*-ADPr or PAR activates RNF146 E3 ubiquitin ligase activity. a. Domain structure of RNF146, with constructs used in this study shown: RNF146(RING), residues 30-89; RNF146(RING-WWE), residues 30-183. Five potential TNKS-binding motifs are shown in orange and numbered I through V in Roman numerals. **b**. Coomassie-stained E2~Ub/lysine reactivity assays of full-length RNF146 *(top)* and RNF146(RING-WWE) *(bottom)* with the E2 UbcH5c. Active RING domains enhance the reactivity of E2~Ub with lysine and therefore speed the disappearance of the E2~Ub species with the corresponding appearance of free E2 and Ub. The WWE domain does not bind ADP-ribose (ADPr)[13].

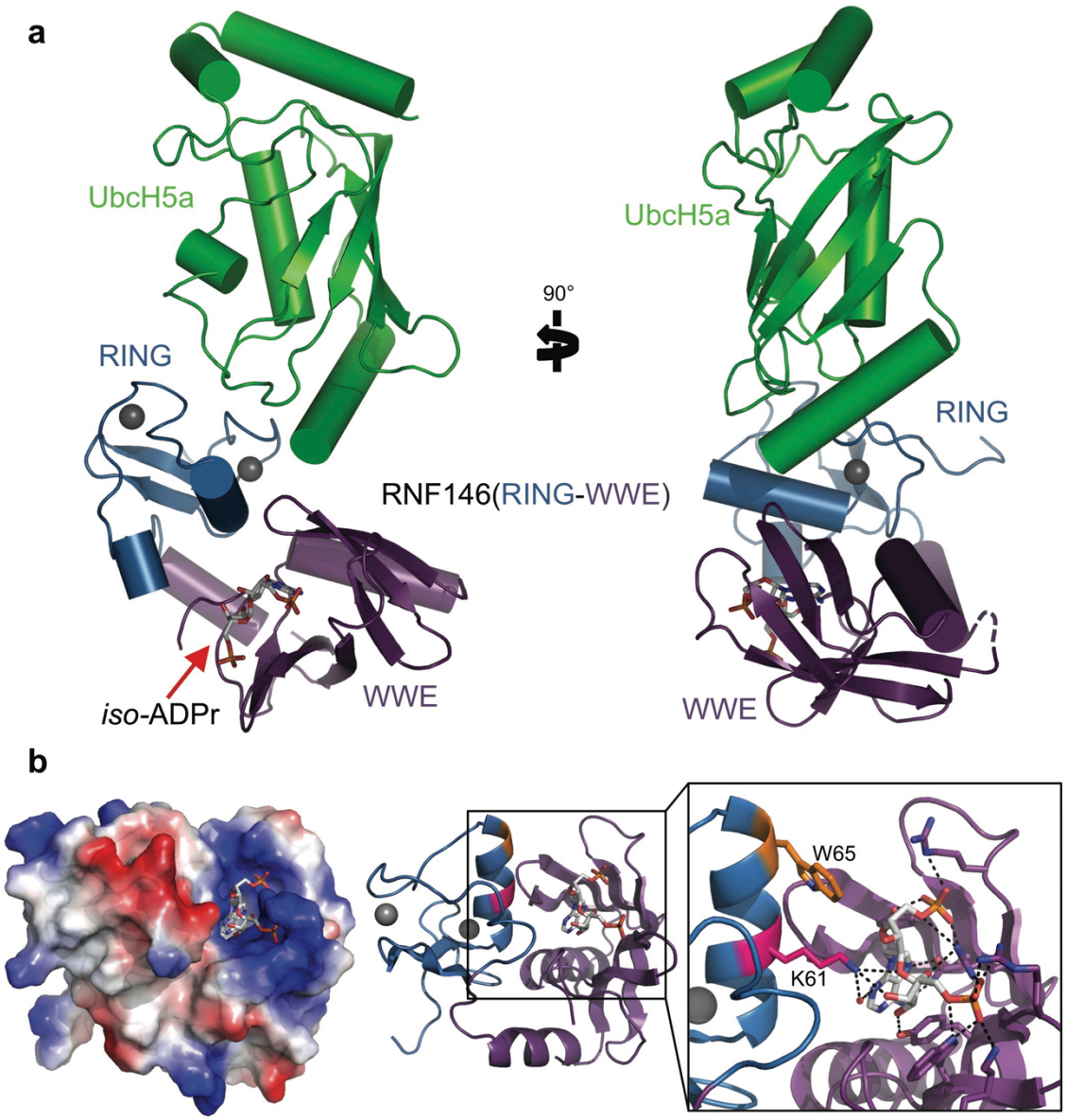

Figure 2 | Crystal structure of the RNF146(RING-WWE)/UbcH5a/*iso*-ADPr complex. a. Cartoon representation of the RNF146/UbcH5a complex with RING domain colored blue, WWE domain colored purple, and UbcH5a colored green. Zn^{2+} ions are shown as grey spheres, and the *iso*-ADPr ligand is represented as sticks. **b.** The RNF146/*iso*-ADPr interface. (*Left)* Surface electrostatic view of RNF146(RING-WWE), showing the *iso*-ADPr/PAR binding pocket; *(Center)* same view, cartoon representation; (*Right)* close-up view of *iso*-ADPr pocket. Polar contacts between protein and the ligand, *iso*-ADPr, are indicated by dashed lines; RING residues K61 (magenta) and W65 (orange) are highlighted.

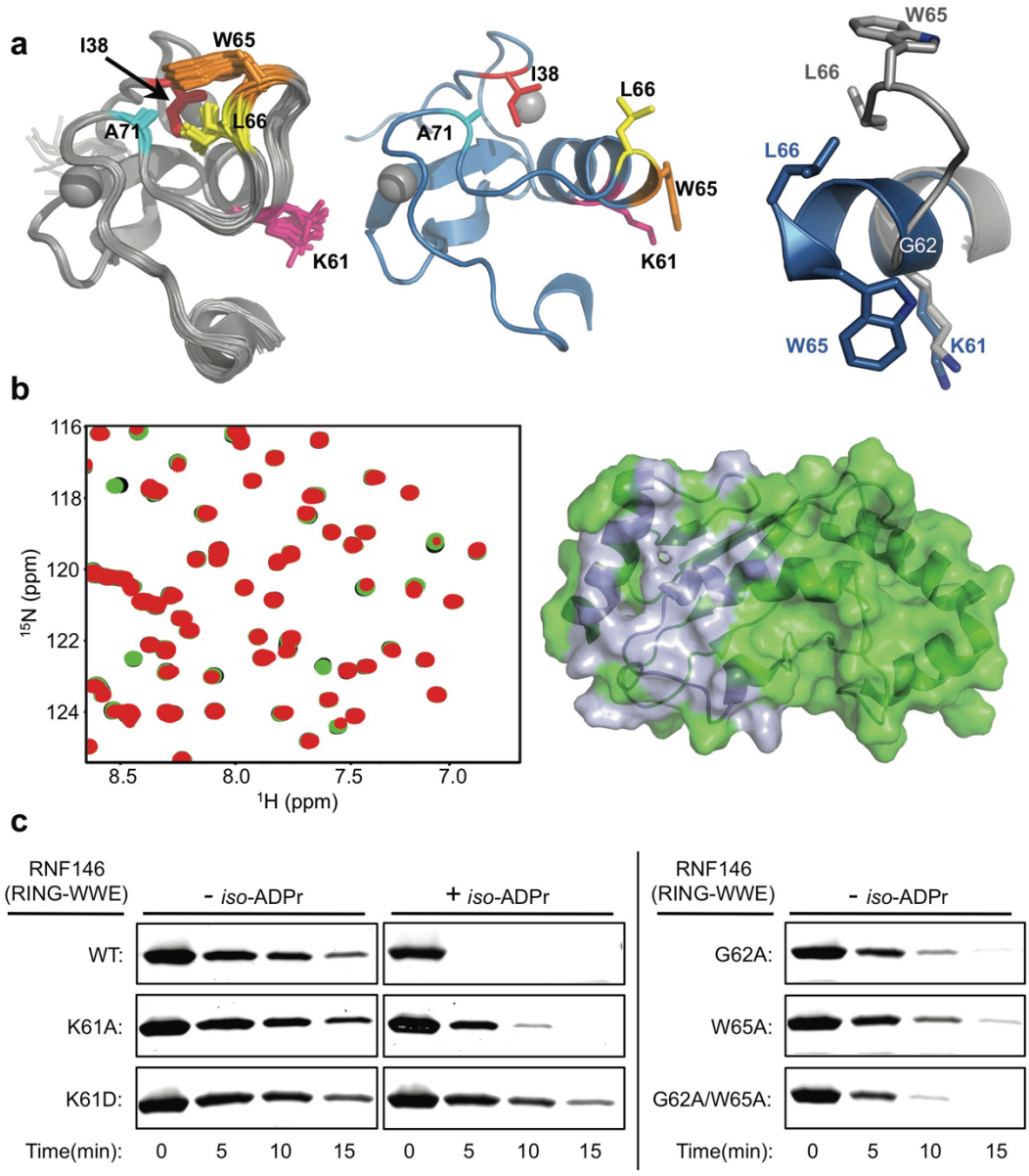

Figure 3 | Mechanism of RNF146 PAR-mediated RING activation. a, (*Top left)* Apo-RNF146 RING domain solution structure ensemble (residues 30-85; PDB 2D8T). I38, L66, A71 and W65 form a hydrophobic cluster in all members of the ensemble. *(Top center)* The RING domain of the RNF146(RING-WWE)/UbcH5a/*iso*-ADPr complex (blue) adopts a canonical RING structure shown in the same orientation as the structure in the left panel. *(Top right)* Helix 1 of the RNF146 RING domain in our complex aligned with a representative NMR structure. Upon *iso*-ADPr binding, helix 1 is extended following G62 and W65 undergoes a dramatic relocation. **b,** (*Left)* ^{1}H-^{15}N HSQC of ^{15}N-UbcH5c (S22R/C85S) alone (black), with 0.25 molar equivalence (m.e.) RNF146(RING-WWE) (green), and with 0.25 m.e. RNF146(RING-WWE) plus 0.5 m.e. of *iso*-ADPr (red). *(Right)* Chemical shift perturbations of residues in left panel mapped to the surface of UbcH5c (PDB 2FUH) show the binding surface for RNF146(RING-WWE) (light blue, on green E2). **c,** E2~Ub/lysine reactivity assays of RNF146(RING-WWE) mutants with the E2 UbcH5c; full gels are shown in Extended Data Fig. 8a.

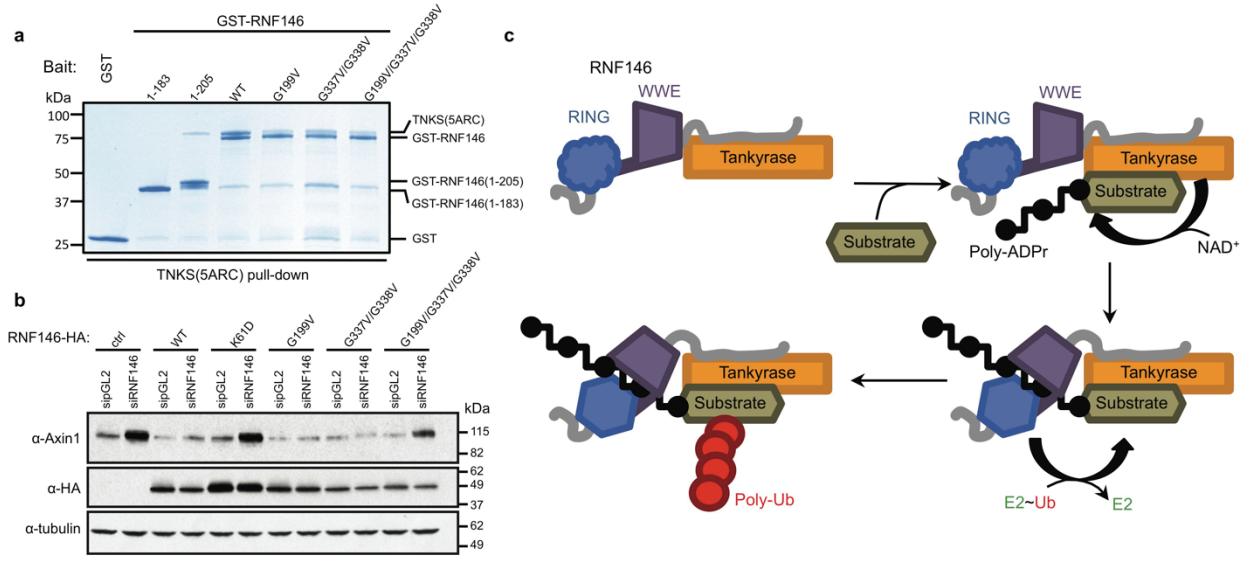

Figure 4 | RNF146 and TNKS form a tight complex critical to PARdU *in vivo*. a, GST pull-downs of GST-tagged RNF146 variants with untagged TNKS(5ARC) (residues 173-961), demonstrate a direct interaction between RNF146 and the five ARCs of TNKS. The interaction likely involves multiple TNKS-binding sites in RNF146 as various RNF146 mutations reduce but do not abolish TNKS binding (inputs are shown in Extended Data Fig. 9d). **b,** Axin turnover rescue assay shows that both the TNKS-RNF146 interaction and the RNF146 allosteric switch are important for PARdU in cells. **c,** Proposed TNKS-RNF146 PARdU model. RNF146 is inactive when bound to non-PARylated TNKS in the cell. Upon substrate binding to TNKS and subsequent PARylation, RNF146 binds an internal unit of PAR. This causes a conformational change in the RING domain, which activates its ligase activity, enabling the polyubiquitination of substrate.

References

1 Gibson, B. A. & Kraus, W. L. New insights into the molecular and cellular functions of poly(ADP-ribose) and PARPs. *Nat Rev Mol Cell Biol* **13**, 411-424 (2012).

2 Hottiger, M. O., Hassa, P. O., Luscher, B., Schuler, H. & Koch-Nolte, F. Toward a unified nomenclature for mammalian ADP-ribosyltransferases. *Trends Biochem Sci* **35**, 208-219 (2010).

3 Luo, X. & Kraus, W. L. On PAR with PARP: cellular stress signaling through poly(ADP-ribose) and PARP-1. *Genes Dev* **26**, 417-432 (2012).

4 Wang, Y., Dawson, V. L. & Dawson, T. M. Poly(ADP-ribose) signals to mitochondrial AIF: a key event in parthanatos. *Experimental neurology* **218**, 193-202 (2009).

5 Virag, L. 50Years of poly(ADP-ribosyl)ation. *Molecular aspects of medicine* **34**, 1043-1045 (2013).

6 Hsiao, S. J. & Smith, S. Tankyrase function at telomeres, spindle poles, and beyond. *Biochimie* **90**, 83-92 (2008).

7 Huang, S. M. *et al.* Tankyrase inhibition stabilizes axin and antagonizes Wnt signalling. *Nature* **461**, 614-620 (2009).

8 Levaot, N. *et al.* Loss of Tankyrase-mediated destruction of 3BP2 is the underlying pathogenic mechanism of cherubism. *Cell* **147**, 1324-1339 (2011).
9 Guettler, S. *et al.* Structural basis and sequence rules for substrate recognition by Tankyrase explain the basis for cherubism disease. *Cell* **147**, 1340-1354 (2011).
10 Callow, M. G. *et al.* Ubiquitin Ligase RNF146 Regulates Tankyrase and Axin to Promote Wnt Signaling. *PloS one* **6**, e22595 (2011).
11 Zhang, Y. *et al.* RNF146 is a poly(ADP-ribose)-directed E3 ligase that regulates axin degradation and Wnt signalling. *Nat Cell Biol* **13**, 623-629 (2011).
12 Kang, H. C. *et al.* Iduna is a poly(ADP-ribose) (PAR)-dependent E3 ubiquitin ligase that regulates DNA damage. *Proceedings of the National Academy of Sciences of the United States of America* **108**, 14103-14108 (2011).
13 Wang, Z. *et al.* Recognition of the iso-ADP-ribose moiety in poly(ADP-ribose) by WWE domains suggests a general mechanism for poly(ADP-ribosyl)ation-dependent ubiquitination. *Genes Dev* **26**, 235-240 (2012).
14 Wenzel, D. M., Lissounov, A., Brzovic, P. S. & Klevit, R. E. UBCH7 reactivity profile reveals parkin and HHARI to be RING/HECT hybrids. *Nature* **474**, 105-108 (2011).
15 Zheng, N., Wang, P., Jeffrey, P. D. & Pavletich, N. P. Structure of a c-Cbl-UbcH7 complex: RING domain function in ubiquitin-protein ligases. *Cell* **102**, 533-539 (2000).
16 Das, R. *et al.* Allosteric regulation of E2:E3 interactions promote a processive ubiquitination machine. *The EMBO journal* **32**, 2504-2516 (2013).
17 Dou, H. *et al.* Structural basis for autoinhibition and phosphorylation-dependent activation of c-Cbl. *Nature structural & molecular biology* **19**, 184-192 (2012).
18 Bentley, M. L. *et al.* Recognition of UbcH5c and the nucleosome by the Bmi1/Ring1b ubiquitin ligase complex. *The EMBO journal* **30**, 3285-3297 (2011).
19 Campbell, S. J. *et al.* Molecular insights into the function of RING finger (RNF)-containing proteins hRNF8 and hRNF168 in Ubc13/Mms2-dependent ubiquitylation. *The Journal of biological chemistry* **287**, 23900-23910 (2012).
20 Yin, Q. *et al.* E2 interaction and dimerization in the crystal structure of TRAF6. *Nature structural & molecular biology* **16**, 658-666 (2009).
21 Pruneda, J. N. *et al.* Structure of an E3:E2~Ub complex reveals an allosteric mechanism shared among RING/U-box ligases. *Molecular cell* **47**, 933-942 (2012).
22 Plechanovova, A., Jaffray, E. G., Tatham, M. H., Naismith, J. H. & Hay, R. T. Structure of a RING E3 ligase and ubiquitin-loaded E2 primed for catalysis. *Nature* **489**, 115-120 (2012).
23 Hodson, C., Purkiss, A., Miles, J. A. & Walden, H. Structure of the human FANCL RING-Ube2T complex reveals determinants of cognate E3-E2 selection. *Structure* **22**, 337-344 (2014).
24 Dou, H., Buetow, L., Sibbet, G. J., Cameron, K. & Huang, D. T. BIRC7-E2 ubiquitin conjugate structure reveals the mechanism of ubiquitin transfer by a RING dimer. *Nature structural & molecular biology* **19**, 876-883 (2012).
25 Brzovic, P. S. *et al.* Binding and recognition in the assembly of an active BRCA1/BARD1 ubiquitin-ligase complex. *Proceedings of the National Academy of Sciences of the United States of America* **100**, 5646-5651 (2003).
26 Morrone, S., Cheng, Z., Moon, R. T., Cong, F. & Xu, W. Crystal structure of a Tankyrase-Axin complex and its implications for Axin turnover and Tankyrase substrate

recruitment. *Proceedings of the National Academy of Sciences of the United States of America* **109**, 1500-1505 (2012).
27 Gao, Y. *et al.* Overexpression of RNF146 in non-small cell lung cancer enhances proliferation and invasion of tumors through the Wnt/beta-catenin signaling pathway. *PloS one* **9**, e85377 (2014).
28 Andrabi, S. A. *et al.* Iduna protects the brain from glutamate excitotoxicity and stroke by interfering with poly(ADP-ribose) polymer-induced cell death. *Nat Med* **17**, 692-699 (2011).
29 Brzovic, P. S., Lissounov, A., Christensen, D. E., Hoyt, D. W. & Klevit, R. E. A UbcH5/ubiquitin noncovalent complex is required for processive BRCA1-directed ubiquitination. *Molecular cell* **21**, 873-880 (2006).
30 Pruneda, J. N., Stoll, K. E., Bolton, L. J., Brzovic, P. S. & Klevit, R. E. Ubiquitin in motion: structural studies of the ubiquitin-conjugating enzyme approximately ubiquitin conjugate. *Biochemistry* **50**, 1624-1633 (2011).
31 Otwinowski, Z. & Minor, W. *Processing of X-ray diffraction data collected in oscillation mode*. Vol. 276 (Academic Press, 1997).
32 Adams, P. D. *et al.* PHENIX: a comprehensive Python-based system for macromolecular structure solution. *Acta Crystallogr D Biol Crystallogr* **66**, 213-221 (2010).
33 Emsley, P., Lohkamp, B., Scott, W. G. & Cowtan, K. Features and development of Coot. *Acta Crystallogr D Biol Crystallogr* **66**, 486-501 (2010).
34 CCP4. The CCP4 suite: programs for protein crystallography. *Acta Crystallogr. D* **50**, 760-763 (1994).
35 DeLano, W. L. & Brunger, A. T. Helix packing in proteins: prediction and energetic analysis of dimeric, trimeric, and tetrameric GCN4 coiled coil structures. *Proteins* **20**, 105-123. (1994).
36 Delaglio, F. *et al.* NMRPipe: a multidimensional spectral processing system based on UNIX pipes. *J Biomol NMR* **6**, 277-293 (1995).
37 Johnson, B. A. & Blevins, R. A. NMR View: A computer program for the visualization and analysis of NMR data. *J Biomol NMR* **4**, 603-614 (1994).
38 Yeh, T. Y. *et al.* Tankyrase recruitment to the lateral membrane in polarized epithelial cells: regulation by cell-cell contact and protein poly(ADP-ribosyl)ation. *The Biochemical journal* **399**, 415-425 (2006).

Materials and Methods

Plasmids, protein expression and purification

Human RNF146 was subcloned into a pET-28a vector with an N-terminal His_6 and T7 tags and a TEV cleavage site, and a pGEX-6P-2 vector with an N-terminal GST and C-terminal His_6 tag. Mouse RNF146(RING-WWE) (residues 30-183), which has an identical protein sequence to human RNF146 in this region, was subcloned into a pGEX-4T-1 vector with an N-terminal GST tag and TEV cleavage site. GST-tagged human Tankyrase 1 fragment containing all five ankyrin repeat clusters (TNKS(5ARC); residues 173-961) was expressed from a pGEX-4T-1 vector with an N-terminal GST tag and TEV cleavage site. Full-length mouse TNKS was cloned into pET-15b plasmid. Mutants and truncations of RNF146 were generated using site-directed mutagenesis (Stratagene) and confirmed by sequencing. BRCA1/BARD1 (residues 1-112/1-115 respectively), UbcH5a, UbcH5b, UbcH5c, Ubiquitin (Ub), UbcH5c(S22R/C85S), and wheat E1 were purified as previously described[25,29]. The oxyester linked E2-O-Ub conjugate (UbcH5c(S22R/C85S)-O-Ub) was generated and purified as previously described[30].

All *Escherichia coli* (BL21) cultures were grown to an OD of 0.6-1.2 in LB media or minimal MOPS media supplemented with ^{15}N-ammonium chloride (Cambridge Isotope Labs) for NMR spectroscopy. Protein expression was induced in the presence of 200 μM IPTG at 16 °C or 24 °C for 16-18 hrs. Bacterially expressed GST-RNF146(RING-WWE) or GST-RNF146(RING) (residues 30-89) were bound to Glutathione Sepharose 4B resin (GE Healthcare), washed, and eluted with 10 mM glutathione in a buffer containing 25 mM sodium phosphate pH 7.6 and 200 mM NaCl. GST was then cleaved from proteins using a His_6-TEV protease for 1 hour at 37 °C (or overnight at 4 °C) and the samples were dialyzed over night at 4 °C into 4 L of phosphate buffer (25 mM sodium phosphate pH 7.6, 200 mM NaCl). Dialyzed

proteins were then run through Ni^{2+} NTA resin (GE Healthcare) to capture TEV and subsequently Glutathione Sepharose 4B resin to capture GST. After concentrating in the presence of 2 mM DTT, RNF146(RING-WWE) was purified using Superdex 75 (GE Healthcare) equilibrated with 25 mM phosphate pH 7.0, 150 mM NaCl,. Similarly, TNKS(5ARC) was purified using Glutathione Sepharose 4B resin, followed by on-column TEV cleavage overnight at 4 °C. The untagged TNKS(5ARC) were subsequently purified by anion exchange column using a Q column (GE Healthcare). Full-length mouse TNKS1 was partially purified by Ni^{2+} NTA resin (GE Healthcare). Full-length His_6-T7-RNF146 was purified using a Ni^{2+} NTA resin (GE Healthcare), followed by ion exchange on a HiTrap Q column (GE Healthcare) and size exclusion chromatography using a Superdex 200 10/300 column (GE Healthcare). Protein concentrations were determined by their UV absorbance at 280 nm, and double checked with Coomassie-stained SDS-PAGE.

Lysine reactivity assay

For Coomassie or Oriole (BioRad) stained gels, UbcH5~Ub conjugates were generated in a solution containing 100 μM E2, 1.5 μM wheat E1, 200 μM Ub (K0 mutant: K6R, K11R, K29R, K33R, K48R K63R, and K27M), 2.5 mM $MgCl_2$, and 2 mM ATP (Sigma-Aldrich) in phosphate buffered saline at 37 °C for 30 min. The conjugate was purified by SEC prior to E2~Ub/lysine reactions. E2~Ub conjugates were added to E3 samples (WT or mutant full-length RNF146, RNF146(RING-WWE), or RNF146(RING)) for a final concentration of 25 μM E2 and 4 or 8 μM E3 (all reactions in Figure 3c were performed at 8 μM E3), and 25 μM *iso*-ADPr where indicated. Time zero samples were taken just before addition of buffered L-lysine HCl (Sigma-Aldrich) to a final concentration of 40 mM and incubated at 35 °C. Time points were collected

between 1 and 15 minutes; the reactions were quenched in 2x non-reducing SDS loading buffer, and analyzed by SDS-PAGE.

For western blot analysis, 5 μM UbcH5a enzyme was charged with 0.5 μM E1, 5 μM Ub (HA-tagged, K0 mutant: K6R, K11R, K29R, K33R, K48R K63R, and K27M), 10 mM $MgCl_2$ and 5 mM ATP for 30-40 min at 37 °C. Reaction mixtures were added to tubes containing E3 for a final concentration of 5 μM E3 and 10 μM *iso*-ADPr when appropriate. Time zero samples were taken just before addition of buffered L-lysine HCl (Sigma-Aldrich) to a final concentration of 25 mM and incubated at 35 °C. Reactions were quenched in 2x non-reducing SDS loading buffer, analyzed by western blots with mouse anti-HA (mAb, Covance, MMS-101P).

Auto-ubiquitination

In vitro auto-ubiquitination was performed in a reaction mixture containing 1 μM E1, 3 μM UbcH5c, 45 μM ubiquitin, 5 μM $MgCl_2$, and 3 μM His_6-T7-RNF146. PAR or *iso*-ADPr was added to a final concentration of about 20 μM (ADPr units) or 10 μM respectively. ATP was added to a final concentration of 5 μM after collecting time zero samples. The samples were then incubated at 37 °C and time points were collected between 0 and 12 min. Reactions were quenched with 10x reducing SDS loading buffer, boiled, and analyzed by western blot using mouse anti-T7 antibody (mAb, Novagen, 69522).

Limited proteolysis

Limited proteolysis was performed by incubating 10 μg RNF146(RING-WWE) (residues 30-183) or RNF146(Linker-WWE) (residues 83-183) with 50 ng subtilisin (Sigma-Aldrich) in the presence or absence of 150 μM *iso*-ADPr for 1 hour at room temperature. The reaction was

quenched with 5x SDS loading buffer and the resulting digests were resolved by SDS-PAGE and stained with Coomassie.

SEC-MALS

SEC-MALS experiments were performed at room temperature with a Superdex 200 10/300 column (GE Healthcare) and a miniDAWN TREOS MALS detector (Wyatt Technology). About 200 μg of full-length RNF146, TNKS(5ARC) and TNKS(5ARC)/RNF146 complex were injected in each run. The column was run with buffer containing 20 mM Tris-HCl pH 7.5, 150 mM NaCl and 2 mM DTT. The light scattered by a protein is directly proportional to its weight-average molecular mass and concentration.

Crystallization of the RNF146(RING-WWE)/UbcH5a/*iso*-ADPr complex

RNF146(RING-WWE) was bound to a SP anion exchange column (GE Healthcare) and then eluted with buffer containing 20 mM Tris-HCl pH 7.0, 5% (v/v) glycerol, 2 mM DTT, and 500 mM NaCl. The protein was eluted with a salt concentration of ~150 mM NaCl and was subsequently concentrated to 2.4 mg/mL for crystallization. RNF146(RING-WWE) was mixed with *iso*-ADPr ligand in a microcentrifuge tube for a final concentration of 133 μM protein to 267 μM ligand and incubated on ice for 30 min. Eighty microliters of this solution was mixed with 20 μL of His_6-UbcH5a in a 25 mM sodium phosphate pH 7.0, 150 mM NaCl buffer, for final concentrations of 120 μM E2 and 106 μM E3. This mixture was incubated on ice for 30 min. Crystals were obtained using the hanging drop method by adding 1 μL of the above protein-ligand mixture to 1 μL of a well solution containing 800 mM sodium citrate, 80 mM Tris-HCl pH 7.0, 160 mM NaCl, 4 mM DTT, and 20 mM trimethylamine HCl. Crystals formed in 24-36

hrs at room temperature. Crystals were frozen with liquid nitrogen in a cryoprotectant composed of 800 mM sodium citrate, 96 mM Tris-HCl pH 7.0, 280 mM NaCl, 5 mM DTT, and 20% (v/v) glycerol.

X-ray data collection and structure determination

Crystal screening and data collection were performed at the ALS, beamline 8.2.1. All diffraction data were processed by the HKL2000 package[31] in the space group $P2_12_12$. The structure was determined, at 1.9 Å resolution, by single-wavelength anomalous dispersion (SAD) using one data set collected at a wavelength of 1.28295 Å, which was also used for refinement (Extended Data Table 1). The zinc sites and the initial phases were determined by PHENIX[32]. Four zinc sites were found in one asymmetric unit, and the experimental electron density map clearly showed the presence of two RNF146(RING-WWE)/UbcH5a complexes with two ligands in one asymmetric unit. The complex model was improved using iterative cycles of manual rebuilding with the program COOT[33] and refinement with Refmac5 of the CCP4 6.4.0 program suite[34]. There are no Ramachandran outliers (96.0% most favored, 4.0% allowed). The electrostatic potential surfaces shown were generated with the APBS tool in Pymol[35].

Isothermal titration calorimetry

ITC was performed on a VP-ITC Microcal colorimeter (Microcal) at 25 °C for RNF146(RING-WWE) and the RNF146(RING-WWE) mutants. Protein and *iso*-ADPr were buffer exchanged into 20 mM HEPES pH 7.5, 150 mM NaCl, 1 mM DTT using size exclusion chromatography on a Superdex 75 10/300 column (GE Healthcare), eluting at a final concentration of ~15-20 μM. The ligand, *iso*-ADPr, was diluted in the same buffer to ~500 μM.

Both ligand and protein were degassed before use. Ligand was injected in 5 μL quantities every 5 min for a total of 25-40 injections into a 1.4218 mL protein chamber. Data were analyzed using Origin 7.0, fitting curves to a one-site model.

NMR spectroscopy

Two-dimensional (^{15}N, ^{1}H)-HSQC-TROSY experiments where performed on a Bruker 500 MHz AVANCE II NMR spectrometer. All data were obtained with 200 μM ^{15}N-labeled protein. Data were processed with NMRPipe[36], and peak intensities (I) and chemical shift perturbations (CSPs) were measured in NMRViewJ[37] (One Moon Scientific). Peak intensity changes of ^{15}N-labeled E2 (UbcH5c S22R/C85S) were measured relative to free E2 ($I_{E3\ bound}/I_{free}$), and peaks affected by binding were identified by one standard deviation away from the mean $I_{E3\ bound}/I_{free}$ value. Chemical shift perturbations were determined by the equation $\Delta\delta_j = [(\Delta\delta_j\ ^{15}N/5)^2 + (\Delta\delta_j\ ^{1}H)^2]^{1/2}$; peaks with CSPs greater than one standard deviation from the mean were considered significantly perturbed. Both peak broadening and CSPs were mapped onto the E2 surface (PDB: 2FUH)[29] to show residues affected by E3 binding. For (^{15}N, ^{1}H)-HSQC-TROSY experiments of the oxyester linked E2-O-Ub conjugate (UbcH5c(S22R/C85S)-O-Ub), Ub and UbcH5c peak intensities and CSPs were analyzed separately as indicated above. For NMR experiments of the E2-O-Ub conjugate, peak broadening and CSPs were mapped onto the UbcH5b and Ub surfaces of the BIRC7/UbcH5b-O-Ub structure[24] (PDB: 4AUQ) to show residues most affected when E3 binds.

GST pull-down assays

Approximately 3 μM of purified GST or GST-RNF146 (wt, truncations, or mutants) and about 6.7 μM of untagged TNKS(5ARC) were incubated with 25 μL of GSH sepharose 4B resin (GE Healthcare) for 1 hour at room temperature in binding buffer (40 mM Tris-HCl pH 8.0, 100 mM NaCl, 0.04% (v/v) Tween 20, 2 mM DTT; total volume of 200 μL). The beads were then washed with 200 μL buffer three times. Proteins were resolved on SDS-PAGE and stained with Coomassie.

Full-length TNKS pull-down assays were performed using GST-RNF146-R163A, a mutant that is deficient in binding poly(ADP-ribose)[11]. Proteins were resolved via SDS-PAGE and the full-length TNKS, GST, and GST-RNF146-R163A were visualized by western blot analysis using anti-TNKS (pAb, rabbit, Abcam, ab86279) and anti-GST (mAb, mouse, GenScript, A00865) antibodies.

Immunoprecipitation

HEK293T cells (ATTC, CRL-11268) were transfected with indicated plasmids with Fugene HD (Promega). Thirty-six hours after transfection, cells were lysed with IP buffer (20 mM Tris-HCl pH 7.4, 150 mM NaCl, 1% (v/v) Triton X-100, supplemented with protease inhibitors and phosphatase inhibitors) and cleared by centrifugation. Flag-tagged proteins were immunoprecipitated from lysates with Flag-agarose beads (Sigma-Aldrich), and washed in IP buffer. Proteins bound to the beads were resolved by SDS-PAGE and analyzed by immunoblotting. Cells were authenticated by SNP testing and confirmed as mycoplasma negative by a PCR based assay.

RNF146 knockdown and rescue assay

siRNA-mediated knockdown and cDNA overexpression of RNF146 were described previously[11]. siRNA-resistant HA-tagged RNF146 (wild type) and indicated mutants were subcloned into pcDNA4-TO. T-REx-293 cells (Life Technologies) were transfected with these plasmids and selected with Blasticidin to establish stable lines that express RNF146 in a Doxycycline-inducible manner. siRNAs against RNF146 and luciferase (as negative control) were transfected with Lipofectamine RNAiMax (Life Technologies). Sequences of siRNAs used are: RNF146 5'-GCACGUUUUCUGCUAUCUAdTdT-3', antisense, 5'-UAGAUAGCAGAAAACGUGCdTdT-3' (Qiagen); pGL2 (luciferase), sense, 5'-CGUACGCGGAAUACUUCGAdTdT-3', antisense, 5'-UCGAAGUAUUCCGCGUACGdTdT-3' (Dharmacon). 72 hours after siRNA transfection and Doxycycline induction, cells were lysed in RIPA buffer (50 mM Tris-HCl pH 7.4, 150 mM NaCl, 1% (v/v) NP-40, 0.5% sodium deoxycholate, 0.1% SDS, 1 mM EDTA) supplemented with protease inhibitor cocktail (Roche) and phosphatase inhibitor cocktail (Thermo Scientific). Cell lysates were resolved by SDS-PAGE and analyzed by immunoblotting with rabbit anti-Axin1 (mAb, Cell Signaling Technology, 2075), rat anti-HA (mAb, Roche, 12158167001), and mouse anti-tubulin (mAb, Sigma, T5168). T-REx-293 cells were authenticated by SNP testing and confirmed as mycoplasma negative by a PCR based assay.

Extended/Supplementary Figures

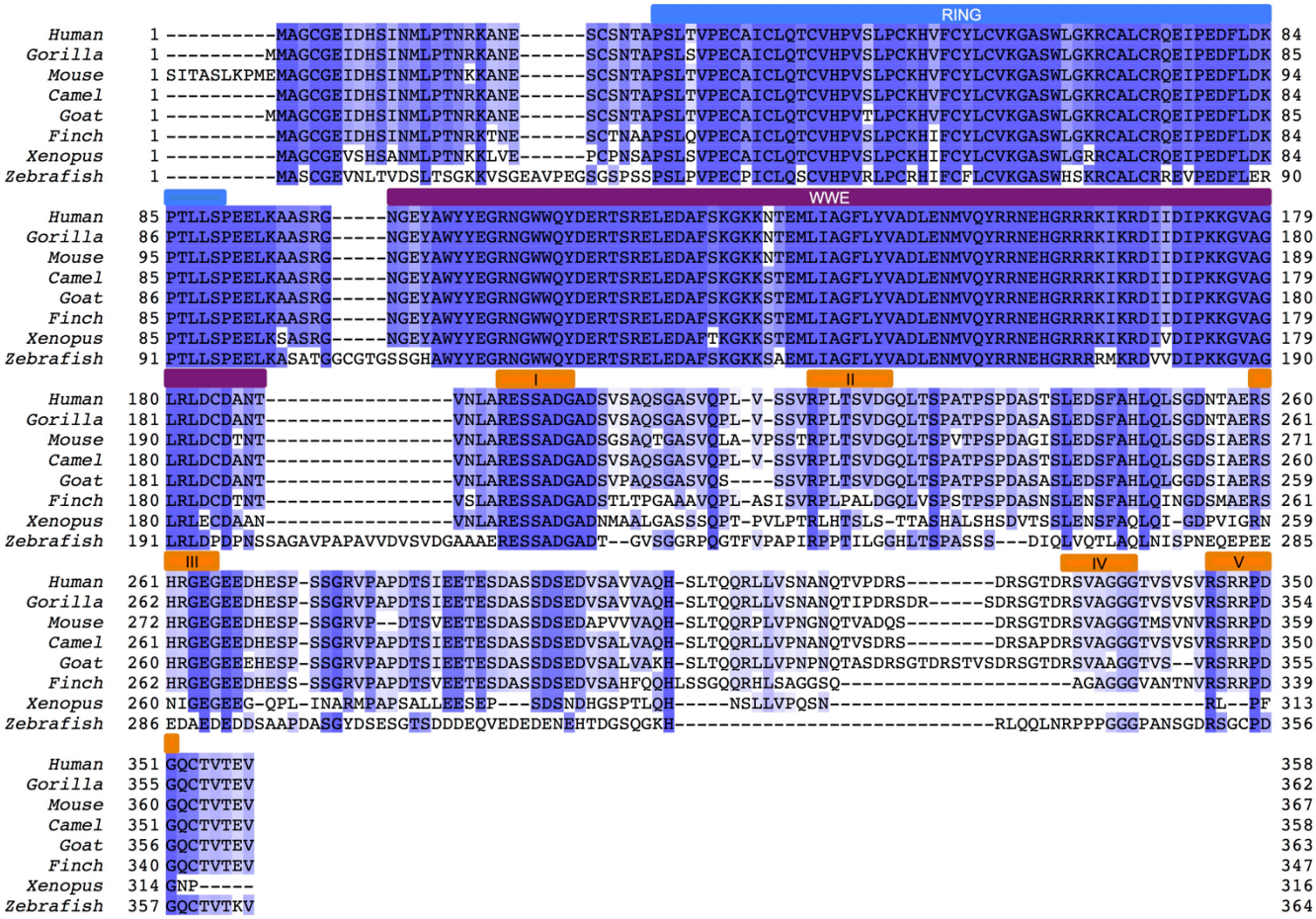

Extended Data Figure 1 | Multiple sequence alignment (MSA) of RNF146 orthologs. The colored bars above the sequence alignment indicate regions of interest in human RNF146: RING domain (blue), WWE domain (purple), and potential TNKS binding motifs, numbered I through V (orange). While there are no apparent RXXGDG TNKS binding motifs, the five potential binding motifs indicated here are based on the TNKS-substrate interface plasticity demonstrated by a recent crystal structure of the Axin-TNKS complex[26].

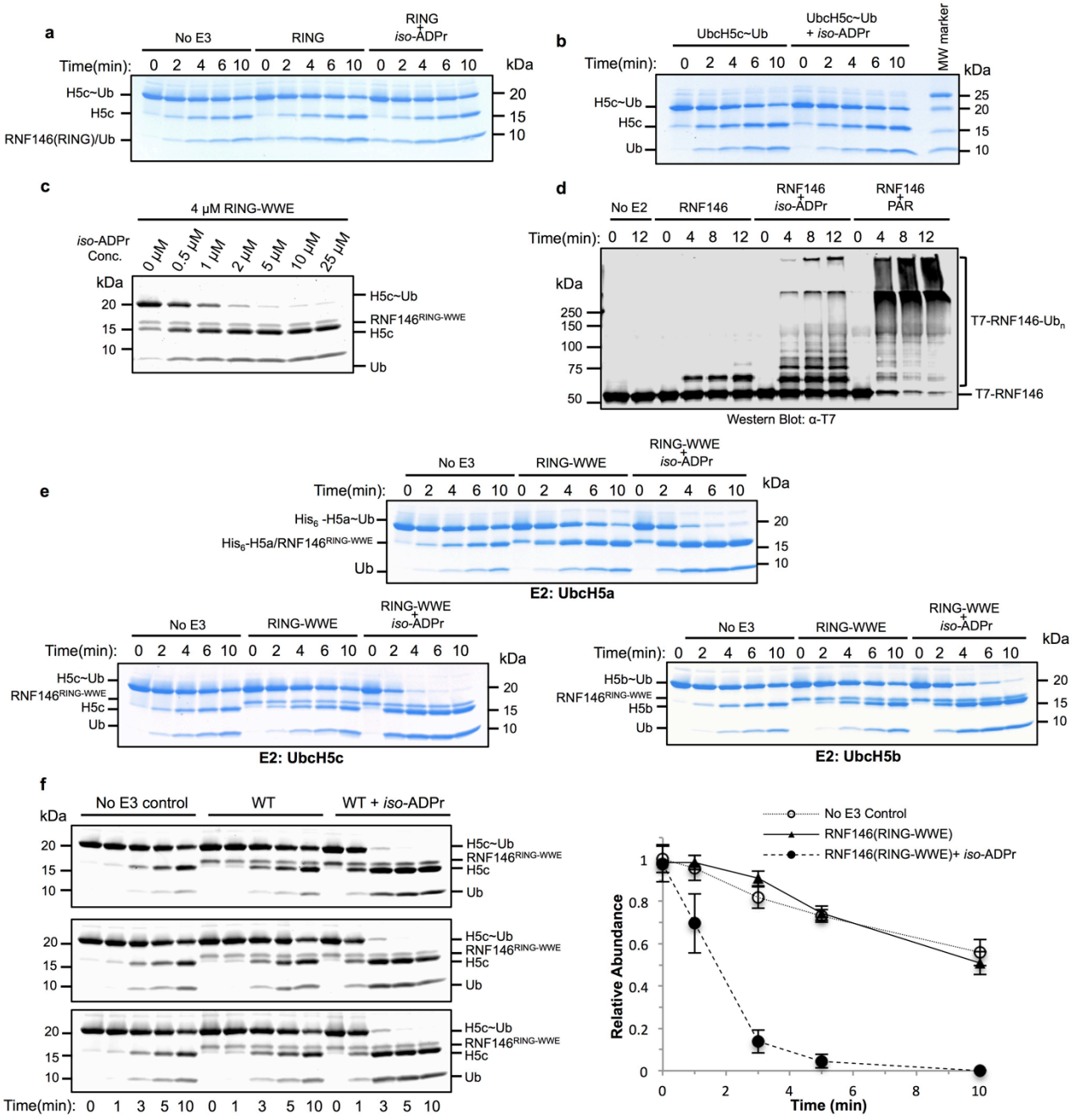

Extended Data Figure 2 | Both PAR and *iso*-ADPr can activate RNF146 E3 ligase activity. **a,** Coomassie-stained E2~Ub/lysine reactivity of the RNF146 RING domain with and without *iso*-ADPr. The RING domain does not enhance E2~Ub conjugate reactivity in the absence or presence of ligand. **b,** Intrinsic lysine reactivity of the UbcH5c~Ub conjugate with and without *iso*-ADPr. *iso*-ADPr does not enhance the reactivity of the conjugate in the absence of RNF146. **c,** Oriole-stained E2~Ub/lysine reactivity with increasing *iso*-ADPr (3 min after lysine addition). The rate of E2~Ub/lysine reactivity is increased as a function of [*iso*-ADPr] up to 5 μM ligand addition (1.2 equiv.), consistent with the affinity of RNF146 for *iso*-ADPr (see Extended Data Fig. 3). **d,** Auto-ubiquitination of full-length RNF146 in the absence or presence of *iso*-ADPr or PAR polymer. Image shows western blot for T7-tagged RNF146. Because full-length RNF146 and the RING-WWE fragment have similar abilities to enhance E2~Ub reactivity (see Figure 1), the additional auto-ubiquitination seen with PAR is likely due to increased local concentration of RNF146 near PAR polymers, allowing auto-ubiquitination in trans. **e,** E2/lysine reactivity of

UbcH5a, UbcH5b, and UbcH5c ubiquitin conjugates with RNF146(RING-WWE) in the absence or presence of *iso*-ADPr (Coomassie-stained). All three isoforms function with ligand-activated RNF146. **f,** Technical triplicates of RNF146(RING-WWE) E2~Ub/lysine reactivity assays (Oriole-stained; *left*) and a plot of relative densitometry values of the E2~Ub conjugate (*right*). Error bars indicate the mean +/- one standard deviation from three separate experiments. All times are given in minutes. "No E3" samples do not contain RNF146.

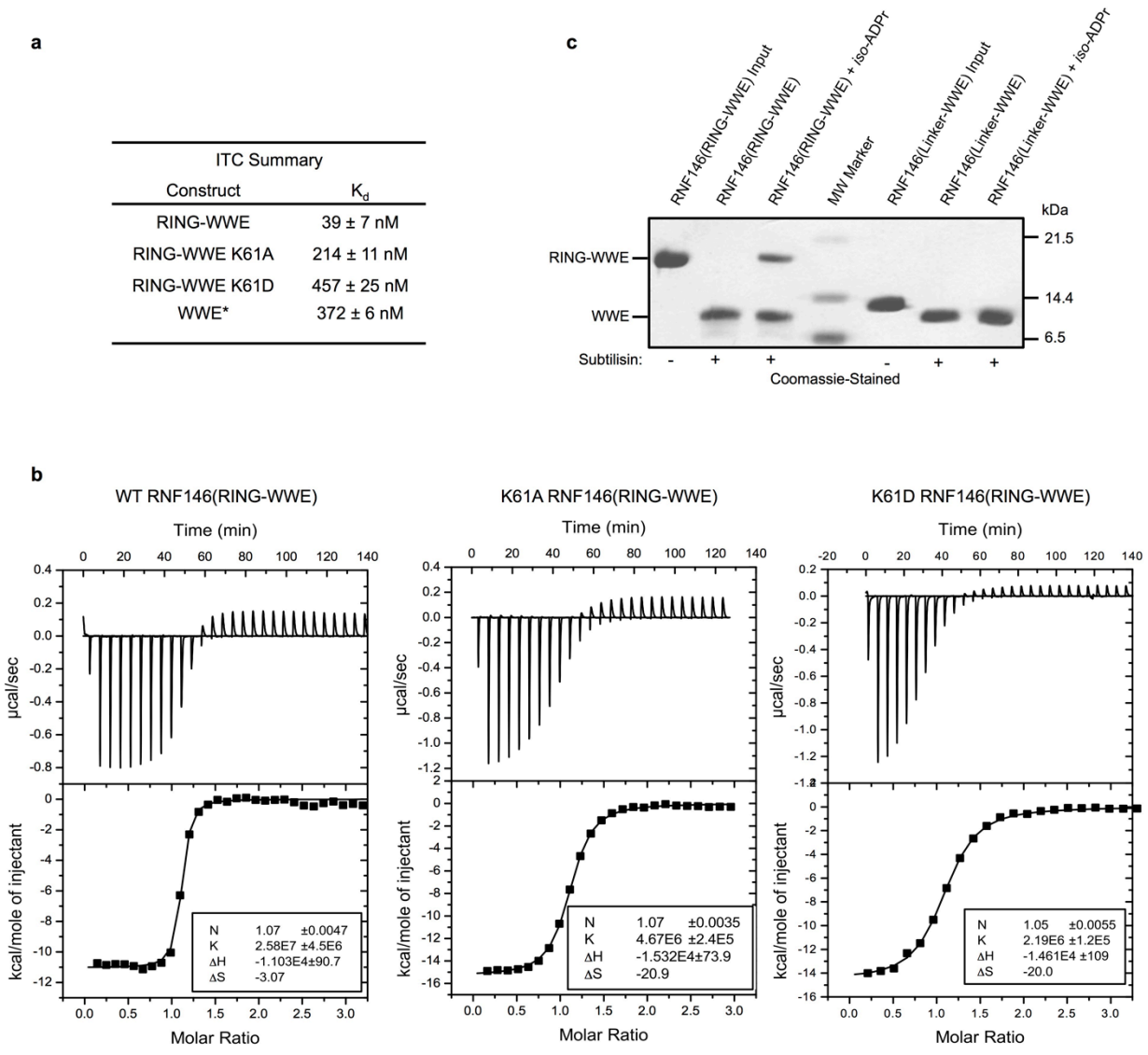

Extended Data Figure 3 | Both RNF146 RING and WWE domains contribute to *iso*-ADPr binding. a, Summary of *iso*-ADPr binding (K_d values) for RNF146(RING-WWE) obtained from the ITC titrations in the current work, and for the WWE-only fragment (previously published; indicated by asterisk)[13]. These data indicate that the RING domain contributes to *iso*-ADPr binding. **b,** Raw ITC titrations of RNF146(RING-WWE) fragments: (left to right) WT, K61A, and K61D. **c,** Limited proteolysis of RNF146(RING-WWE) and of a construct of RNF146 including the linker between the RING and WWE domains, and the WWE domain (RNF146(Linker-WWE); residues 83-183). Both appear to result in the same product when treated with subtilisin. The RING-WWE construct is more resistant to subtilisin in the presence of ligand.

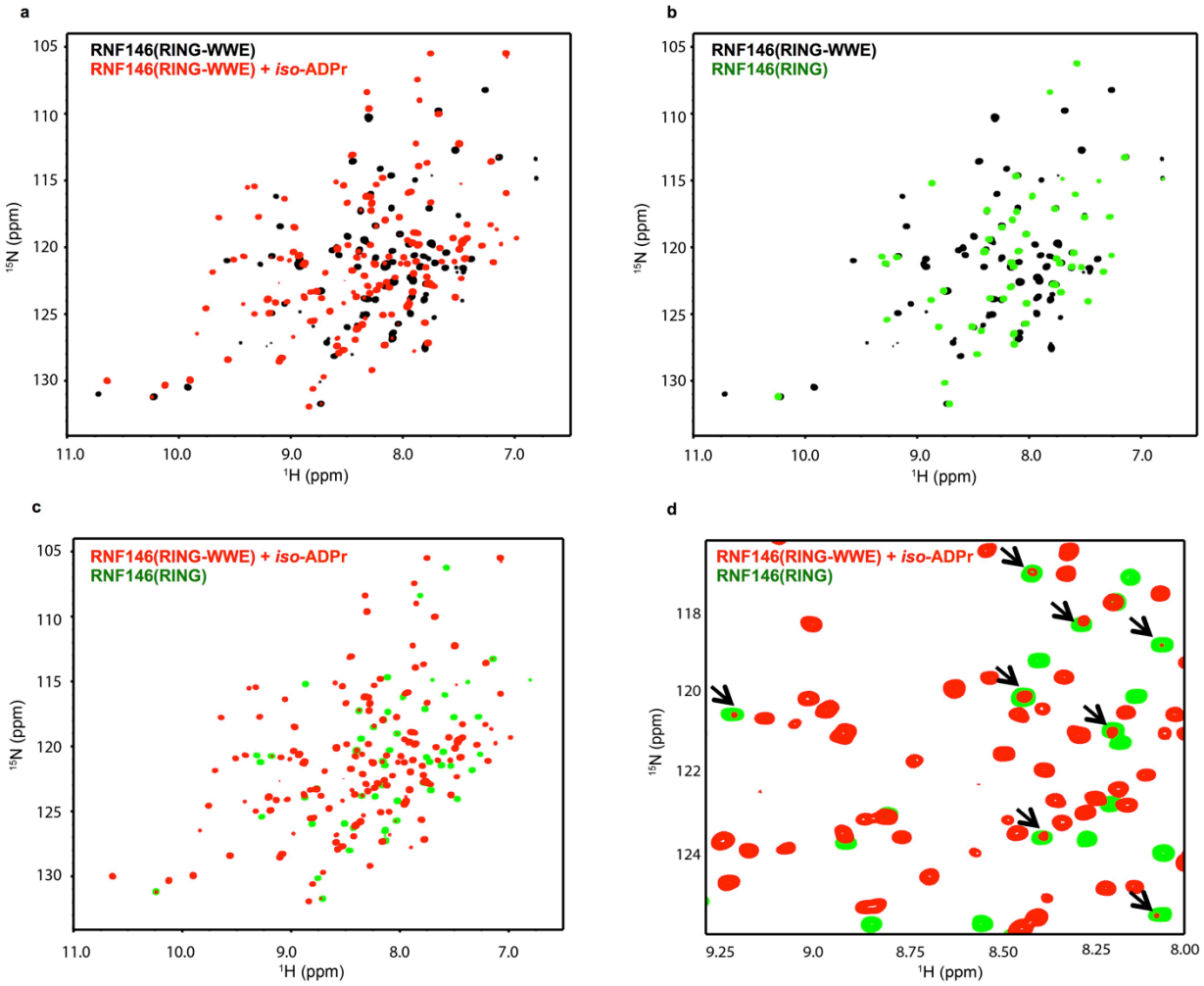

Extended Data Figure 4 | ^{1}H-^{15}N HSQC-TROSY spectra of RNF146 reveal a conformational change in the RING domain upon *iso*-ADPr binding. **a,** RNF146(RING-WWE) spectra in the absence (black) and presence (red) of saturating *iso*-ADPr concentrations show a dramatic change in a majority of amide chemical environments. **b,** Overlay of the RNF146(RING-WWE) spectrum (black) with the spectrum of the RNF146 RING-only domain (green) in the absence of *iso*-ADPr. Nearly all RING-only peaks overlay with a peak in the RING-WWE fragment spectrum, confirming that the RING-only domain adopts the same conformation as the RING domain in the larger fragment. **c,** Overlay of the liganded RING-WWE spectrum (red) with the isolated RING domain (green) shows very few corresponding peaks between the two spectra, indicating environment changes of most RING domain peaks in the presence of *iso*-ADPr consistent with a conformational change. Importantly, there are no changes in the spectrum of the RING-only construct when *iso*-ADPr is added under these conditions (data not shown). **d,** Close-up of panel c to illustrate that the RING domain samples a minor conformational state in liganded RNF146(RING-WWE). The minor peaks all correspond to RING peaks of unliganded RNF146 (black arrows). Therefore, the RING domain can still sample the non-activated conformation when saturated with ligand. Spectra were obtained with 200 µM protein and 300 µM *iso*-ADPr (saturating conditions).

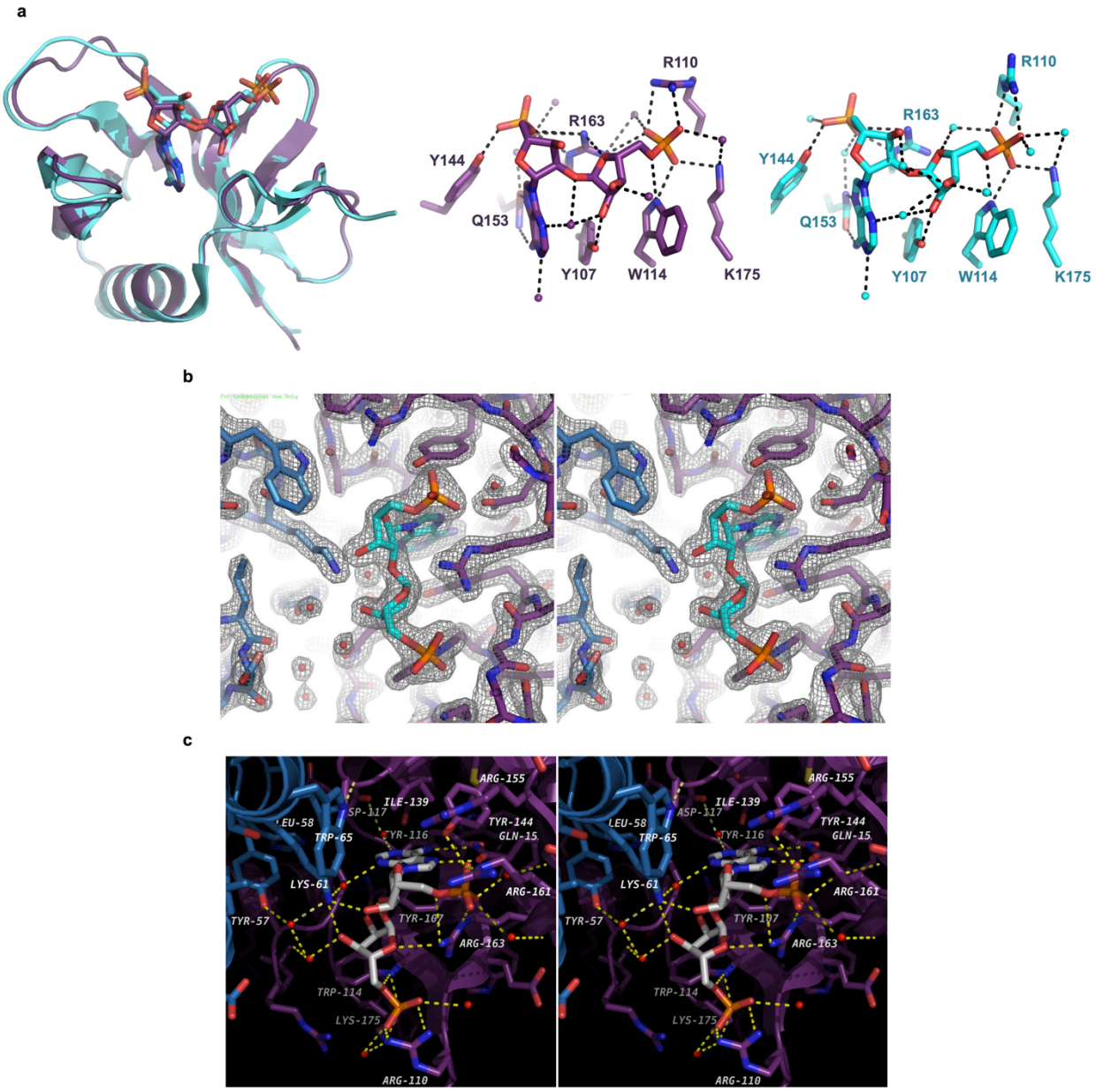

Extended Data Figure 5 | Comparison of ligand binding in the RNF146(RING-WWE)/UbcH5a/*iso*-ADPr complex and in the WWE-only structure. a, (*Top left*) Superposition of the WWE domain of the RNF146(RING-WWE)/UbcH5a/*iso*-ADPr complex (purple) and the previous *iso*-ADPr/WWE structure (cyan, PDB 3V3L)[13]. (*Top center*) WWE residues involved in binding *iso*-ADPr in the RNF146(RING-WWE)/UbcH5a/*iso*-ADPr complex (purple) and (*Top right*) in the previous *iso*-ADPr/WWE structure (cyan). Waters are shown as non-bonded spheres; hydrogen bonds are shown as dashed lines. Side-chain contacts between ligand and protein are maintained in both structures. **b,** Stereoview of the RNF146(RING-WWE)/UbcH5a/*iso*-ADPr complex ligand binding site showing the 2Fo-Fc map (grey mesh) contoured at 1.5 σ. The ligand and waters are well defined within the binding site. Waters are shown as red non-bonded spheres, *iso*-ADPr is shown in cyan, and the RING and WWE domains are colored as in Fig. 2a. **c,** Stereoview of the *iso*-ADPr binding site indicating residues within 4.5 Å of the ligand. Protein and ligand are represented as sticks, waters as red non-bonding spheres, and hydrogen bonds as dashed yellow lines. The RING and WWE domains and ligand are colored as in Fig. 2a.

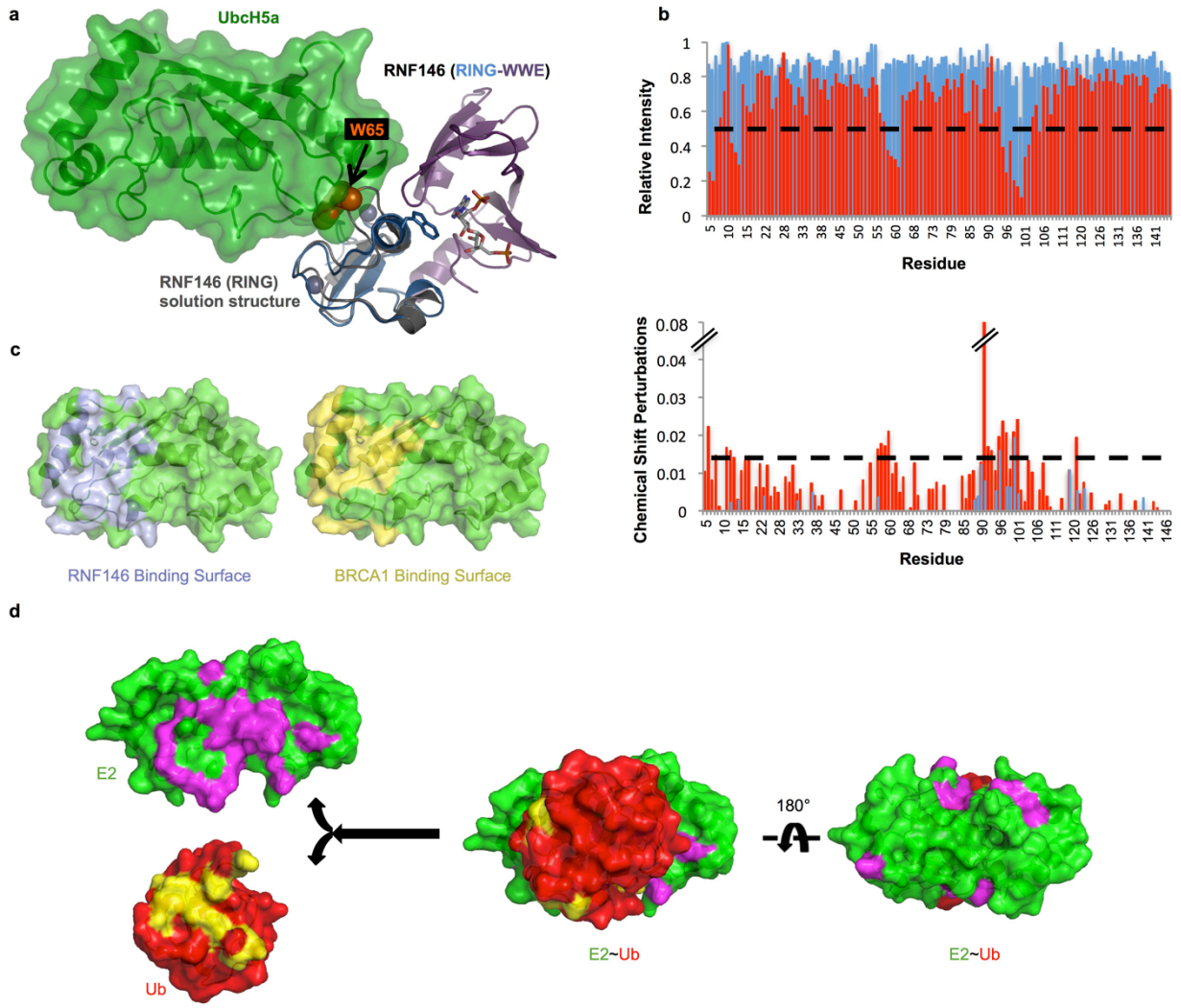

Extended Data Figure 6 | Rotation and crystal packing at the E2-E3 binding interface of the RNF146(RING-WWE)/UbcH5a/*iso*-ADPr complex. a, Superposition of the E2 in the RNF146(RING-WWE)/UbcH5a/*iso*-ADPr (colored as in Figure 2a) with a representative RING E3-E2 structure, the Bmi1/Ring1b-UbcH5c complex (grey) (PDB 3RPG)[18]. The WWE domain is excluded for clarity. Boxes show close-up views of the RING domains revealing a rotation of the RING domain relative to the E2. (*Bottom right*) RING domains rotated 90° to show the E2 binding surface of the E3s. The RING of the RNF146(RING-WWE)/UbcH5a/*iso*-ADPr structure is rotated relative to Ring1b-UbcH5c and other E3-E2 complexes[15-20,23] (indicated by red arrow) when the E2s are aligned. **b,** A close-up view of the E2-E3 interface of the RNF146(RING-WWE)/UbcH5a/*iso*-ADPr complex shows that RING residue R74 (yellow) is too far (~7.7 Å) from the E2 Q92 (magenta) carbonyl to make the hydrogen bond observed in activated E3-E2~Ub structures[17,21,22,24]. The side chain of R74 in the RING domain packs against F128 (orange), a WWE domain residue of a symmetry-related molecule in this crystal form. It is likely that crystal packing interferes with the formation of the "allosteric" hydrogen bond. **c,** E2~Ub/lysine reactivity with RNF146(RING-WWE)-R74A shows a dependence of RNF146 activity on the allosteric arginine[17,21,22,24] with or without ligand. Because RNF146 activation requires R74, which does not make contacts with the E2 in our structure, and because RNF146 shows canonical E2 binding in solution (see Extended Data Fig. 7), we conclude that the orientation of RNF146 in the RNF146(RING-WWE)/UbcH5a/*iso*-ADPr complex is likely an unproductive E2-E3 association. The observed rotation is likely a crystallographic artifact.

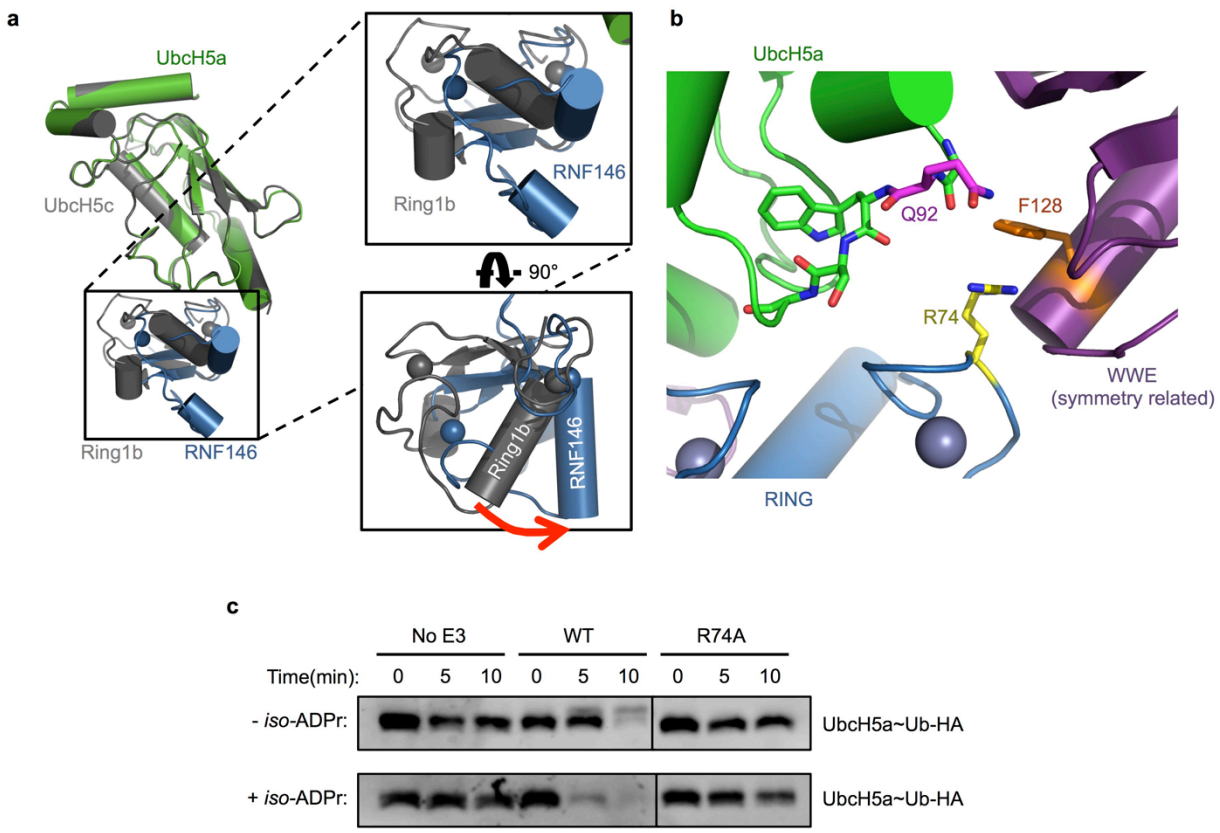

Extended Data Figure 7 | RNF146/*iso*-ADPr binding allows the RING domain to bind and activate a ubiquitin conjugating enzyme (E2). a, (*Left*) Superposition of the RING domain of unliganded RNF146 (PDB 2D8T; grey, Trp 65 is shown as orange spheres) with the RNF146(RING-WWE)/UbcH5a/*iso*-ADPr complex (colored as in Fig 2a), shows a clash of Trp 65 with UbcH5a at the E2-E3 binding interface. This clash is observed when the RNF146 RING structure (2D8T) is aligned with all other E2-E3 structures[15-20,23]. **b,** Peak broadening (*Top*; intensity relative to free E2) and chemical shift perturbations (CSPs; *bottom*) of ^{15}N-UbcH5c(S22R/C85S) resonances (data are from the spectra shown in Figure 3b). Histograms shown in blue compare the spectral properties of free E2 to E2 plus RNF146(RING-WWE); histograms shown in red compare free E2 to E2 plus RNF146(RING-WWE) and *iso*-ADPr. Dashed lines indicate one standard deviation from the mean value of the liganded (red) plots. Values below and above the dashed lines for the relative intensities and CSPs respectively are plotted on the E2 surface shown in panel c and Figure 3b. **c,** (*Left*) The RNF146(RING-WWE) binding surface inferred from data in panel b (light blue, on green E2), is compared with (*right*) the BRCA1/BARD1 binding surface on E2 (yellow, on green E2; residues 1-112 and residues 26-115, respectively) previously inferred by an analogous experiment[25]. When the NMR perturbations are mapped to the surface of UbcH5c, the revealed binding sites are very similar, and are consistent with previously reported binding surfaces for RING E3s on free ubiquitin conjugating enzymes[15-20,23]. **d,** Chemical shift perturbations and broadening of resonances from ^{15}N-E2~Ub conjugate (UbcH5c(S22R/C85S)-O-Ub) upon RNF146(RING-WWE)/*iso*-ADPr binding (determined by the same method as shown in panel b, but with only 0.125 mol. equiv. E3 added to minimize hydrolysis of the E2~Ub oxyester during NMR data collection). (*Left*) Perturbed residues are mapped onto UbcH5b (magenta on green E2) and ubiquitin (yellow on red ubiquitin). (*Center and right*) Perturbed residues mapped onto the structure of E2~Ub as it appears in the E3/E2~Ub complex of BIRC7/UbcH5b-Ub (PDB 4AUQ; BIRC7 not shown for clarity)[24] show that the surfaces highlighted in the left panel are buried in the "closed" state. The data show that RNF146 activates the E2~Ub conjugate by inducing the closed conformation[17,21,22,24]. Because only the most perturbed residues are mapped to the E2~Ub surface, the E3 binding surface is not highlighted on the E2 in panel d.

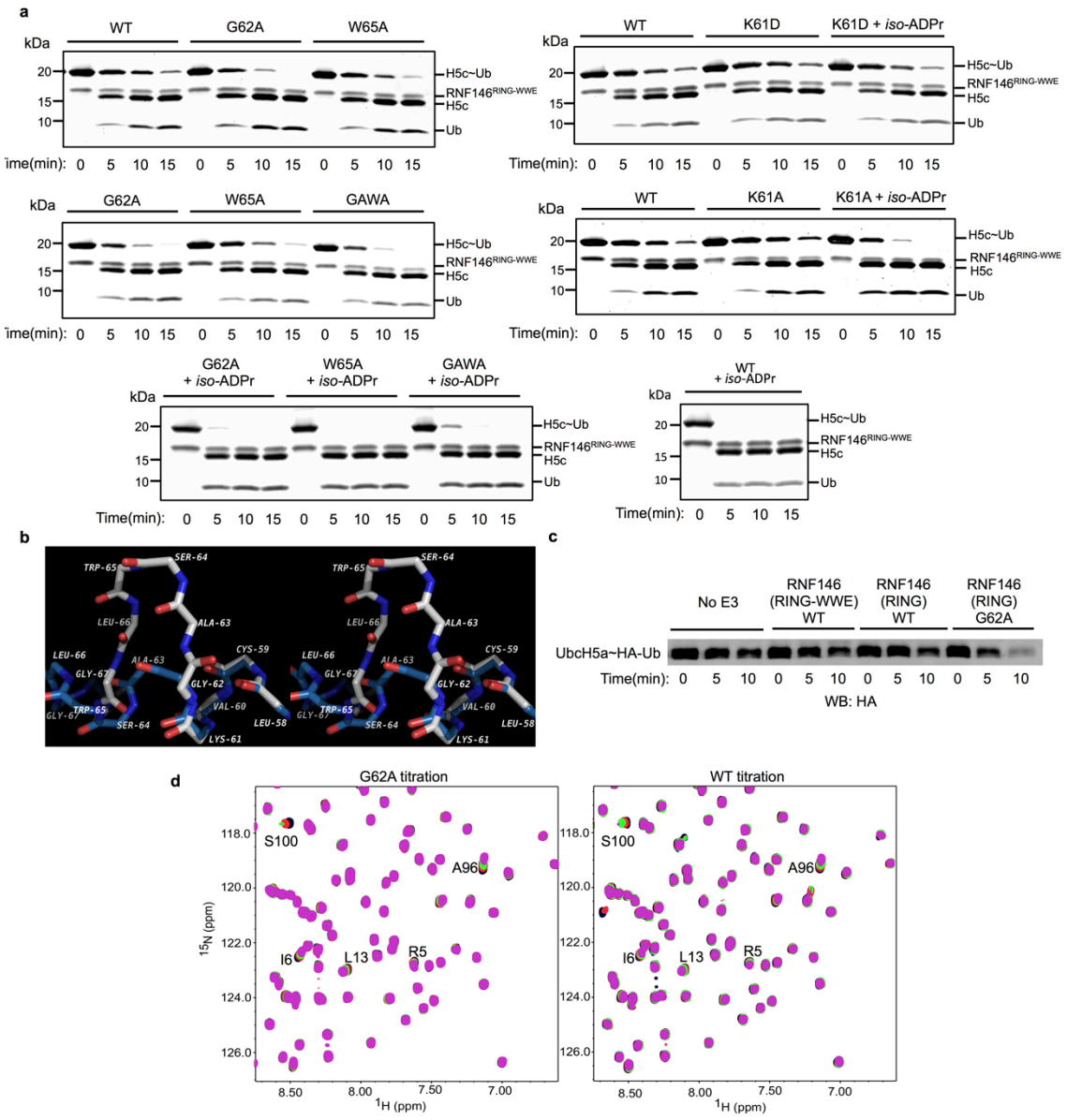

Extended Data Figure 8 | Stabilizing Helix 1 of RNF146 activates the RING domain. **a,** Complete images of gels shown in Figure 3c (Oriole-stained) for G62A, W65A, G62A/W65A (GAWA), K61A and K61D mutants of RNF146(RING-WWE) with and without *iso*-ADPr. G62A and GAWA mutants show reduced enhancement with *iso*-ADPr relative to wild type, likely due to a clash of the Ala side chain with a turn in the WWE domain at position 62 (data not shown). **b,** Alignment of RNF146(RING) solution structure (PDB 2D8T; white) and the crystal structure determined in this study (blue) shown in stereoview. Side chains are excluded for clarity; the backbone is represented by sticks. Comparison of the conformation of Gly 62 in the two structures suggests a need for a small side chain at position 62 to allow the structural transition from the inactive to active form of RNF146. **c,** Anti-HA western blot of the E2~Ub/lysine reactivity assay of RNF146(RING-WWE) compared with RNF146(RING) and RNF146(RING)-G62A showing enhanced reactivity for the G to A mutation. **d,** (*Left*) ^{1}H-^{15}N HSQC TROSY of ^{15}N-UbcH5c(S22R/C85S) in the presence of 0.0 (black), 0.25 (red), 0.5 (green), and 1.0 (magenta) mol. equiv. of RNF146(RING) G62A. (*Right*) The same experiment performed with WT RNF146(RING). The most perturbed residues, indicated by letter and position (S100, etc.), show increased chemical shift perturbations for the RNF146(RING)-G62A mutant.

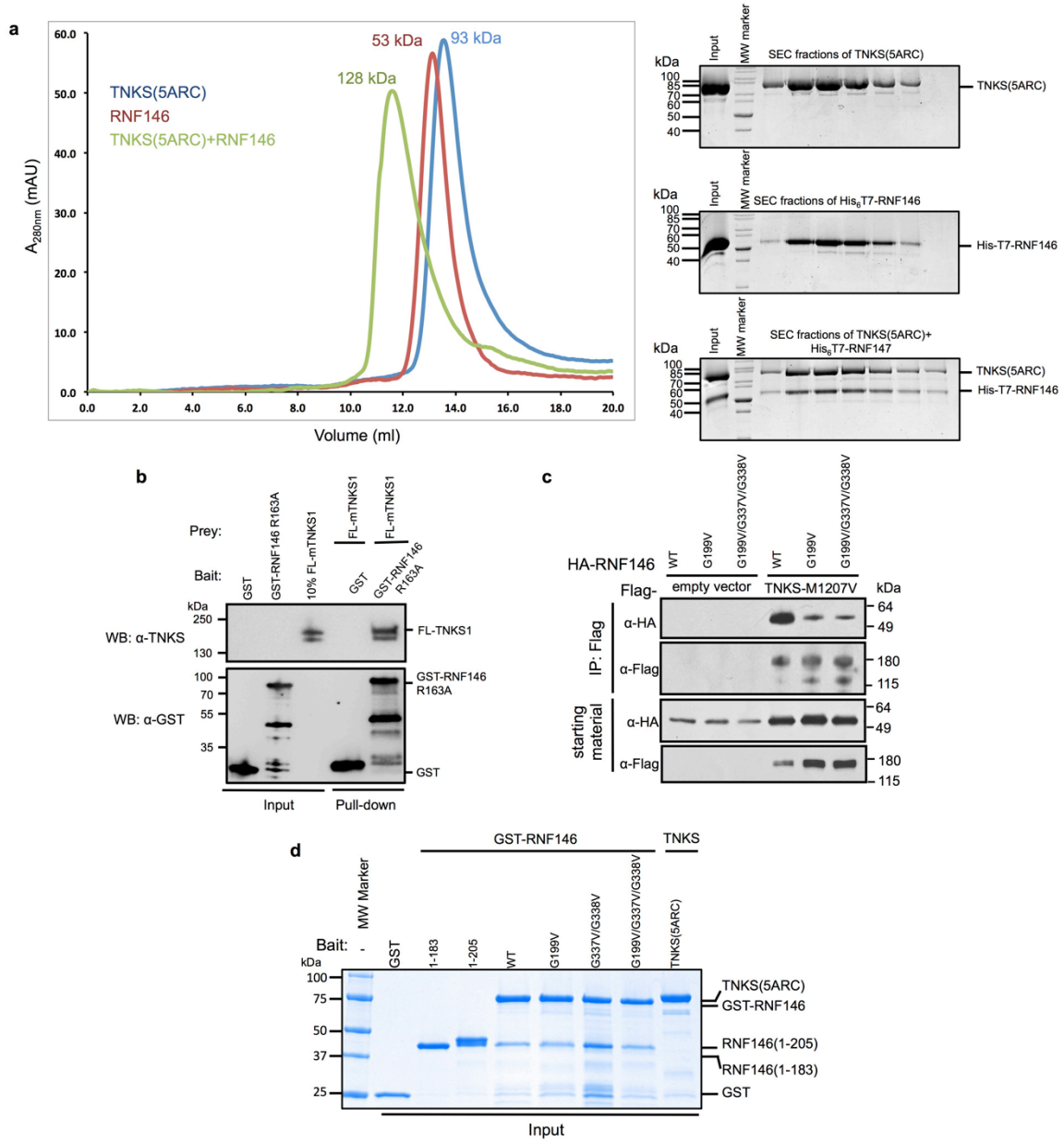

Extended Data Figure 9 | RNF146 directly interacts with TNKS. a, (*Left*) SEC profiles of untagged TNKS(5ARC) (blue), His_6T7-RNF146 (red), and a 1:1 mixture of these proteins (green). Numbers above the peaks indicate the average mass obtained by multi-angle static light scattering (MALS) for each peak. His_6T7-RNF146 and TNKS(5ARC) co-migrate as a single peak with an apparent mass of 128 kDa. (*Right*) Coomassie-stained SDS-PAGE analysis of the SEC peaks in left panel show the presence of both proteins within the peak of the TNKS(5ARC)/His_6T7-RNF146 complex (*Bottom right*). **b,** GST pull-down of partially purified full-length mouse tankyrase-1 (FL-mTNKS1) with GST tagged RNF146-R163A (PAR-binding deficient RNF146 mutant)[11]. Full-length mTNKS1 can be pulled down by GST-RNF146, but not GST. **c,** Co-immunoprecipitation of HA-RNF146 variants with transiently transfected flag-tagged TNKS-M1207V (catalytically inactive mutant). The M1207V mutation prevents auto-PARylation of TNKS and therefore PAR-mediated interactions between RNF146 and TNKS[38]. Under the experimental conditions, both the motif I mutant, G199V, and the motifs I+IV mutant, G199V/G337V/G338V, significantly reduce the RNF146-TNKS interaction. **d,** Coomassie-stained SDS-PAGE of proteins used in the GST pull-down assay shown in Figure 4a (inputs). Samples were used in a 1:2 ratio (3 μM GST-RNF146 to 6.7 μM TNKS(5ARC)) for these GST pull-down experiments.

Extended Data Table 1 Data collection, phasing and refinement statistics

	RNF146(RING-WWE)/UbcH5a/*iso*-ADPr complex **Zn^{2+} SAD**
Data collection	
Space group	$P2_12_12$
Cell dimensions	
a, *b*, *c* (Å)	133.67, 61.69, 94.35
α, β, γ (°)	90, 90, 90
Resolution (Å)	50.0 - 1.90 (1.96 - 1.90)*
R_{sym}(%)	9.2 (45.9)*
$I/\sigma I$	34.4 (2.5)*
Completeness (%)	95.6 (71.4)*
Redundancy	7.8 (4.6)*
Refinement	
Resolution (Å)	50.0 - 1.90
No. reflections (test set)	55779 (2994)
R_{work}/ R_{free}	18.6 / 22.2
No. atoms	
Protein	4886
Ligand	72
Zn^{2+}	4
Water	371
B-factors	
Protein	16.3
Ligand	31.0
Zn^{2+}	31.5
Water	42.4
R.m.s deviations	
Bond lengths (Å)	0.009
Bond angles (°)	1.4

This diffraction dataset was collected from a single crystal.
5% randomly selected reflections were used as a test set.
*Highest resolution shell is shown in parenthesis.

CHAPTER 3

Structural basis for tankyrase-RNF146 interaction reveals extended tankyrase-binding motifs

Paul A. DaRosa[1], Rachel E. Klevit[1], and Wenqing Xu[2]

[1] Department of Biochemistry, University of Washington, Seattle, WA 98195
[2] Department of Biological Structure, University of Washington, Seattle, WA 98195

Note on Chapter 3: The following manuscript is an early draft. The content and material presented herein may change substantially prior to publication.

Abstract

Poly(ADP-ribosyl)ation (PARylation) catalyzed by the tankyrase enzymes (Tankyrase-1/2; referred to either as TNKSs or simply tankyrase) is involved in mitosis, telomere length regulation, GLUT-4 vesicle transport, and cell growth and differentiation. Together with the E3 ubiquitin ligase RNF146 (a.k.a. Iduna), tankyrases regulate the cellular concentrations of several important proteins including Axin, 3BP2, and the angiomotin proteins. These substrates of tankyrases are first PARylated then ubiquitylated by RNF146, which is allosterically activated by binding to the PAR polymer. Each tankyrase substrate is recognized by a tankyrase-binding motif (TBM). Here we show that RNF146 binds directly to tankyrases through at least four motifs in its C-terminus, which may bind to four different ankyrin repeat cluster (ARC) subdomains in the tankyrase substrate-binding domain. Three of these RNF146 motifs represent novel, extended TBMs one additional amino acid in length. Individually the motifs in RNF146 display weak binding, but together mediate a strong multivalent interaction with the substrate-binding region of TNKS, forming a tight one-to-one complex. A crystal structure of the first RNF146 noncanonical TBM in complex with the second ARC of TNKS shows how an extended motif can be accommodated in a peptide-binding groove on tankyrases. Therefore, this structure

confirms the existence of a new class of extended TBMs that could exist in other tankyrase-binding proteins.

Introduction

Tankyrase-1/2 constitute two of the six members of the human poly(ADP-ribose) polymerase (PARP) enzymes. The PARP family of proteins generate the post-translational modification poly(ADP-ribose) (PAR), a large negatively charged polymer with widespread cellular significance for cellular functions. Protein PARylation has implications in a myriad of processes including, DNA damage repair, cell death,[1] cell division,[2–5] and vesicle translocation.[6,7] The tankryases (TNKSs) have a particularly important role in cell growth, division, and differentiation.[8–17] As regulators of multiple signal transduction pathways including Wnt, SRC, and Hippo signaling, tankyrases are important drug targets for cancer therapies.[18–20]

When compared with other PARP enzymes the TNKS proteins have a unique domain composition (Figure 1A) containing a PARP catalytic domain at the far C-terminus closely coupled to a SAM domain responsible for TNKSs polymerization.[21–26] After a histidine, serine, proline rich segment at the N-terminus (a region lacking in tankyrase-2), TNKSs contain a large ankyrin repeat domain composed of five conserved subdomains or ankyrin repeat clusters (ARCs) connected by conserved linkers. With the exception of ARC3, each ARC recognizes a tankyrase-binding motif (TBM) in a highly conserved binding groove (Supplemental Figure S1) having the form RXXΦDG where X is any amino acid, and Φ is a small hydrophobic. However, considerable sequence variability is allowed at each position except the conserved Arg and Gly.[27] All tankyrase substrates to date contain one or more TBMs. Hence, it is likely that peptides can

be utilized to block substrate binding to TNKSs as a means of a highly specific TNKS inhibition.[28]

There have been a number of reports that TNKSs can regulate the cellular concentrations of several proteins including TRF1,[11,12] 3BP2,[8,27] Axin-1/2,[9] BLF1, CASC3,[10,29] CPAP,[4] PTEN,[16] and most recently the angiomotin (AMOT) family of proteins[13,14,17] in a PARylation dependent manor. The PARylated forms of BLF1, CASC3, and the disease related proteins PTEN, Axin, 3BP2, and the angiomotins are confirmed substrates of RNF146 (Figure 1B), which targets these proteins for degradation by conjugation with ubiquitin chains.[8–10,13,14,16,17]

Protein ubiquitination is a post-translational modification involved in all cellular processes. In the ubiquitin (Ub) cascade, a ubiquitin activating enzyme (E1) activates and transfers Ub to a Ub conjugating enzyme (E2), creating a thioester linkage between C-terminal glycine of Ub and the active site cysteine of the E2, forming an E2~Ub conjugate. This cascade is completed when a Ub ligase (E3) mediates the transfer of Ub to a lysine residue of a substrate or a growing Ub chain. RING E3s, the largest class of E3 ligases, catalyze the direct transfer of Ub from the E2~Ub conjugate to substrate. Classically E3s are responsible for targeting substrate via protein-protein interactions with the substrate directly. However, RNF146 does not contain any known substrate recognition domains (Figure 1B).

RNF146 was previously shown to bind the internal structural unit of the PAR polymer (known as *iso*-ADPr) via its WWE domain and RING domains.[30,31] The PAR ligand acts as an allosteric activator of the E3 ligase through a conformational change in the RING domain.[31] Hence, PAR acts as a signal for RNF146 activation. It was also observed that RNF146 binds to tankyrase via its C-terminal region and that this association is required for Axin turnover.[31] Thus the C-terminus of RNF146 may dictate substrate specificity or localize RNF146 with substrates

through its interaction with TNKSs, allowing the E3 to target proteins PARylated by TNKSs but not other PARPs. However, the specifics of the RNF146-tankyrase interaction have not yet been investigated.

Here we show that the C-terminal fragment of RNF146 can form a one to one complex with the complete ankyrin repeat region of tankyrase and that at least four motifs in RNF146 mediate this interaction. Three of these motifs in RNF146 are non-canonical, including a one-residue extension in the previously defined binding sequence. We report the crystal structure of a non-canonical tankyrase-binding motif of RNF146 with ARC2 of mouse tankyrase-1. This structure reveals a binding mode similar to those of previous reported TBM-Tankyrase interactions, but shows how an extended motif can be accommodated on the tankyrase scaffold, expanding the possible list of tankyrase substrates and interacting partners.

Results and Conclusions

RNF146 binds to tankyrases via its flexible C-terminal tail

RNF146 contains two characterized domains at its N-terminus, a RING domain and a WWE domain that comprise the protein's ubiquitin E3 ligase activity and PAR binding function, respectively. The C-terminal region of RNF146, however, is predicted to be intrinsically disordered (data not shown). Consistent with these predictions, NMR spectroscopy (^{1}H-^{15}N HSQC) shows a lack of 1H dispersion typical of disordered proteins (Supplemental Figure S2A).

RNF146 has been reported to interact with tankyrase-1 (referred to as tankyrase or TNKS here forth) via its flexible C-terminus downstream of its WWE PAR-binding domain (see Figure 1B).[31] When this region was removed no interaction with tankyrase was observed.[31] In agreement with this previous study we observe that a C-terminal fragment of RNF146 is

necessary for its interaction with the substrate binding region of tankyrase-1 (TNKS(5ARC)) via GST pull-down assays (Figure 2A). While GST-tagged RNF146 can pull-down TNKS(5ARC), a construct of RNF146 lacking the C-terminus, RNF146(ΔC-term) (residues 1-183), cannot (Figure 2A, lane 2 versus 1). Furthermore, the C-terminus of RNF146 (residues 184-358; RNF146(ΔN-term)) appears to be sufficient for the RNF146-tankyrase interactions (Figure 2A, Lane 7) despite lacking a folded protein structure. Indeed, the ΔN-term fragment of RNF146 retains tight binding with tankyrase as indicated by their co-elution on a size exclusion column in a one-to-one complex (Figure 2B). Therefore, the flexible C-terminal region of RNF146 is necessary and sufficient for its interaction with TNKS.

The RNF146-TNKS interaction is mediated by at least 4 motifs in the RNF146 C-terminus

Tankyrases recognize proteins via their ARC domains in the ankyrin repeat region where ARCS1, 2, 4, and 5 all contain a conserved peptide binding grooves that recognize a tankyrase-binding motif (TBM) (see Figure 1A and Supplemental Figure S1).[21] Canonical TBMs follow the form RXXΦDG where X is any amino acid, and Φ is small hydrophobic residue such as Ala, Pro, and Gly. However, only the Arg and Gly of this motif are strictly invariant positions.[27] It was previously proposed that RNF146 has five similar motifs in its disordered C-terminus that closely resemble other canonical tankyrase motifs (Figure 1C; Supplemental Figure S2B).[31] However, with the exception of motif 4 (RSVAGG), all of the TNKS binding motifs are one or two residues longer than previously identified TNKS binding sequences. Importantly, a mutation in motif 1, has a larger effect on tankyrase binding than motif 4, which matches the TBM consensus motif more closely.[31] However, previously only two of these motifs in RNF146 were tested, showing that motif 1 and 4 are important for the RNF146-Tankyrase interaction and that mutation of these motifs together attenuates Axin turnover in cells.[31] We therefore tested the

remaining motifs using GST pull-down assays in which the obligate Gly in each motif is mutated to a Val residue. In agreement with a previous report, motif 1 contributes to full-length RNF146 binding to TNKS(5ARC) as evident by a reduction in tankyrase-1 (TNKS1) binding upon mutation of motif 1 (Figure 2A, lane 3). Surprisingly, mutants in motifs 3 and 5 show that both of these additional motifs contribute to the interaction of RNF146 with TNKS1 (Figure 2A, lanes 3, 5, and 6), though motif 1 mutant reproducibly showed a stronger effect on binding. In contrast, mutation of motif 2 does not appear to affect the interaction of RNF146 with TNKS1 significantly (Figure 2A, lane 4). Hence, four of the five putative TBMs in RNF146 contribute to the RNF146-TNKS interaction despite the apparent one-residue insertion in three of the RNF146 TBMs not previously characterized in tankyrase binders.

RNF146 exhibits multivalent binding to tankyrases

The retention of binding upon mutation of specific motifs suggests a multivalent binding of RNF146 to the ankyrin repeats of TNKSs in which a number of motifs in RNF146 bind to one or more ARCs in tankyrases. To determine if RNF146 can interact with multiple tankyrase ARCs we also performed pull-down experiments with individual ARC domains in TNKS1 and the C-terminus of RNF146. Indeed, RNF146 can interact with at least 3 of the four individual ARC domains (Figure 2C). ARC1 displays weak binding to RNF146 as indicated by a lack of a GST pull-down of the RNF146 C-terminus (Figure 2C). Lower affinities for ARC1 of canonical TBMs are due in part to a lack of a hydrogen-binding moiety at the glycine gate where tyrosine/phenylalanine residues on TNKSs sandwich the conserved Gly of the TBM. A tyrosine at this position can be a hydrogen bond donor to a backbone carbonyl of the TBM.[27,32,33] However, ARC1 lacks this Tyr. Instead, ARC1 has a Phe in its place, which cannot hydrogen bond with the TBM (See Supplemental Figure S1).

To test weather RNF146 requires multiple interactions at once we performed GST pull-down assays in the presence of a competitive inhibitor that is known to simultaneously bind two sites of TNKSs, Axin(1-80) (Axin, residues 1-80)[32,33] and SEC in the presence of a large excess of RNF146. When Axin(1-80) is added as a competitor in GST pull-down assays RNF146 was easily competed off by a one-to-one equivalence of Axin:TNKS1 (Supplemental Figure S3A). Indicating that competition with at most two of the TNKS sites disrupts RNF146 binding significantly. Furthermore, when RNF146(ΔN-term) is added in a large (6 fold) excess of RNF146 in size exclusion chromatography, RNF146 still forms a one-to-one complex with TNKS1 (Supplemental Figure S3B). These data establish that RNF146 has multiple binding motifs that are capable of binding to multiple binding sites on tankyrases, most of which do not match the TBM consensus sequence.[27] Together and in combination with the relatively low affinity of a single TBM-ARC interaction observed (see below), these data show multivalency in the RNF146-TNKSs interaction that may be disrupted easily by a TNKS substrate such as Axin. Whether TNKS substrates can displace RNF146, or if they can both weakly associate simultaneously to the ankyrin repeat region of TNKSs *in vivo* requires further investigation.

RNF146 motif 1 can bind to tankyrase-1 similarly to canonical TBMs

Because motif 1 appears to have the largest impact on TNKS binding,[31] and because RNF146 displays binding characteristics that appear to be consistent with previously characterized canonical TBMs, we decided to explore the possibility that RNF146 motif 1 can bind to a single ARC of TNKS, despite not conforming to the canonical RXXΦDG sequence (instead containing an insertion of an additional amino acid between the key R and G residues). GST-RNF146(motif1) can pull-down a fragment of TNKS1 including ARC2 and 3 (TNKS(ARC2-3); Figure 3A). Furthermore, ITC analysis shows that the binding affinity of this

interaction is ~6 uM (Figure 2B), demonstrating that this extended TBM has an affinity similar to canonical TBMs (in the range of 0.3-20).[27,32–34] Notably, the low affinity observed for this isolated motif 1-TNKS1 interaction supports the hypothesis that RNF146 uses multiple motifs to bind tankyrases simultaneously, because the full C-terminus and TNKS(5ARC) region forms a tight 1:1 complex by SEC (Figure 2B) indicated much tighter binding when all binding sites are available. To structurally characterize the non-canonical motif 1-ARC2 binding site, we determined a crystal structure at 1.93 Å resolution of RNF146(motif 1) (residues 184-205) in complex with TNKS(ARC2-3) (residues 308-655) (Table1).

The overall architecture of the TNKS1-RNF146 complex is similar to other structures solved of TBMs bound to ARC2;[32,34] two molecules of ARC2-3 reside in the asymmetric unit forming cross pattern with a pseudo two-fold axis of symmetry resulting from an ankyrin repeat swap following the ARC2/3 helical linker (Figure 4A). One copy of the RNF146(motif1) peptide is bound to each ARC2 module with clear electron density (Figure 4 and Supplemental Figure S4A). When the two sites are compared in the asymmetric unit, the two peptides have a very similar backbone conformation (Supplemental Figure S4B). The extra residue within the RNF146 TBM is accommodated by the ARC2 binding site by diverting a three residue segment of the main chain away from the canonical TBM trajectory (Figure 4B and C). In brief, R193 of RNF146 falls into the “arginine cradle” where hydrophobic interactions with the aliphatic chain of arginine are supplied by Trp-427, and a Phe-427 interacts with the guanadinium head group via pi stacking. Glu-438 supplies a complementary charge-charge interaction with R193 at the base of the arginine cradle. The “aromatic glycine sandwich” is also maintained in this non-canonical RNF146-TNKS interaction in which Try-372 and Try-405 form a “gate” in which only a glycine can be accommodated.[27] The central region of RNF146(motif1) makes a number of

Van der Waals interactions and hydrogen bonds, including the aforementioned Tyr-carbonyl hydrogen bond previously observed (which may explain the lower binding affinity to ARC1).[27,32,34] Here, this hydrogen bond is exemplified by the interaction of TNKS1 Tyr-405 and the backbone carbonyl of RNF146(motif 1) Ala-197 (see Figure 3B, center panel). Interestingly, the length of the RNF146 TBM is accommodated within this central region. Relatively poor side-chain density for the Ser-195 likely indicates that this side-chain can be flexible (Supplemental Figure 4SC); there do not appear to be any protein-protein interactions at this position. The Ser-196 side-chain hydroxyl and Ala-197 main-chain carbonyl groups form a bifurcated hydrogen-bond with the Try-405 side-chain and may contribute to the interaction of RNF146(motif 1) with TNKSs. In addition, RNF146 Glu-194 forms salt bridges with TNKS1 Arg-361 and Lys-393.

When compared with canonical-TBM interactions the placement of the most conserved residues in the TBM (i.e. the obligate arginine at the N-terminus and the last four residues including the ΦDG motif) are nearly identical (Figure 4C). Therefore, the RNF146(motif1)-TNKS interaction behaves much like a canonical TBM, where the sequence rules previously established must still apply to the conserved arginine and the downstream ΦDG. Importantly, modeling suggests that the remaining two non-canonical TBMs seen in RNF146 (motif 3 and 5) can easily be spatially accommodated in this binding mode. However, the specific interactions of residues within these motifs with the TNKSs binding sites are likely to be accommodated differently, as the residues between the conserved Gly and Arg of motif 1 are not necessarily conserved for motifs 3 and 5 (see Figure 1C). Still, these data open the possibility that extended TNKS binding motifs may exist in other proteins.

Discussion

The RNF146-TNKS interaction was previously shown to be important for Axin turnover *in vivo*.[31] This study expands the complexity of this unique interaction. First, this study presents a new type of TBM that is extended by one amino acid. The sequence variation in TBMs has previously been well studied.[27] However, these studies have focused entirely on consensus sequences with a length of 4 amino acids between the conserved arginine and glycine (i.e. RXXΦDG). Here we have shown the accommodation of an extra amino acid in this motif, giving the form RXXXΦDG. This could considerably increase the number of predicted TBMs in the proteome. Indeed, we searched a list of experimentally determined tankyrase interacting proteins previously published[16] for proteins that contain similar extended motifs in predicted disordered regions of these proteins. The search results returned more than 350 putative TBM motifs, including 150 extended motifs. While most proteins containing extended TBMs also contain canonical TBMs (similarly to RNF146), there are a number of proteins that only contain an extended binding motif that may bind to TNKS including Fbox-only protein 50, Desmin, Negative elongation factor E, and Eukaryotic initiation factor 4A-I (Supplemental Table S1).

The question of the true tertiary structure of the RNF146-TNKS interaction is further confounded by the presence of an oligomerization domain in TNKS, known as the SAM domain. Recently it was shown that the SAM domain in TNKS can form long, helical, head-to-tail oligomers[24–26] with their N and C-termini facing away from the helical center. Hence, many TNKS ankyrin repeats will presumably be in very close proximity within larger TNKS scaffolds. Still, the one-to-one TNKS-RNF146 complex may suggest that RNF146 binds in a specific orientation that allows for substrate PARylation and subsequent ubiquitylation. It was recently shown that Axin can remodel the conformation of the TNKS(5ARC) region when it binds due to

flexibility of the linkage between ARC3 and ARC4.[33] RNF146 may have a similar effect on the TNKS(5ARC) region, which could have direct implications on the access of RNF146 or substrates to the PARP active site. It is worth nothing that, while our crystal structure shows that the ARC2-3 fragment is present as a repeat swapped dimer similarly to previous TNKS(ARC2-3),[32,34] in larger TNKS fragments such as 5ARC we do not see dimerization in either the free TNKS(5ARC) or bound to RNF146 (Figure 2B). Hence the dimerization may be a crystallographic artifact. Consistent with this we also do not observe dimerization of TNKS(5ARC) with Axin(1-80) (data not shown) despite ARC2-3 fragment forming a dimer in the presence of Axin(1-80).[32] Although this lack of dimerization of the TNKS(5ARC) fragment is also noted in another study,[33] we could not rule out the possibility that within the larger tankyrase scaffolds such a dimerization may exist.

Figures:

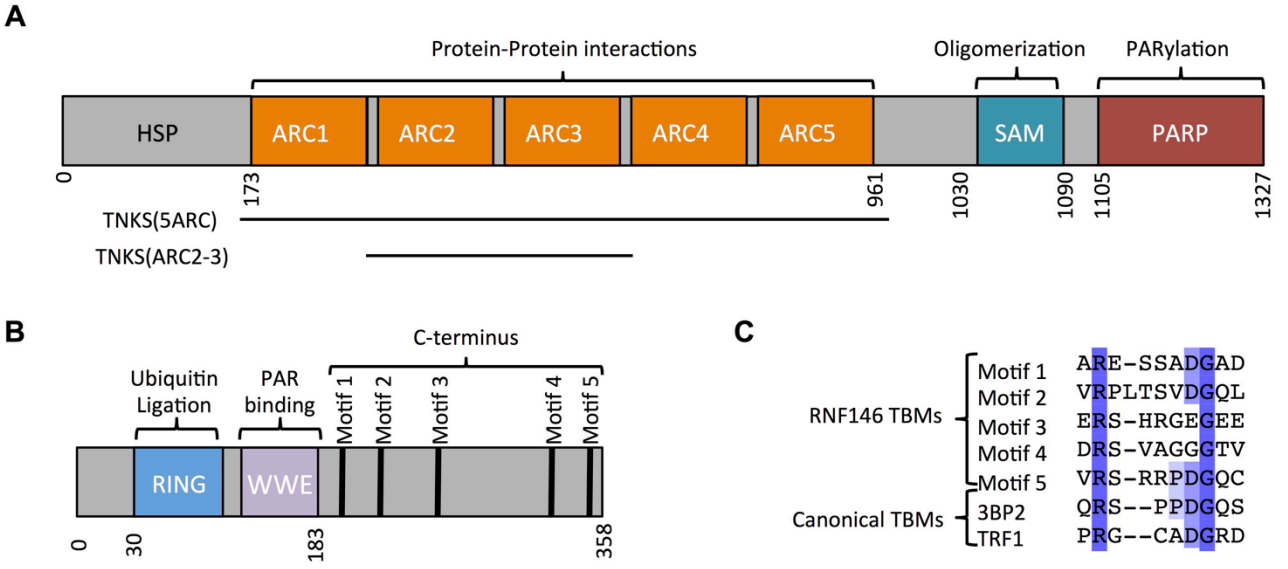

Figure 1 | Domain architecture of RNF146 and Tankyrase-1/2
(A) Linear schematic of tanyrase-1/2 indicating domains and domain functions (above). Tankyrase-2 is approx. 83 % identical to tankyrase-1, but lacks the N-terminal histidine, serine, proline rich region (HSP). **(B)** Linear schematic of RNF146 showing domain location and functions. Motif 1-5 are indicated within the disordered C-terminal domain. **(C)** Sequence of the TBM-like motifs in RNF146 indicated in (B). The canonical TBMs from 3BP2 and TRF1 are shown for comparison and follow the form of RXXΦDG. The term Φ represents any smaller hydrophic residue such as G, A, P, and V. X; any amino acid. PAR; Poly(ADP-ribose); PARylation; poly(ADP-ribosyl)ation. ARC; ankyrin repeat cluster. SAM; sterile alpha motif.

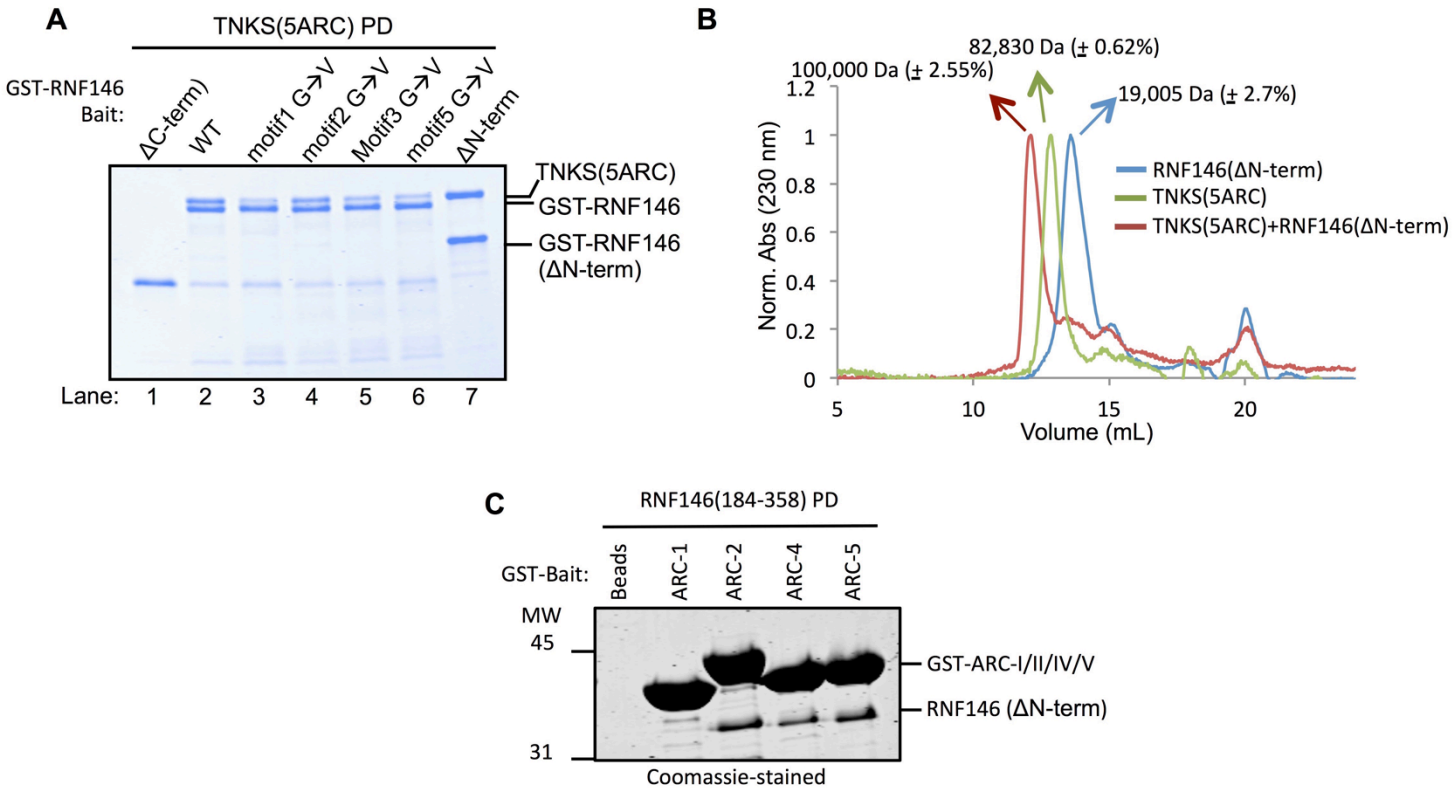

Figure 2 | RNF146 binds to tankyrase via 4 motifs in its flexible C-terminus.
(A) GST pull-downs of TNKS(5ARC) (residues 171-961) with GST tagged RNF146 constructs and mutants. Mutants shown as G→V are Gly to Val mutations in the obligate Gly of the TBM. motif1 G→V, G199V; motif2 G→V, G226V; motif3 G→V, G265V; motif5 G→V, G351V; RNF146(ΔN-term), residues 184-358; RNF146(ΔC-term), residues 1-183. **(B)** Size exclusion chromatography (SEC) of TNKS(5ARC) (green) and RNF146(ΔN-term) (blue) and a one-to-one mixture of the two (red). Molecular weights given were determined via SEC-multi-angle light scattering (SEC-MALS). **(C)** GST pull-downs of RNF146(ΔN-term) with GST-tagged TNKS fragments. ARC1, residues 171-328; ARC2, residues 308-484; ARC4, residues 655-800, ARC5, residues 800-961.

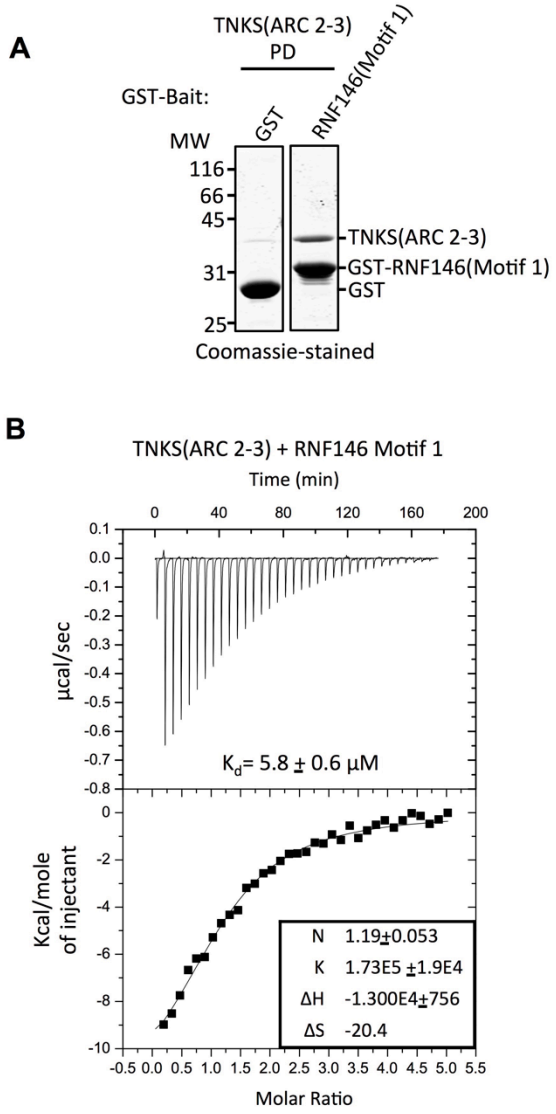

Figure 3 | Non-canonical RNF146 motif 1 binds ARC2 with an affinity similar to other TBM-TNKS interactions.
(A) GST pull-downs of TNKS(ARC2-3) (residues 308-655) by GST-RNF146(motif 1) (residues 184-205) showing weak interaction between RNF146(motif 1) and TNKS ARC2. **(B)** Isothermal titration calorimetry (ITC) of TNKS(ARC2-3) with RNF146(motif 1) titration curves and resulting thermodynamic parameters. A K_d of 5.8 $\pm$ 0.6 µM was measured.

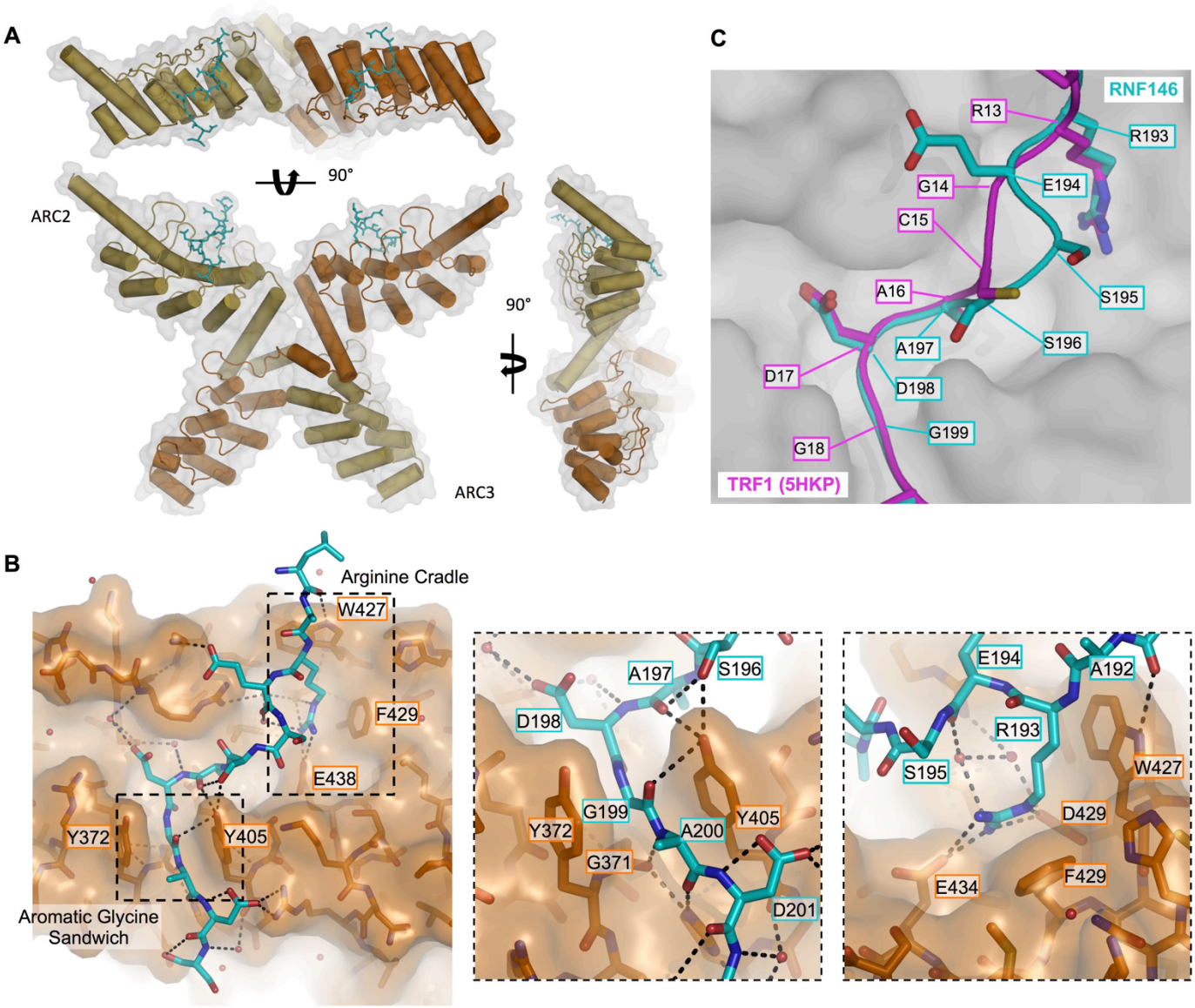

Figure 4 | Structure of the RNF146(motif 1)-TNKS(ARC2-3) interaction
(A) Overall structural architecture of the RNF146(motif 1)-TNKS(ARC2-3) complex showing two copies of TNKS(ARC2-3) (yellow and orange) shown as a cartoon with helices shown as cylinders, and two peptides of RNF146(motif 1) (cyan) shown as sticks. ARC2 and ARC3 are indicated. Three angles are shown. **(B)** (*Left*) The motif 1 binding site on ARC2 showing the location of the arginine cradle and the aromatic glycine sandwich (dashed rectangles), and select residues. (*Middle*) A close-up of the Aromatic glycine sandwich shown in (A) and (*right*) the arginine cradle indicated in the left panel shown from an alternate angle. RNF146(motif 1) is shown as in (A), ARC2 is shown as sticks with its surface shown as orange. **(C)** Comparison of the peptides bound to ARC2 for RNF146(motif 1) (cyan) and TRF1 (magenta; PDB 5HKP).[34] Interactions in the arginine cradle and the aromatic glycine sandwich are maintained despite the extended RNF146 TBM. Residues are marked near their c-alpha atom with line.

Table 1 | Crystallographic data collection and refinement statistics

	TNKS(ARC2-3)/RNF146(Motif1)
Data collection	
Space group	*C121*
Cell dimensions	
a, *b*, *c* (Å)	134.02, 103.28, 75.16
α, β, γ (°)	90.0, 106.9, 90.0
Resolution (Å)	50.0 - 1.93 (1.96 - 1.93)*
R_{sym}(%)	5.4 (46.5)*
$I/\sigma I$	52.8 (2.5)*
Completeness (%)	97.0 (71.8)*
Redundancy	3.6 (2.3)*
Refinement	
Resolution (Å)	50.0 - 1.93
No. reflections	71212
R_{work}/ R_{free}	18.7 / 22.2
No. atoms	5344
Protein	4898
Motif1 peptide	148
Water	298
B-factors	
Protein	27.3
Motif1 peptide	29.2
Water	42.6
R.m.s deviations	
Bond lengths (Å)	0.014
Bond angles (°)	1.6

This diffraction dataset was collected from a single crystal.
*Highest resolution shell is shown in parenthesis.
5% randomly selected reflections were used as a test set.

References

1. D'Amours D, Desnoyers S, D'Silva I, Poirier GG (1999) Poly(ADP-ribosyl)ation reactions in the regulation of nuclear functions. Biochem. J. 342:249–268.

2. Dynek JN, Smith S (2004) Resolution of sister telomere association is required for progression through mitosis. Science. 304:97–100.

3. Chang P, Coughlin M, Mitchison TJ (2005) Tankyrase-1 polymerization of poly(ADP-ribose) is required for spindle structure and function. Nat. Cell Biol. 7:1133–1139.

4. Kim MK, Dudognon C, Smith S (2012) Tankyrase 1 regulates centrosome function by controlling CPAP stability. EMBO Rep. 13:724–732.

5. Ozaki Y, Matsui H, Asou H, Nagamachi A, Aki D, Honda H, Yasunaga S, Takihara Y, Yamamoto T, Izumi S, et al. (2012) Poly-ADP Ribosylation of Miki by tankyrase-1 Promotes Centrosome Maturation. Mol. Cell 47:694–706.

6. Yeh T-YJ, Sbodio JI, Tsun Z-Y, Luo B, Chi N-W (2007) Insulin-stimulated exocytosis of GLUT4 is enhanced by IRAP and its partner tankyrase. Biochem. J. 402:279–290.

7. Guo HL, Zhang C, Liu Q, Li Q, Lian G, Wu D, Li X, Zhang W, Shen Y, Ye Z, et al. (2012) The Axin/TNKS complex interacts with KIF3A and is required for insulin-stimulated GLUT4 translocation. Cell Res 22:1246–1257.

8. Levaot N, Voytyuk O, Dimitriou I, Sircoulomb F, Chandrakumar A, Deckert M, Krzyzanowski PM, Scotter A, Gu S, Janmohamed S, et al. (2011) Loss of Tankyrase-mediated destruction of 3BP2 is the underlying pathogenic mechanism of cherubism. Cell 147:1324–1339.

9. Callow MG, Tran H, Phu L, Lau T, Lee J, Sandoval WN, Liu PS, Bheddah S, Tao J, Lill JR, et al. (2011) Ubiquitin ligase RNF146 regulates tankyrase and Axin to promote Wnt signaling. PLoS One 6.

10. Zhang Y, Liu S, Mickanin C, Feng Y, Charlat O, Michaud G a, Schirle M, Shi X, Hild M, Bauer A, et al. (2011) RNF146 is a poly(ADP-ribose)-directed E3 ligase that regulates axin degradation and Wnt signalling. Nat. Cell Biol. 13:623–9.

11. Smith S, Giriat I, Schmitt A, de Lange T (1998) Tankyrase, a Poly(ADP-Ribose) Polymerase at Human Telomeres. Science. 282:1484 LP-1487.

12. Chang W, Dynek JN, Smith S (2003) TRF1 is degraded by ubiquitin-mediated proteolysis after release from telomeres. Genes Dev. 17:1328–1333.

13. Wang W, Li N, Li X, Tran MK, Han X, Chen J (2015) Tankyrase Inhibitors Target YAP by Stabilizing Angiomotin Family Proteins. Cell Rep. 13:524–532.

14. Campbell CI, Samavarchi-Tehrani P, Barrios-Rodiles M, Datti A, Gingras A-C, Wrana JL (2016) The RNF146 and tankyrase pathway maintains the junctional Crumbs complex through regulation of angiomotin. J. Cell Sci. 129:3396 LP-3411.

15. Matsumoto Y, Larose J, Kent OA, Lim M, Changoor A, Zhang L, Storozhuk Y, Mao X, Grynpas MD, Cong F, et al. (2017) RANKL coordinates multiple osteoclastogenic pathways by regulating expression of ubiquitin ligase RNF146. J. Clin. Invest. 127.

16. Li N, Zhang Y, Han X, Liang K, Wang J, Feng L, Wang W, Songyang Z, Lin C, Yang L, et al. (2015) Poly-ADP ribosylation of PTEN by tankyrases promotes PTEN degradation and tumor growth. Genes Dev. 29:157–170.

17. Wang H, Lu B, Castillo J, Zhang Y, Yang Z, McAllister G, Lindeman A, Reece-Hoyes J, Tallarico J, Russ C, et al. (2016) Tankyrase Inhibitor Sensitizes Lung Cancer Cells to Endothelial Growth Factor Receptor (EGFR) Inhibition via Stabilizing Angiomotins and Inhibiting YAP Signaling. J. Biol. Chem. 291:15256–15266.

18. Haikarainen T, Krauss S, Lehtio L (2014) Tankyrases: structure, function and therapeutic implications in cancer. Curr. Pharm. Des. 20:6472–88.

19. Lehtio L, Chi NW, Krauss S (2013) Tankyrases as drug targets. FEBS J. 280:3576–3593.

20. Riffell JL, Lord CJ, Ashworth A (2012) Tankyrase-targeted therapeutics: expanding opportunities in the PARP family. Nat. Rev. Drug Discov. 11:923–36.

21. Sbodio JI, Lodish HF, Chi N-W (2002) Tankyrase-2 oligomerizes with tankyrase-1 and binds to both TRF1 (telomere-repeat-binding factor 1) and IRAP (insulin-responsive aminopeptidase). Biochem. J. 361:451–459.

22. De Rycker M, Venkatesan RN, Wei C, Price CM (2003) Vertebrate tankyrase domain structure and sterile alpha motif (SAM)-mediated multimerization. Biochem. J. 372:87–96.

23. De Rycker M, Price CM (2004) Tankyrase polymerization is controlled by its sterile alpha motif and poly(ADP-ribose) polymerase domains. Mol. Cell. Biol. 24:9802–12.

24. DaRosa PA, Ovchinnikov S, Xu W, Klevit RE (2016) Structural insights into SAM domain-mediated tankyrase oligomerization. Protein Sci. 25:1744–1752.

25. Mariotti L, Templeton CM, Ranes M, Paracuellos P, Cronin N, Beuron F, Morris E, Guettler S (2016) Tankyrase Requires SAM Domain-Dependent Polymerization to Support Wnt-β-Catenin Signaling. Mol. Cell 63:498–513.

26. Riccio AA, McCauley M, Langelier M-F, Pascal JM (2016) Tankyrase Sterile α Motif Domain Polymerization Is Required for Its Role in Wnt Signaling. Structure 24:1573–1581.

27. Guettler S, LaRose J, Petsalaki E, Gish G, Scotter A, Pawson T, Rottapel R, Sicheri F (2011) Structural Basis and Sequence Rules for Substrate Recognition by Tankyrase Explain the Basis for Cherubism Disease. Cell 147:1340–1354.

28. Xu W, Lau YH, Fischer G, Tan YS, Chattopadhyay A, de la Roche M, Hyvönen M, Verma C, Spring DR, Itzhaki LS (2017) Macrocyclized Extended Peptides: Inhibiting the Substrate-Recognition Domain of Tankyrase. J. Am. Chem. Soc. 139:2245–2256.

29. Huang S-M a, Mishina YM, Liu S, Cheung A, Stegmeier F, Michaud G a, Charlat O, Wiellette E, Zhang Y, Wiessner S, et al. (2009) Tankyrase inhibition stabilizes axin and antagonizes Wnt signalling. Nature 461:614–620.

30. Wang Z, Michaud GA, Cheng Z, Zhang Y, Hinds TR, Fan E, Cong F, Xu W (2012) Recognition of the iso-ADP-ribose moiety in poly(ADP-ribose) by WWE domains suggests a general mechanism for poly(ADP-ribosyl)ation-dependent ubiquitination. Genes Dev. 26:235–240.

31. DaRosa PA, Wang Z, Jiang X, Pruneda JN, Cong F, Klevit RE, Xu W (2014) Allosteric activation of the RNF146 ubiquitin ligase by a poly(ADP-ribosyl)ation signal. Nature 517:223–226.

32. Morrone S, Cheng Z, Moon RT, Cong F, Xu W (2012) Crystal structure of a Tankyrase-Axin complex and its implications for Axin turnover and Tankyrase substrate recruitment. Proc. Natl. Acad. Sci. 109:1500–1505.

33. Eisemann T, McCauley M, Langelier M-F, Gupta K, Roy S, Van Duyne GD, Pascal JM (2017) Tankyrase-1 Ankyrin Repeats Form an Adaptable Binding Platform for Targets of ADP-Ribose Modification. Structure 24:1679–1692.

34. Li B, Qiao R, Wang Z, Zhou W, Li X, Xu W, Rao Z (2016) Crystal structure of a tankyrase 1 telomere repeat factor 1 complex. Acta Crystallogr. Sect. F 72:320–327.

35. Tropea JE, Cherry S, Waugh DS Expression and Purification of Soluble His6-Tagged TEV Protease. In: Doyle SA, editor. High Throughput Protein Expression and Purification: Methods and Protocols. Totowa, NJ: Humana Press; 2009. pp. 297–307.

36. Otwinowski Z, Minor W (1997) Processing of X-ray diffraction data collected in oscillation mode. Macromol Crystallogr Part A 276: 307–326.

37. McCoy AJ (2007) Solving structures of protein complexes by molecular replacement with Phaser. Acta Crystallogr. Sect. D 63:32–41.

38. Langer GG, Hazledine S, Wiegels T, Carolan C, Lamzin VS (2013) Visual automated macromolecular model building. Acta Crystallogr. D. Biol. Crystallogr. 69:635–641.

39. Emsley P, Lohkamp B, Scott WG, Cowtan K (2010) Features and development of Coot. Acta Crystallogr. D. Biol. Crystallogr. 66:486–501.

40. Murshudov GN, Skubak P, Lebedev AA, Pannu NS, Steiner RA, Nicholls RA, Winn MD, Long F, Vagin AA (2011) REFMAC5 for the refinement of macromolecular crystal structures. Acta Crystallogr. D. Biol. Crystallogr. 67:355–367.

41. Winn MD, Ballard CC, Cowtan KD, Dodson EJ, Emsley P, Evans PR, Keegan RM, Krissinel EB, Leslie AGW, McCoy A, et al. (2011) Overview of the CCP4 suite and current developments. Acta Crystallogr. D. Biol. Crystallogr. 67:235–242.

42. Delaglio F, Grzesiek S, Vuister GW, Zhu G, Pfeifer J, Bax A (1995) NMRPipe: A multidimensional spectral processing system based on UNIX pipes. J. Biomol. NMR 6:277–293.

43. Johnson BA, Blevins RA (1994) NMR View: A computer program for the visualization and analysis of NMR data. J. Biomol. NMR 4:603–614.

Materials and methods

Protein Expression and Purification

All mouse tankyrase fragments including ARC1 (residues 171-328), ARC2 (residues 308-484), ARC4 (residues 655-800), ARC5 (residues 800-961), ARC2-3 (residues 308-655), and 5ARC (residues 171-961) were subcloned into a pGEX-4T-1 plasmid with N-terminal GST tag followed by an added TEV cleavage site. Full-length human RNF146 and RNF146(ΔN-term) (residues 184-358), and deletions were cloned into a pGEX-6P-2 vector with an added C-terminal His_8-tag for purification. RNF146(ΔC-term) (residues 1-183) was generated by addition of a stop codon into the full-length RNF146 construct. All mutations were generated by site-directed mutagenesis (Stratagene) of the above constructs and confirmed by sequencing.

All proteins were produced in *Escherichia coli* (BL21(DE3)) cells in either LB media or MOPs minimal media (for RNF146(ΔN-term)), or MOPs minimal media containing 15N ammonium chloride (Cambridge Isotope Labs) for ^{1}H-^{15}N HSQC experiments (NMR). Cultures were grown at 37 °C to an optical density (at 600 nm) between 0.6 and 1.2, cooled to 16 °C before induction with isopropyl β-D-1-thiogalactopyranoside (IPTG) (Thermo Fisher Scientific) at a final concentration of 100-400 μM. Cultures expressed overnight (for about 16 hours) at 16 °C, spun down to pellet cells, and resuspended in 20 mM Tris pH 7.6, 200 mM NaCl, 2 mM Dithiothreitol (DTT) and frozen for future lysis. Cells were thawed at room temperature and lysed via French pressure cell press in the presence of phenylmethane sulfonyl fluoride (PMSF) (Pierce), and centrifuged at ~1500xg before application to affinity columns. GST-tagged ARC1,

ARC2, ARC4, and ARC5 and TNKS(5ARC) were bound to Glutathione Sepherose 4B (GE Healthcare) columns, washed with five column volumes of binding buffer (20 mM Tris pH 7.6, 200 mM NaCl, 2 mM DTT) and eluted with binding buffer containing 15 mM glutathione, followed by size exclusion chromatography. Tankyrase fragments ARC2-3 and TNKS(5ARC) were similarly bound to glutathione beads, followed by overnight cleavage with tabacco etch virus (TEV) protease (purified as previously described)[35] on the column. After elution from Glutathione Sepherose 4B, ARC2-3 was further purified by cation-exchange chromatography (SP column; GE Healthcare) and gel filtration using a Superdex 200 column (GE Healthcare). GST-cleaved TNKS(5ARC) was then eluted from the column followed by anion exchange chromatography using a HiTrap Q HP column (GE healthcare) and size exclusion chromatography (Superdex 200; GE Healthcare). GST-tagged full-length, mutants, and truncations of RNF146 purified using Glutathione Sepherose 4B (GE Healthcare), followed by Ni-NTA (Quiagen) for affinity purification using the C-terminal His_8-tag, then anion exchange chromatography (HiTrap Q HP, GE Healthcare), and gel filtration using a Superdex 75 column (GE Healthcare). RNF146 samples prepared without a GST tag were similarly purified, but GST was cleaved using TEV protease prior to Ni-affinity purification. Axin(1-80) was purified as previously described.[32] The RNF146 peptide used for crystallography, residues 190-203 (NLARESSADGADS) was purchased (United Biosystems). The peptide mass was used to generate a stock solution of a known concentration in water. The concentration of peptide was confirmed by UV absorbance at 205 nm.

GST pull-down assays

GST pull-down assays using GST-tagged RNF146 (or fragments or mutants thereof) were performed as previously described.[31] Assays containing the competitive inhibitor Axin (residues

1-80) were similarly peformed, but Axin was pre-incubated with 2 μM TNKS(5ARC) and 2 μM GST-RNF146 prior to washing steps with the indicated concentrations. For pull-down experiments in which GST-RNF146(motif 1) (residues 184-205) were used as bait, about 100 μg of TNKS(ARC2-3) was incubated with ~50 μg of GST-RNF146(motif 1), and 20 μL of glutathione sepherose 4B (GE Healthcare) in a microcentrifuge tube fore 30 min on ice prior to washing 4 times with 100 μL of wash buffer (40 mM Tris pH 8.0, 100 mM NaCl, 2 mM DTT, 0.04% Tween-20). GST pull-down assays with GST-tagged tankyrase fragments were performed with ~100 μg individual GST-ARCs and ~50 μg RNF146(ΔN-term), and 20 μL glutathione sepherose 4B beads. Pull-downs were performed as above with same volume of wash buffer and wash cycles.

Protein crystallization, data Collection, and refinement

TNKS(ARC2-3) was buffer exchange into 20 mM Tris pH 8.0, 100 mM NaCl, 2 mM DTT using a Superdex 200 10/300 column (GE healthcare) and concentrated to 240 μM. RNF146(motif 1) peptide (residues 190-203, NLARESSADGADS) was added to the above solution from a stock solution of 10 mM in water to give a final concentration of 1 mM peptide. One microliter of this solution was combined with 1 μL of a well solution containing 30 mM sodium citrate pH 5.6, 60 mM ammonium acetate, 27% 2-methyl-2,4-pentanediol (MPD) and crystalized via the hanging drop method at 4 °C. Crystals formed between 2 and 3 days. Crystals were dehydrated overnight by soaking in a cryoprotectant containing 16 mM Tris pH 8.0, 80 mM NaCl, 24 mM sodium citrate pH 5.6, 48 mM ammonium acetate, 0.5 mM RNF146(motif 1) peptide, and 28% MPD before being frozen in liquid nitrogen for structure determination.

Data was collected at ALS, beamline 8.2.2. and diffraction datasets were processed using HKL2000 software package[36] with the C2 space group. The structure phase was determined by

molecular replacement by searching with ARC2 and ARC3 structures from the PDB 3UTM[32] as the initial search model using Phaser,[37] followed by automated and manual model building using ARPwarp[38] and Coot[39]. The structure was refined to 1.93 Å using iterative model building using Coot and refinement using Refmac5[40] in the CCP4 7.0 software package.[41]

NMR Spectroscopy

^{1}H-^{15}N HSQC-TROSY experiments were performed on a 500 mHz Bruker Avance II NMR spectrometer using ~400 μM ^{15}N labeled RNF146(ΔN-term) in 25 mM sodium phosphate pH 7.0, 150 mM NaCl, and 10% D_2O. Raw NMR data was processed using NMRpipe,[42] and analyzed in NMRviewJ (One Moon Scientific).[43]

Isothermal titration calorimetric

Isothermal titration calorimetry (ITC) was performed using a VP-ITC Microcal calorimeter (Malvern Instruments). Proteins/peptides were buffer exchanged (or resuspended) in 20 mM HEPES pH 7.5, 150 mM NaCl and degassed for ITC analysis at 20 °C. Five-hundred micromolar (500 μM) RNF146(motif 1) peptide (residues 190-203; sequence NLARESSADGADS) (United Biosystems) (titrant) was injected into 15 μM TNKS(ARC2-3) (titrand) every five minutes for a total of 40 injections at a volume of 5 μL each. Data was analyzed using the Origin 7.0 software (OriginLab Corp).

Analytical gel filtration and Multi-Angle Light Scattering

Analytical size exclusion chromatography (SEC) and SEC-MALS (multi-angle light scattering) experiments were performed using a 24 mL superdex 200 10/300 column (GE Healthcare) in a running buffer composed of 20 mM Tris pH 7.5, 150 mM NaCl, 2 mM DTT. A miniDAWN TREOS MALS detector (Wyatt Technology) was used for SEC-MALS. About 200 μg of TNKS(5ARC) or RNF146 was used for SEC-MALS experiments, or 200 μg TNKS(5ARC) and

~45 µg RNF146(ΔN-term) for a one-to-one molar ratio. For analytical SEC experiments only 100 µg of TNKS(5ARC) were used with a with a large molar excess (>6 fold) of RNF146(ΔN-term). Ultraviolet detection of eluted proteins was monitored at 230 nm and 280 nm.

Supplemental Figures:

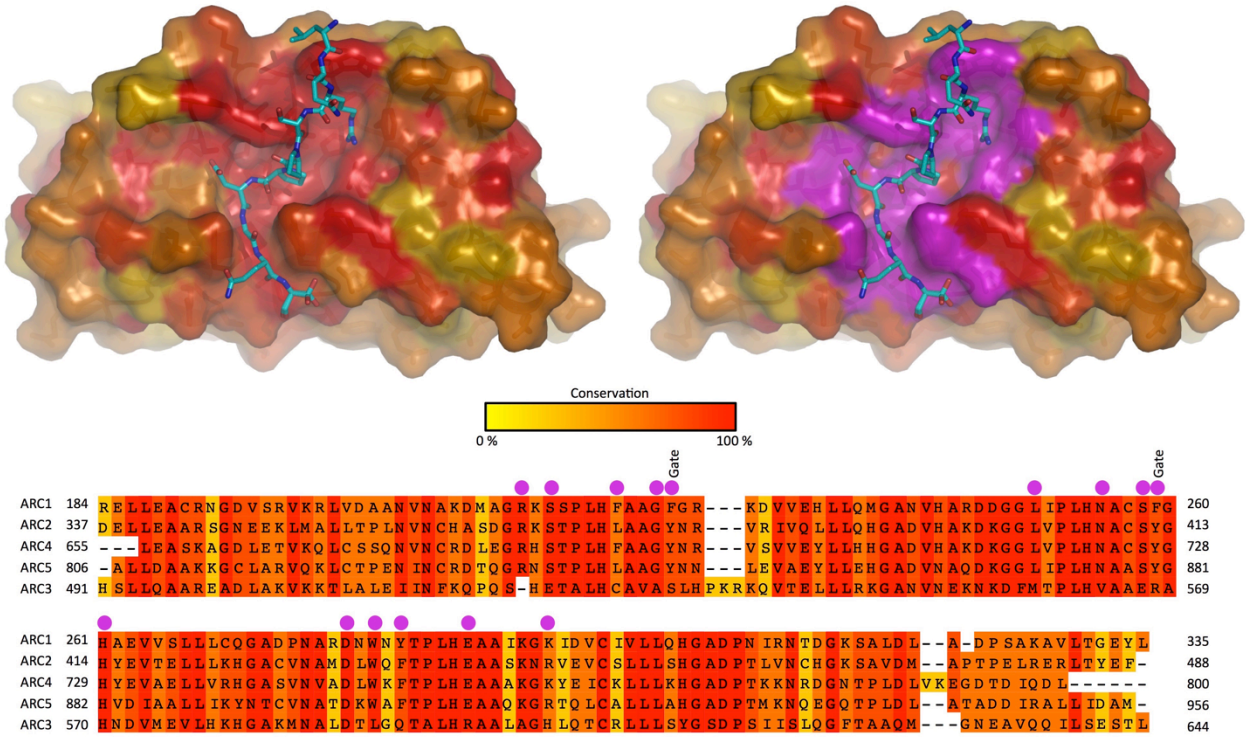

Supplemental Figure S1 | Sequence conservation of the tankyrase ARC binding groove (*Top left*) Sequence conservation between ARCS1, 2, 4, and 5 mapped onto the surface of the crystal structure of ARC4 bound to the TBM of 3BP2 shown in cyan (PDB 3TWR).[27] (*Top right*) all residues that are within 4 Å of the 3BP2 peptide are shown as magenta; other residues colors shown as in left. (*Bottom*) Sequence alignment of all five ARCs of tankyrase 1 showing high conservation across sequences. Magenta sequences circles above sequence show location of the residues highlighted in *top right*. The "Gate" label refers to the Tyr/Phe present at the aromatic glycine sandwich of the binding groove. The sequence of ARC3 is shown as comparison, and has very low sequence identity with the other ARCs at the peptide binding site.

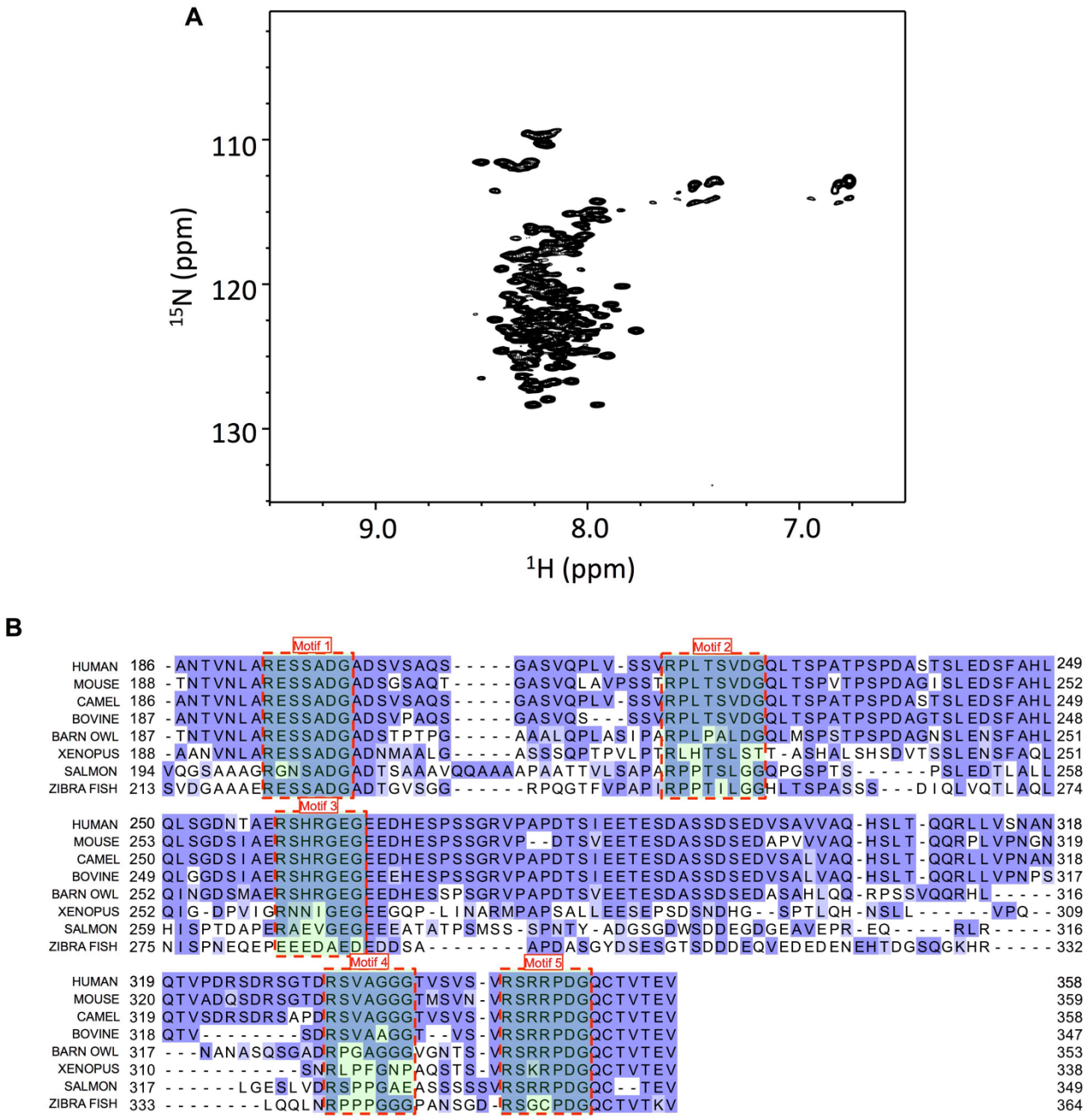

Supplemental Figure S2 | TBM-like motifs in the disordered RNF146 C-terminus
(A) ^{1}H-^{15}N-HSQC of the C-terminus of RNF146 (residues 134-358) showing low dispersion of resonances in the proton dimension typical of disordered proteins. **(B)** Multiple sequence alignment showing conservation of proposed TBMs in RNF146 based on their similarity to other canonical TBMs showing variable conservation. The first motif (motif 1) structurally characterize in this study, and the last motif (motif 5) are the best conserved from mammals through zebra fish.

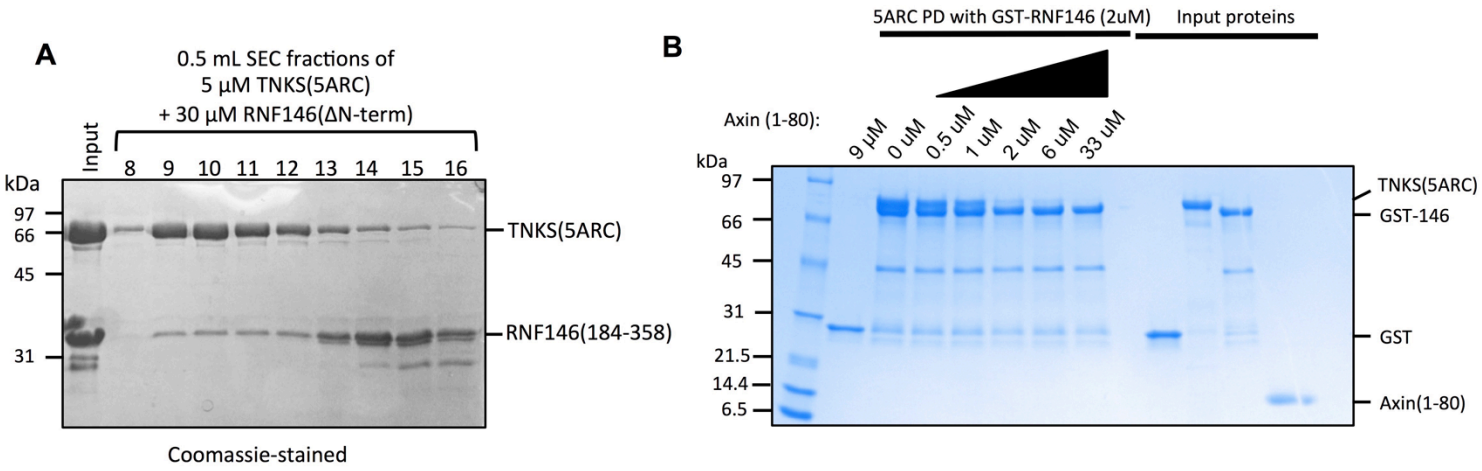

Supplemental Figure S3 | RNF146 displays tight binding to tankyrase but is competed off by Axin

(A) SDS-PAGE analysis of eluted fractions from a size exclusion chromatography run performed as in Figure 1B with a large excess of RNF146(ΔN-term) (6 fold). Despite the large excess of one component, RNF146 forms a one-to-one complex with TNKS(5ARC). **(B)** GST pull-down experiments of TNKS(5ARC) with GST-RNF146 in the presence of increasing quantities of Axin(1-80). All three proteins were mixed and incubated for 60 min on ice in the presence of GST affinity resin prior to performing the pull-down experiment. Axin(1-80) competes off RNF146 stoichiometrically indicating that it binds more tightly than RNF146, and RNF146 cannot bind sufficiently to the remaining unoccupied tankyrase sites.

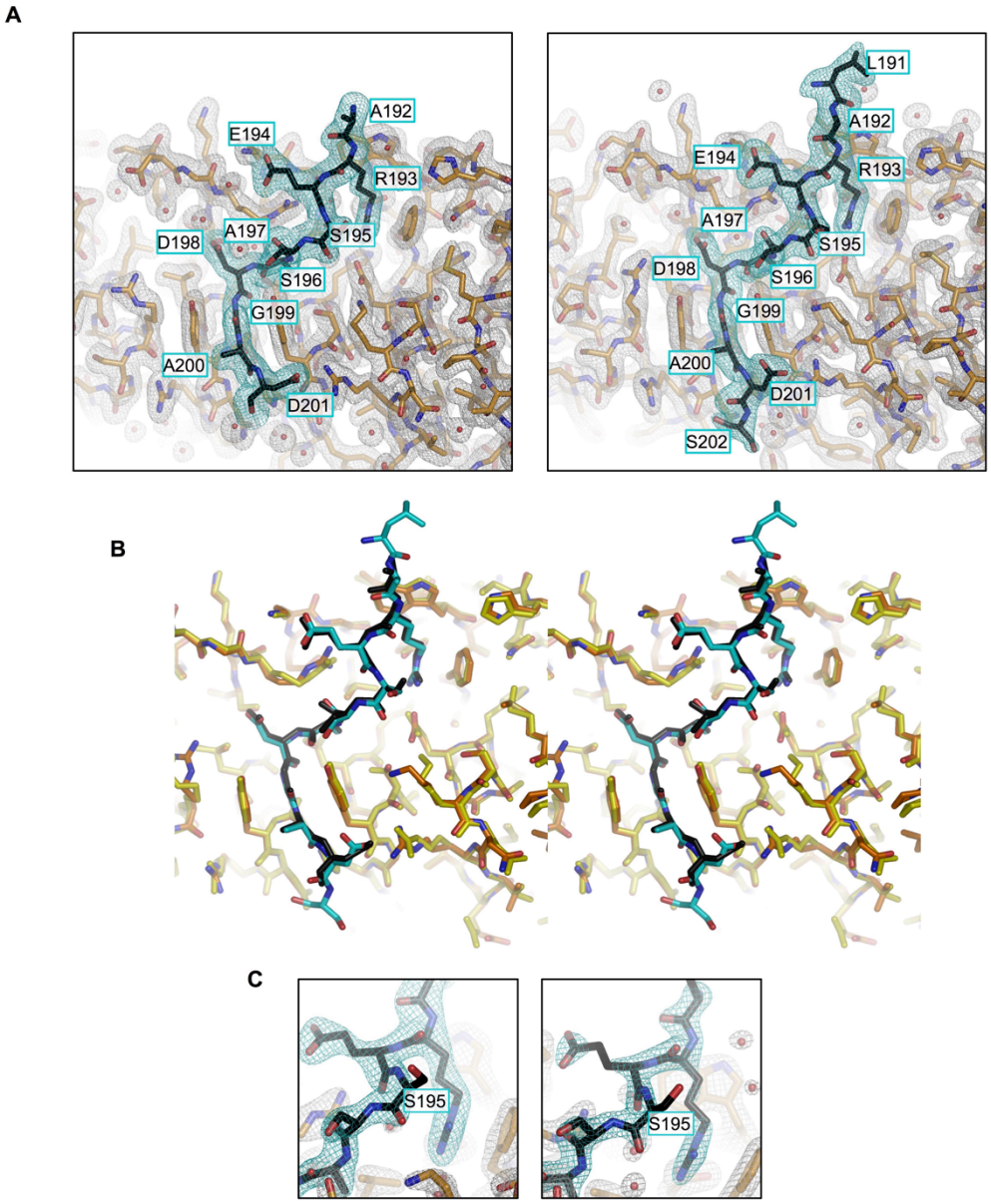

Supplemental Figure S4 | Comparison of the two peptide binding sites in the asymmetric unit

(A) RNF146(motif 1) peptides bound to both ARC2 modules in the asymmetric unit shown as sticks with $2F_o$-F_c electron density map at 1σ. Peptide is shown as black with cyan electron density map tankyrase is shown as orange with grey map. Residues for RNF146 are labeled. **(B)** Stereoview of the structures of each tankyrase-RNF146 complex in the asymmetric unit overlaid. One copy of the complex is shown as orange (tankyrase) and cyan (RNF146), the other in yellow (tankyrase) and black (RNF146). The conformation of each peptides is nearly identical (RMSD = 0.23 Å). **(C)** $2F_o$-F_c electron density map (shown as cyan mesh) for each of the peptides (black) at 1.5σ showing relatively low density for the Ser-195 side chain.

Supplemental Table 1 | Search results of TBMs from TNKS interaction proteins

Protein	Start Position	Sequence	End Position	Motif Type
RIMB1_HUMAN	1058	RTMSPHG	1064	Extended
RIMB1_HUMAN	1137	REMAKG	1142	Canonical
RIMB1_HUMAN	1405	RRRGGG	1410	Canonical
RIMB1_HUMAN	1563	RGRSATG	1569	Extended
RIMB1_HUMAN	1585	RGQDGSG	1591	Extended
FBX50_HUMAN	5	REGHALG	11	Extended
FBX50_HUMAN	107	RSPNPEG	113	Extended
C9JDE9_HUMAN	3	RLQVVLG	9	Extended
RL4_HUMAN	188	RMRAGKG	194	Extended
TAOK1_HUMAN	970	RRTASG	975	Canonical
HMCN1_HUMAN	5416	RKTCPEG	5422	Extended
EWS_HUMAN	300	RGRGRG	305	Canonical
EWS_HUMAN	314	RGGRGGG	320	Extended
EWS_HUMAN	471	RGGPGG	476	Canonical
EWS_HUMAN	486	RMGGRG	491	Canonical
EWS_HUMAN	506	RGNPSG	511	Canonical
EWS_HUMAN	563	RGRGGPG	569	Extended
EWS_HUMAN	581	RGGPGG	586	Canonical
EWS_HUMAN	607	RGGFGGG	613	Extended
EWS_HUMAN	614	RRGGPG	619	Canonical
EWS_HUMAN	632	RRGGRG	637	Canonical
NUCL_HUMAN	656	RGGGRG	661	Canonical
NUCL_HUMAN	666	RGGGRG	671	Canonical
NUCL_HUMAN	679	RGRGGFG	685	Extended
NUCL_HUMAN	691	RGGRGGG	697	Extended
AEDO_HUMAN	22	RGSGGG	27	Canonical
AEDO_HUMAN	33	RDAASG	38	Canonical
ETFA_HUMAN	3	RAAAPG	8	Canonical
DESM_HUMAN	58	RTSGGAG	64	Extended
DNJA2_HUMAN	380	RGSGGG	385	Canonical
CDC7_HUMAN	21	RFQAEG	26	Canonical
ZN703_HUMAN	544	RYHPYG	549	Canonical
CHD3_HUMAN	117	RRKKGEG	123	Extended
CHD3_HUMAN	1335	RNLGKG	1340	Canonical
CHD3_HUMAN	1662	RERPEG	1667	Canonical
CHD3_HUMAN	1675	REDVKG	1680	Canonical
APRV1_HUMAN	84	RMAGSG	89	Canonical
CDC37_HUMAN	286	RLGPGG	291	Canonical
FBP1L_HUMAN	499	RESPEG	504	Canonical
DDX5_HUMAN	12	RDRGFG	17	Canonical
DDX5_HUMAN	482	RSRGRG	487	Canonical
DDX5_HUMAN	559	RTGNPTG	565	Extended
IF2B1_HUMAN	167	RRGGFG	172	Canonical
TARA_HUMAN	196	RSPVGG	201	Canonical
TARA_HUMAN	1253	RGSAPPG	1259	Extended
TARA_HUMAN	1316	RKSEAAG	1322	Extended
TARA_HUMAN	1595	RKDPAG	1600	Canonical
TARA_HUMAN	1690	RSTAKG	1695	Canonical
SEMG1_HUMAN	165	RLWVHG	170	Canonical
LMNA_HUMAN	627	RSVGGSG	633	Extended
LRCH4_HUMAN	393	RREEPAG	399	Extended
LRCH4_HUMAN	439	RAVVGG	444	Canonical
RL27A_HUMAN	26	RKHPGG	31	Canonical
RL27A_HUMAN	32	RGNAGG	37	Canonical
PLPL6_HUMAN	351	RTSPVRG	357	Extended
PLPL6_HUMAN	376	RPPDPTG	382	Extended
PLPL6_HUMAN	461	REQPAG	466	Canonical
NELFE_HUMAN	144	RELGPDG	150	Extended
RL8_HUMAN	147	RVKLPSG	153	Extended
RL8_HUMAN	226	RRDAPAG	232	Extended
AXIN2_HUMAN	23	RPPVPG	28	Canonical
AXIN2_HUMAN	57	RNEDGLG	63	Extended
AXIN2_HUMAN	595	REGGAPG	601	Extended
KLRG2_HUMAN	105	RNGEAPG	111	Extended
KLRG2_HUMAN	129	RVKPVG	134	Canonical
KLRG2_HUMAN	202	RASPAEG	208	Extended
SHIP2_HUMAN	960	RLKPEG	965	Canonical
SHIP2_HUMAN	1096	RPPLPPG	1102	Extended
SHIP2_HUMAN	1192	RASGLG	1197	Canonical
RBM8A_HUMAN	35	RKGRGFG	41	Extended
RBM8A_HUMAN	152	RGPPKG	157	Canonical
RS26_HUMAN	10	RAKKGRG	16	Extended
RS26_HUMAN	100	RFRPAG	105	Canonical
HNRPU_HUMAN	250	REDHGRG	256	Extended
HNRPU_HUMAN	720	RGGAPG	725	Canonical
HNRPU_HUMAN	739	RGGGGG	744	Canonical
RENT2_HUMAN	1151	RKGPPLG	1157	Extended
RENT2_HUMAN	1251	RYQHPKG	1257	Extended
U17L7_HUMAN	389	REPRALG	395	Extended
RL29_HUMAN	109	RARIAKG	115	Extended
SEMG2_HUMAN	165	RLWVHG	170	Canonical
F117A_HUMAN	9	RGGGAWG	15	Extended
F117A_HUMAN	18	RGGAGG	23	Canonical
F117A_HUMAN	58	RRDGGG	63	Canonical
ID4_HUMAN	12	RKAPSG	17	Canonical
IF4B_HUMAN	278	RRAFGSG	284	Extended
IF4B_HUMAN	545	RGPGDG	550	Canonical
NKD2_HUMAN	15	RRESPEG	21	Extended
NKD2_HUMAN	96	REGPRG	101	Canonical
ROA2_HUMAN	238	RGFGDG	243	Canonical
ROA2_HUMAN	266	RGGYGGG	272	Extended
RS2_HUMAN	26	RGGFGSG	32	Extended
RS2_HUMAN	34	RGRGRG	39	Canonical
RS2_HUMAN	40	RGRGRG	45	Canonical
RS2_HUMAN	46	RGRGARG	52	Extended
CE170_HUMAN	1570	RFNPDG	1575	Canonical
GPBL1_HUMAN	109	RSGGGTG	115	Extended
SOGA3_HUMAN	26	RLHPEG	31	Canonical
SOGA3_HUMAN	58	RSPVGAG	64	Extended
SOGA3_HUMAN	96	RGGGGG	101	Canonical
SOGA3_HUMAN	194	RGWRGKG	200	Extended
SOGA3_HUMAN	232	RNSGSG	237	Canonical
SOGA3_HUMAN	289	RSSPVSG	295	Extended
SOGA3_HUMAN	773	REGPIG	778	Canonical
H4_HUMAN	4	RGKGGKG	10	Extended
GTSE1_HUMAN	179	RLTRAPG	185	Extended
GTSE1_HUMAN	220	RAASVRG	226	Extended
GTSE1_HUMAN	363	RPALPAG	369	Extended
STRN4_HUMAN	18	RPLGSG	23	Canonical
STRN4_HUMAN	335	RRCTVDG	341	Extended
UIMC1_HUMAN	132	RPLATG	137	Canonical
UIMC1_HUMAN	708	RTKAGRG	714	Extended
RN166_HUMAN	14	RQPPAG	19	Canonical
SAPC2_HUMAN	137	RKPLPLG	143	Extended
SAPC2_HUMAN	207	RAPRARG	213	Extended
SAPC2_HUMAN	217	RHTIASG	223	Extended
RS20_HUMAN	66	RKTPCG	71	Canonical
ACOT8_HUMAN	16	RGDPPG	21	Canonical
IRS2_HUMAN	6	RHGPPG	11	Canonical
IRS2_HUMAN	381	RPVSVAG	387	Extended
IRS2_HUMAN	531	RDGGGG	536	Canonical
IRS2_HUMAN	718	RTFPASG	724	Extended
IRS2_HUMAN	1137	RADPQG	1142	Canonical
PARD3_HUMAN	249	RVEPVG	254	Canonical
DISC1_HUMAN	47	RSSTGPG	53	Extended
DISC1_HUMAN	169	RRVRAAG	175	Extended
DISC1_HUMAN	223	RGEAEG	228	Canonical
BRE1A_HUMAN	146	RERGEG	151	Canonical
TXLNG_HUMAN	10	RGRGGG	15	Canonical
TXLNG_HUMAN	106	REEIPGG	112	Extended
TXLNG_HUMAN	115	RTDPPDG	121	Extended
ABR_HUMAN	63	RSQGGG	68	Canonical
NPM_HUMAN	142	RSAPGG	147	Canonical
AMOL1_HUMAN	157	RQEPQG	162	Canonical
TFE2_HUMAN	6	RMAPVG	11	Canonical
TFE2_HUMAN	158	RRRAADG	164	Extended
TFE2_HUMAN	174	RKVPPG	179	Canonical
TFE2_HUMAN	371	RAGAPG	376	Canonical
CC85B_HUMAN	151	RGGPSG	156	Canonical
CC85B_HUMAN	176	RDLGDG	181	Canonical
KHNYN_HUMAN	288	RPQSVGG	294	Extended
EP15R_HUMAN	788	RPKPPSG	794	Extended
LARP1_HUMAN	45	RGGEPDG	51	Extended
LARP1_HUMAN	338	RGRGRG	343	Canonical
LARP1_HUMAN	344	RGRGRG	349	Canonical
LARP1_HUMAN	654	RRHPGG	659	Canonical
LARP1_HUMAN	1038	RHSVVAG	1044	Extended
HEXI1_HUMAN	58	RPGPEG	63	Canonical
HNRPM_HUMAN	410	RLGGAG	415	Canonical
HNRPM_HUMAN	418	RMGAGLG	424	Extended
HNRPM_HUMAN	456	RMGPLG	461	Canonical
HNRPM_HUMAN	485	RMGAGMG	491	Extended
HNRPM_HUMAN	531	RMVPAG	536	Canonical
HNRPM_HUMAN	591	RMGPAMG	597	Extended
HNRPM_HUMAN	606	RMGLAMG	612	Extended
DDX17_HUMAN	81	RGGGFG	86	Canonical
DDX17_HUMAN	92	RDRGGFG	98	Extended
DDX17_HUMAN	555	RGGGGG	560	Canonical
DDX17_HUMAN	610	RAGYANG	616	Extended
UBP22_HUMAN	4	RPEPEG	9	Canonical
HNRPK_HUMAN	246	RRGRPVG	252	Extended
HNRPK_HUMAN	263	RMPPGRG	269	Extended
TERF1_HUMAN	13	RGCADG	18	Canonical
CAMP3_HUMAN	472	RLLPDG	477	Canonical
CAMP3_HUMAN	666	RPAGEG	671	Canonical
CAMP3_HUMAN	767	RRSPGPG	773	Extended
CAMP3_HUMAN	999	RPRAAG	1004	Canonical
CAMP3_HUMAN	1030	RSPARG	1035	Canonical
CAMP3_HUMAN	1071	RAPSPSG	1077	Extended
CS043_HUMAN	6	RRAEPQG	12	Extended
CS043_HUMAN	105	RKGGPG	110	Canonical
IF4A1_HUMAN	10	RDNGPDG	16	Extended
UBP25_HUMAN	1049	RTPADG	1054	Canonical
SNX33_HUMAN	95	RSGGGSG	101	Extended
SNX33_HUMAN	131	RAGGLG	136	Canonical
MCL1_HUMAN	6	RNAVIG	11	Canonical
MCL1_HUMAN	45	RREIGGG	51	Extended
MCL1_HUMAN	78	RPPPIG	83	Canonical
MCL1_HUMAN	187	REQATG	192	Canonical
THAP4_HUMAN	92	RGAGGHG	98	Extended
THAP4_HUMAN	173	RTPGDG	178	Canonical
HNRH1_HUMAN	212	RPGAGRG	218	Extended
HNRH1_HUMAN	232	RRGAYG	237	Canonical
ERCC6_HUMAN	360	RPEAEG	365	Canonical
HSP72_HUMAN	4	RGPAIG	9	Canonical
FA83H_HUMAN	532	RGLEPSG	538	Extended
FA83H_HUMAN	568	RRGGPEG	574	Extended
FA83H_HUMAN	746	RDPGGG	751	Canonical
FA83H_HUMAN	1001	RLSLGQG	1007	Extended
FA83H_HUMAN	1073	RPPAAG	1078	Canonical
TRI33_HUMAN	52	RAGAEG	57	Canonical
TRI33_HUMAN	873	RIGGDG	878	Canonical
STK26_HUMAN	293	RWKAEG	298	Canonical
NFKB2_HUMAN	160	RSRPQG	165	Canonical
F117B_HUMAN	56	RSGGGG	61	Canonical
F117B_HUMAN	127	RSAAPG	132	Canonical
F117B_HUMAN	468	REPPEG	473	Canonical
MTCL1_HUMAN	55	RPAAPG	60	Canonical
MTCL1_HUMAN	100	RSGGVPG	106	Extended
MTCL1_HUMAN	143	RAGKPPG	149	Extended
MTCL1_HUMAN	243	REPPRG	248	Canonical
MTCL1_HUMAN	257	RGAPPG	262	Canonical
MTCL1_HUMAN	283	RSIPSG	288	Canonical
MTCL1_HUMAN	768	REGPVG	773	Canonical
MTCL1_HUMAN	1566	RDYVEG	1571	Canonical
MTCL1_HUMAN	1795	RPELGPG	1801	Extended
MTCL1_HUMAN	1811	RSPSPIG	1817	Extended
MTCL1_HUMAN	1824	REEGGEG	1830	Extended
MTCL1_HUMAN	1866	RRQAAHG	1872	Extended
TXLNA_HUMAN	503	RRPEGPG	509	Extended
IRS4_HUMAN	413	RLHLPRG	419	Extended
IRS4_HUMAN	499	RGSGGG	504	Canonical
IRS4_HUMAN	563	RPGGGHG	569	Extended
IRS4_HUMAN	816	RSSPLG	821	Canonical
GCC1_HUMAN	618	RRSPVG	623	Canonical
DDX3X_HUMAN	592	RFSGGFG	598	Extended
DDX3X_HUMAN	622	RSGGGG	627	Canonical
DDX3X_HUMAN	632	RGFGGG	637	Canonical
GLCI1_HUMAN	24	RRSAAG	29	Canonical
GLCI1_HUMAN	417	REPPEG	422	Canonical
MRE11_HUMAN	570	RGRGRG	575	Canonical
MRE11_HUMAN	576	RRGGRG	581	Canonical
FGOP2_HUMAN	62	RSTLVMG	68	Extended
TCPH_HUMAN	535	RGRGRG	540	Canonical
CC85C_HUMAN	34	RLRRAEG	40	Extended
CC85C_HUMAN	200	RDVGDG	205	Canonical
CC85C_HUMAN	257	RSIPNG	262	Canonical
RN146_HUMAN	194	RESSADG	200	Extended
RN146_HUMAN	260	RSHRGEG	266	Extended
RN146_HUMAN	333	RSVAGG	338	Canonical
RN146_HUMAN	346	RSRRPDG	352	Extended
CNO11_HUMAN	41	RGGASG	46	Canonical
USP9X_HUMAN	6	RGSPVG	11	Canonical
USP9X_HUMAN	1614	RDDVFG	1619	Canonical
TAOK2_HUMAN	544	RRHQAIG	550	Extended
TAOK2_HUMAN	915	RDPGDG	920	Canonical
TAOK2_HUMAN	1126	RLPVPG	1131	Canonical
HTF4_HUMAN	7	RMAAIG	12	Canonical
HTF4_HUMAN	135	RQDLGLG	141	Extended
HTF4_HUMAN	184	RKVPPG	189	Canonical
HTF4_HUMAN	326	RGNAAG	331	Canonical
HTF4_HUMAN	415	RNHAVG	420	Canonical
ZCHC3_HUMAN	23	RPAARG	28	Canonical
ZCHC3_HUMAN	94	RGDPKG	99	Canonical
ZCHC3_HUMAN	100	RRRDPAG	106	Extended
INP5K_HUMAN	437	REDPLG	442	Canonical
BABA1_HUMAN	28	RSNPEG	33	Canonical
BABA1_HUMAN	48	RSEGEG	53	Canonical
HERC2_HUMAN	4239	RPRQVQG	4245	Extended
AXIN1_HUMAN	22	RPPVPG	27	Canonical
AXIN1_HUMAN	259	RDAAPPG	265	Extended
AXIN1_HUMAN	484	RQSPGPG	490	Extended
AXIN1_HUMAN	647	RRTGHG	652	Canonical
AXIN1_HUMAN	770	RKVGGG	775	Canonical
FNBP1_HUMAN	515	RESPDG	520	Canonical
ARPIN_HUMAN	213	REQGDG	218	Canonical
AMOL2_HUMAN	40	RGGAGTG	46	Extended
AMOL2_HUMAN	71	RQEPQG	76	Canonical
AMOL2_HUMAN	134	RGAPGG	139	Canonical
AMOL2_HUMAN	197	RGPPAEG	203	Extended
AMOL2_HUMAN	230	RYRARG	235	Canonical

Protein	Start Position	Sequence	End Position	Motif Type
AMOL2_HUMAN	488	RLQQALG	494	Extended
AMOL2_HUMAN	526	RQAGAPG	532	Extended
PEX14_HUMAN	310	RMEVQG	315	Canonical
PEX14_HUMAN	350	RRGGDG	355	Canonical
ZN687_HUMAN	122	RMQNGFG	128	Extended
ZN687_HUMAN	1071	RAQGPG	1076	Canonical
ZN687_HUMAN	1101	RGGPGSG	1107	Extended
ZN687_HUMAN	1183	RSDPDG	1188	Canonical
ZN687_HUMAN	1230	RQGAVG	1235	Canonical
CAR10_HUMAN	255	RGPPPG	260	Canonical
CAR10_HUMAN	307	RPGAPG	312	Canonical
CAR10_HUMAN	420	RKQVRG	425	Canonical
CAR10_HUMAN	605	RSPPGG	610	Canonical
CAR10_HUMAN	635	RVLSGPG	641	Extended
CAR10_HUMAN	804	RPKPVG	809	Canonical
TAXB1_HUMAN	712	RGHGTG	717	Canonical
ASPP2_HUMAN	81	RHERPPG	87	Extended
ASPP2_HUMAN	88	RDIVSG	93	Canonical
ASPP2_HUMAN	343	RVAAVG	348	Canonical
CNOT2_HUMAN	198	RNQAFG	203	Canonical
CNOT2_HUMAN	238	RREGSG	243	Canonical
K1522_HUMAN	159	RRSTVLG	165	Extended
K1522_HUMAN	196	RIPTVDG	202	Extended
K1522_HUMAN	205	RGTSGMG	211	Extended
K1522_HUMAN	402	RGSPSG	407	Canonical
K1522_HUMAN	831	RSVGAPG	837	Extended
STRN3_HUMAN	19	RQQQGPG	25	Extended
STRN3_HUMAN	321	RSSGDG	326	Canonical
3BP5_HUMAN	186	RYNAAMG	192	Extended
3BP5_HUMAN	261	RRSSAMG	267	Extended
3BP5_HUMAN	269	RGCGVG	274	Canonical
3BP5_HUMAN	383	RGDRAEG	389	Extended
PABP1_HUMAN	436	RWTAQG	441	Canonical
ASPP1_HUMAN	114	RTENGVG	120	Extended
KIF7_HUMAN	387	RGRRAPG	393	Extended
KIF7_HUMAN	1172	RDHLGEG	1178	Extended
BAIP2_HUMAN	539	REHGDG	544	Canonical
ZBT10_HUMAN	126	RGGGGG	131	Canonical
ZBT10_HUMAN	208	RRSGGDG	214	Extended
LRC47_HUMAN	259	RVGGRG	264	Canonical
LRC47_HUMAN	290	RREGGDG	296	Extended
PP12C_HUMAN	363	RRPGGAG	369	Extended
PP12C_HUMAN	436	RRTAEG	441	Canonical
PP12C_HUMAN	592	RRPRVPG	598	Extended
PP12C_HUMAN	608	RAEAPDG	614	Extended
PP12C_HUMAN	633	RGPAEG	638	Canonical
BRE1B_HUMAN	8	RAAGDG	13	Canonical
BRE1B_HUMAN	519	RAQASG	524	Canonical
PEX5_HUMAN	942	RIVEGQG	948	Extended
KIF1A_HUMAN	942	RIVEGQG	948	Extended
STRN_HUMAN	302	RSAGDG	307	Canonical
RUSC2_HUMAN	87	RSRDGRG	93	Extended
RUSC2_HUMAN	154	RVGRPWG	160	Extended
RUSC2_HUMAN	165	RAGVVEG	171	Extended
RUSC2_HUMAN	345	REGGYG	350	Canonical
RUSC2_HUMAN	636	RATGQG	641	Canonical
RUSC2_HUMAN	667	RARADG	672	Canonical
RUSC2_HUMAN	756	RATGRG	761	Canonical
RUSC2_HUMAN	773	RPSPLG	778	Canonical
RUSC2_HUMAN	784	RSVGPFG	790	Extended
RUSC2_HUMAN	847	RLHGTG	852	Canonical
RUSC2_HUMAN	872	RGGGEG	877	Canonical
RUSC2_HUMAN	900	RRKNPLG	906	Extended
RUSC2_HUMAN	1212	RGQEGPG	1218	Extended
RUSC2_HUMAN	1228	RVKGVG	1233	Canonical
RUSC2_HUMAN	1259	RARWARG	1265	Extended
RUSC2_HUMAN	1318	REGVVEG	1324	Extended
GO45_HUMAN	18	RGAGDG	23	Canonical
F175B_HUMAN	333	RPQAVG	338	Canonical
AMOT_HUMAN	77	RQEPQG	82	Canonical
GMDS_HUMAN	7	RCPSARG	13	Extended
TNKS2_HUMAN	4	RRCAGG	9	Canonical
ARH40_HUMAN	225	RSPGDG	230	Canonical
ARH40_HUMAN	274	RKGAGG	279	Canonical
ARH40_HUMAN	304	RPPGEG	309	Canonical
ARH40_HUMAN	356	RGGGGG	361	Canonical
ARH40_HUMAN	373	RRTGKG	378	Canonical
ARH40_HUMAN	381	RKKRAAG	387	Extended
ARH40_HUMAN	472	RELEGPG	478	Extended
ARH40_HUMAN	966	RRRRADG	972	Extended
CSKI2_HUMAN	414	RSAGSG	419	Canonical
CSKI2_HUMAN	637	RRLAKG	642	Canonical
CSKI2_HUMAN	704	RSRGSG	709	Canonical
CSKI2_HUMAN	730	RNLPEG	735	Canonical
CSKI2_HUMAN	875	RLSSVSG	881	Extended
CSKI2_HUMAN	943	RGSSGEG	949	Extended
CSKI2_HUMAN	963	RPKPAG	968	Canonical

Protein	Start Position	Sequence	End Position	Motif Type
TB182_HUMAN	135	RCAAPG	140	Canonical
TB182_HUMAN	402	RTFPSG	407	Canonical
TB182_HUMAN	764	RGDPGLG	770	Extended
TB182_HUMAN	1251	RESGVG	1256	Canonical
TB182_HUMAN	1363	REHGVG	1368	Canonical
TB182_HUMAN	1397	RELGVG	1402	Canonical
TB182_HUMAN	1446	RPPPSG	1451	Canonical
TB182_HUMAN	1471	RESAASG	1477	Extended
TB182_HUMAN	1508	RPQPDG	1513	Canonical
BCR_HUMAN	116	RPDGEG	121	Canonical
BCR_HUMAN	160	RIRKGHG	166	Extended
BCR_HUMAN	474	RDALVSG	480	Extended
CNOT1_HUMAN	685	RQPPPG	690	Canonical

CHAPTER 4

Adapted from:

Structural insights into SAM domain-mediated tankyrase oligomerization

Paul A. DaRosa[1,2], Sergey Ovchinnikov[1,3], Wenqing Xu[2#], Rachel E. Klevit[1#]

[1] Department of Biochemistry, University of Washington, Seattle, WA 98195
[2] Department of Biological Structure, University of Washington, Seattle, WA 98195
[3] Howard Hughes Medical Institute, University of Washington, Seattle, WA 98195

Published in the journal Protein Science.

Abstract

Tankyrase 1 (TNKS1; a.k.a. ARTD5) and tankyrase 2 (TNKS2; a.k.a ARTD6) are highly homologous poly(ADP-ribose) polymerases (PARPs) that function in a wide variety of cellular processes including Wnt signaling, Src signaling, Akt signaling, Glut4 vesicle translocation, telomere length regulation, and centriole and spindle pole maturation. Tankyrase proteins include a sterile alpha motif (SAM) domain that undergoes oligomerization *in vitro* and *in vivo*. However, the SAM domains of TNKS1 and TNKS2 have not been structurally characterized and the mode of oligomerization is not yet defined. Here we model the SAM domain-mediated oligomerization of tankyrase. The structural model, supported by mutagenesis and NMR analysis, demonstrates a helical, homotypic head-to-tail polymer that facilitates TNKS self-association. Furthermore, we show that TNKS1 and TNKS2 can form (TNKS1 SAM-TNKS2 SAM) hetero-oligomeric structures mediated by their SAM domains. Though wild-type tankyrase proteins have very low solubility, model-based mutations of the SAM oligomerization interface residues allowed us to obtain soluble TNKS proteins. These structural insights will be invaluable for the functional and

biophysical characterization of TNKS1/2, including the role of TNKS oligomerization in protein poly(ADP-ribosyl)ation (PARylation) and PARylation-dependent ubiquitylation.

Significance

Poly(ADP-ribose) is an important post-translational modification. The homologous poly(ADP-ribose) polymerase proteins, tankyrase 1 and 2, are significant drug targets for cancer therapies. The tankyrases contain a polymerizing domain known as a sterile alpha motif (SAM). Using molecular modeling and NMR spectroscopy, we characterize the tankyrase SAM oligomeric structure, establishing a basis for the study of the role of tankyrase oligomerization on its activities, including poly(ADP-ribosyl)ation and recruitment of substrate, and the reported tankyrase-mediated protein turnover.

Abbreviations

TNKS, Tankyrase; ARTD, diphtheria toxin-like ADP-ribosyltransferase; PAR, Poly(ADP-ribose); PARylation, Poly(ADP-ribosyl)ation; PARP, poly(ADP-ribose) polymerase; SAM, sterile alpha motif; PTEN, phosphatase and tensin homolog; GLUT4, glucose transporter 4; ITC, isothermal titration calorimetry; PDB, Protein Data Bank; HSQC, heteronuclear single quantum correlation spectroscopy

Introduction

Tankyrase-1 (TNKS1) and tankyrase-2 (TNKS2) constitute two of the six members of the *bona fide* human poly(ADP-ribose) polymerase (PARP) enzymes. TNKS1/2 Poly(ADP-ribosyl)ate (PARylate) proteins in a myriad of cellular functions including Wnt signaling,[1] Src signaling,[2] Hippo signaling,[3] telomere length regulation,[4] Glut-4 vesicle translocation,[5,6] and mitosis.[7–10] Not only is the PARylation of substrate required for all observed functions of TNKS, but PAR-dependent ubiquitylation mediated by RNF146 is also necessary for many TNKS1/2-mediated regulatory events, including Axin,[11–13] Angiomotin,[3] 3BP2,[2] and PTEN turnover.[14] These diverse regulatory functions have led to an intense focus on the development of TNKS1/2 PARP inhibitors for cancer therapies.[15–17] Characterization of the many protein-protein interactions required for TNKS1/2 function, such as substrate and RNF146 binding,[13] could facilitate more targeted small molecule or mutagenic pathway manipulation. Though the mechanism is currently unclear, TNKS1/2 oligomer formation has been suggested to affect the PARylation of substrates,[1,18] implying a potential regulatory function.

Of the six PARPs, the tankyrase proteins (TNKS) have unique domain compositions and TNKS1 and TNKS2 share ~83 percent identity (Fig. 1A). The sterile alpha motif (SAM) domain in TNKS1/2 is of particular interest because it is adjacent to the PARP domain—a position held by the PARP regulatory domain in other human poly-ADP-ribosylating enzymes.[19] SAM domains are composed of a ~70 amino acid helical structure in which three or four helices cradle a c-terminal helix and act as interaction motifs with diverse functions in signal transduction and transcriptional regulation.[20,21] SAM domains have been shown to mediate protein-protein,[21] protein-RNA,[22–24] and protein-lipid interactions.[25] Furthermore, SAM domains can bind themselves symmetrically, as in the example of Eph4A which forms a homodimer,[26] can bind

other SAM domains (e.g. odin binding to EphA2, and Ste11 binding to Ste50),[27–29] and can form long-range homo-oligomeric/polymeric structures.[30–37] While it is generally accepted that the SAM domain is largely responsible for the oligomerization of TNKS1/2,[38,39] the domain has not yet been structurally or biochemically characterized. It is still unknown whether the domain forms oligomers using multiple interfaces as observed for the SAM domain structure of EphB2 receptor,[40] homotypic oligomers with a single, distinct head-to-tail interface observed for other SAM polymers,[41] or utilizes some heretofore unobserved oligomeric topology. Furthermore, it is unclear whether the reported co-localization of TNKS1 and TNKS2[42] is due to association through SAM domain hetero-binding or mediated through the large ankyrin repeat cluster region (Fig. 1A).[18,43]

Here we model the tankyrase SAM oligomer structure revealing a head-to-tail oligomerization mode, with conserved interfaces for TNKS1 and TNKS2. Model-based mutations of residues in the interface generate monomeric TNKS1 and TNKS2 mutants, providing confirmation of the model. Because of their head-to-tail association, mixtures of two different interface mutants readily form homo- and heteromeric dimers with high affinity, consistent with the notion that TNKS1 and TNKS2 can form homo- and hetero-oligomer structures through their SAM domains. We have identified the residues involved in the SAM-SAM interaction using NMR spectroscopy as further experimental confirmation of the model. The data and the ability to generate well-defined, well-behaved tractable TNKS species will aid in future biophysical and functional characterization of TNKS.

Results

It is known that the tankyrase proteins are very insoluble and likely oligomerize through their SAM domains.[38,39,44] We therefore sought to determine the mode of SAM-domain mediated tankyrase oligomerization with the hope that controlling oligomerization might yield more soluble and therefore structurally and biochemically tractable proteins. We performed a fold prediction of the isolated TNKS1 SAM domain (residues1026-1088) using Rosetta ab initio,[45] which generated models that match a canonical SAM domain fold (Fig. 1B). The top 10 models produced by Rosetta were very similar, with an average pairwise root mean square deviation (RMSD) of 1.99 Å.

A TNKS1 oligomer model was generated from the top-scoring model, using clues from known SAM-SAM interfaces. Using TM-align,[46] the top-scoring Rosetta ab initio model was used to search the PDB for structurally similar domains, independent of sequence homology. From the top hits, all with TM-align score ≥ 0.6, we screened for entries containing multiple SAM-like folds. The TM-align search returned five SAM domains with significant structural similarity to TNKS1 (PDB codes: 3BQ7,[34] 3SEI,[47] 3TAD, 3TAC,[48] 1PK1[32]; 20-31 percent sequence identity) that contained SAM-SAM interfaces. Though the angles between SAM domains differ substantially in these structures, all contained asymmetric SAM-SAM interfaces centered on helix 5 (H5; termed the end-helix or EH surface) and a patch composed of helices 2, 3, and 4 (termed mid-loop or ML surface). By performing structural alignments between our TNKS1 SAM domain model and these SAM-SAM complex structures, we obtained initial docking positions. The RosettaCM[49] protocol was used to refine and generate homotypic TNKS1 SAM oligomer models. Despite different initial SAM-SAM orientations, the models converged on a single relative SAM-SAM angle with a maximum pairwise RMSD for the (dimeric) models of 1.16 Å. The resulting model shows a head-to-tail helical oligomer (Fig. 1B), similar to the

oligomeric structures of several other SAM domains[30–37] in which oligomers of SAM domains form a right-handed helix that contains ~6 protomers per turn. While these structures differ in their helical pitch (primarily determined by the angle between promoters), this helical form is likely adopted by many SAM oligomers.[41] Importantly, in our model the N and C-termini of the SAM domains are directed away from the core of the oligomer (Fig. 1B), consistent with the multi-domain architecture of TNKS1/2. It is unclear how the close proximity of the PARP domain might affect long-range polymer structure.

Inspection of the interface between protomers in our oligomer model revealed that the interaction is a combination of charge-charge and hydrophobic contacts. Notably, amino acids on opposing faces of the TNKS1/2 SAM domain are highly biased to generate electrostatic interactions (Fig. 1C). Furthermore, the residues that are predicted to participate in the interaction are nearly 100 percent conserved between TNKS1 and TNKS2 (Fig. 1D) and tankyrase orthologs (Supporting Information Fig. S1). Hence, this model predicts that the TNKS1 and TNKS2 may form homo and hetero-oligomers through their conserved SAM-SAM interface in a head-to-tail manner.

We attempted to express and purify proteins from *Escherichia Coli* for biochemical characterization, but were unable to purify detectable amounts of wild-type TNKS1 or TNKS2 or fragments containing the SAM domain by conventional means. This is consistent with the reported insolubility of the protein.[38] We therefore used our model to design missense mutations in TNKS1 and TNKS2 that are predicted to disrupt oligomerization. Because of the head-to-tail polymerization mode, we were able to identify potential positions at the interface of protomers in the oligomer, for example Y1073, D1055, and V1056 (Fig. 2A). The head-to-tail oligomerization model predicts that mutations on one surface should generate monomeric SAM domains (see Fig.

3A). Two mutants were generated in the SAM domains of both TNKS1 and TNKS2: Y1073E and D1055A/V1056K (referred to as YE, and DAVK, respectively; tankyrase 1 numbering). The resulting mutant proteins are highly soluble and NMR $^{1}H^{15}N$-HSQC analysis reveals that both mutant SAM-Linker (Fig. 1A) fragments of TNKS are folded as indicated by well-dispersed peaks in the ^{1}H dimension (Fig. 2B). The HSQC spectrum for TNKS1 SAM-Linker(DAVK) was assigned using conventional three-dimensional heteronuclear protocols, and the $^{13}C\alpha/^{13}C\beta$ chemical shifts were analyzed for secondary structure relative to predicted random coiled values (Fig. 2C). The NMR chemical shifts strongly predict five a-helices in locations consistent with our model, though the length of Helix-1 (H1) may be ~1 turn shorter than the Rosetta-predicted structure. The three N-terminal residues of H5 likely experience conformational heterogeneity as indicated by a drop in the chemical shift differences for residue H1075, which neighbors a glycine near the end of H5 (G1074), and by the apparent lack of an NH resonance from Y1073 in the ^{1}H ^{15}N-HSQC spectrum. Notably, conformational flexibility appears to be reduced in the oligomer (see below). Altogether, the NMR spectra are consistent with the predicted SAM fold for the protomers.

SEC-MALS analysis was performed on mutant constructs that include both the SAM and PARP domains (SAM-PARP; Fig. 1A). Each of the constructs migrate at the expected retention volume on a Superdex 200 column and exhibit monomeric molecular weights: TNKS1-YE 33.0 kDa ± 1.73 %, TNKS1-DAVK 33.7 kDa ± 0.986 %, TNKS2-YE 33.5 kDa ± 0.461 %, and TNKS2-DAVK 33.9 kDa ± 0.469 % (Fig. 3A and Fig. 3B top). When YE and DAVK mutants are mixed, the resulting species co-migrate on a SEC column (Fig. 3A and Fig. 3B top), forming a complex near the expected molecular weight of a SAM-PARP dimer (57.8 kDa ± 1.69 % for TNKS1 and 63.0 kDa ± 1.16 % for TNKS2). Consistent with the long-lived interaction detected

by SEC, the binding affinity (K_d) between TNKS1 SAM-Linker DAVK and YE mutants measured by isothermal Titration Calorimetry (ITC) is 469(±38) nM (Fig. 3C left). As the dimers formed between the two mutants likely do so through their unmutated (i.e., native) interface, the data imply a strong propensity of TNKS to form homo-oligomers. As predicted by the strong conservation in the oligomeric interface between TNKS1 and TNKS2, mixtures of TNKS1-YE and TNKS2-DAVK co-elute as a heterodimer, with a molecular weight of 64.1 kDa ± 0.549 % (Fig. 3B bottom). The strength of this interaction was determined to be 427(±20) nM by ITC (Fig. 3C right). Thus, our data reveal a roughly equal preference for TNKS hetero-oligomer formation and TNKS1 homo-oligomerization, confirming that the two proteins can form hetero-oligomers through their SAM domains[42] and are likely to do so *in vivo*. Furthermore, placing SAM mutations in the context of full-length TNKS2 can generate soluble protein (Supporting Information Fig. S2), suggesting that the SAM domain makes a large contribution to the overall oligomeric assembly of TNKS.

To investigate the residues involved in the interaction interface, we performed NMR chemical shift perturbation analysis. Titration of TNKS1 SAM-Linker(YE) into ^{15}N-labeled TNKS1 SAM-Linker(DAVK) produced profound shifts in residues at the beginning of and throughout H5 (Fig. 4A and B). Furthermore, while a peak is not observed for Y1073 in the initial spectrum of ^{15}N-labeled TNKS1 SAM-Linker(DAVK), backbone assignments of the bound domain in a fully saturated sample confirmed the appearance of an amide peak for Y1073 (Fig. 4A). This suggests that Y1073 undergoes a conformational exchange process in the monomeric SAM domain and is stabilized upon dimer formation. Mapping of the most perturbed residues (Fig. 4B) on the surface of the dimer model confirms the predicted surface to be directly involved (Fig. 4C). Importantly, the NMR data indicate that binding only occurs at one interface,

and does not appear to involve multiple surfaces between TNKS1 SAM domains in solution. These results not only provide key support for our model but also indicate that it can be used to identify other candidate residues for monomerizing mutations in the future.

Discussion

We have shown that TNKS polymerizes through its SAM domain in a head-to-tail fashion to form a predicted helical oligomer. Mutations in the SAM domain can generate folded, monomeric proteins that can subsequently dimerize when mixed with complementary surface mutations. Furthermore, we have shown that the native SAM-SAM interactions are relatively strong, with K_d values below 500 nM for TNKS1 homodimerization and for TNKS1/TNKS2 heterodimerization. These values suggest that oligomers formed *in vivo* may contain both homomeric and heteromeric interfaces. Though this work indicates a major role for the SAM domain in TNKS oligomerization, the estimates of TNKS solubility (<40 nM)[38] may imply that other regions, such as the third ankyrin-repeat cluster,[43] may also contribute to oligomeric assembly.

Our results and their structural insights provide a basis to investigate 1) the role of oligomerization for substrate PARylation *in vivo*; and 2) the potential effects of the SAM domain on inhibitor binding.[15,50,51] How TNKS oligomerization affects substrate binding to the ankyrin repeat regions, PARylation activity, and subsequent ubiquitination of key cellular proteins such as Axin and Angiomotin remain to be investigated. It is likely that the multivalent nature of both TNKS oligomerization and its substrate or RNF146 binding will be affected by mutations in the SAM domain. This study provides a path forward towards a fine-grained approach to studying the importance of TNKS oligomerization *in vivo*.

Figures

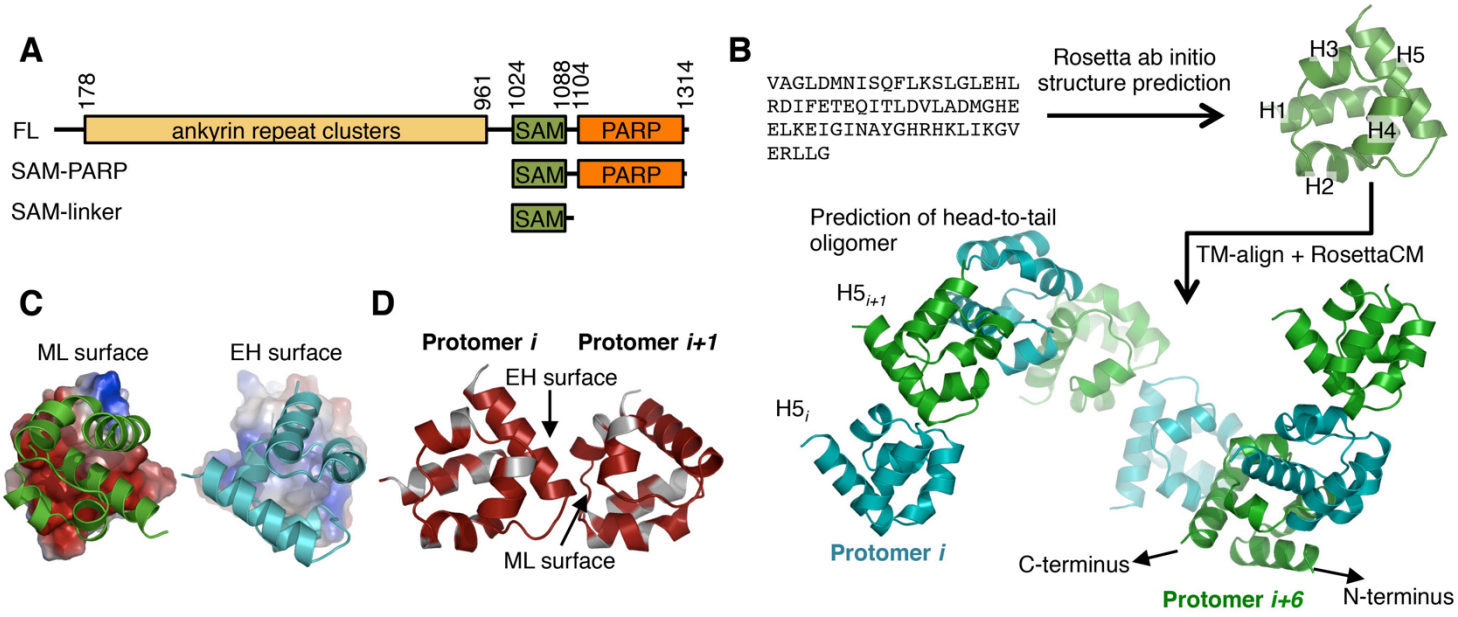

Figure 1 | Modeling tankyrase SAM domain oligomerization. (**A**) The TNKS1 domain architecture and constructs used in this manuscript. TNKS2 is highly homologous to TNKS1, but lacks a ~170 amino acid N-terminal histidine serine proline rich region in Tankyrase 1. FL; full-length. (**B**) Schematic of the TNKS1 SAM domain structure and oligomeric structure prediction workflow. First, the amino acid sequence was used for structure prediction using Rosetta, followed by a TM-align search for similar folds participating in SAM-SAM interactions used as initial docking positions for a RosettaCM TNKS1 oligomer modeling protocol with helical symmetry. H1-5; Helix 1, 2, 3, 4, and 5. Protomers are colored either green or cyan to clarify oligomeric structure. (**C**) Surface charges experienced by opposing faces of the oligomer protomers. Between the two interacting surfaces, the mid-loop (ML) surface (*left*) is negatively charged (red), whereas the end-helix (EH) surface is enriched in positively (blue) charged residues (*right*). (**D**) Conservation of residues between TNKS1 and TNKS2 plotted on the surface of the TNKS1 model showing sequence identity (red) at the interface of the two protomers. White; non-identical. See also Supporting Information Fig. S1.

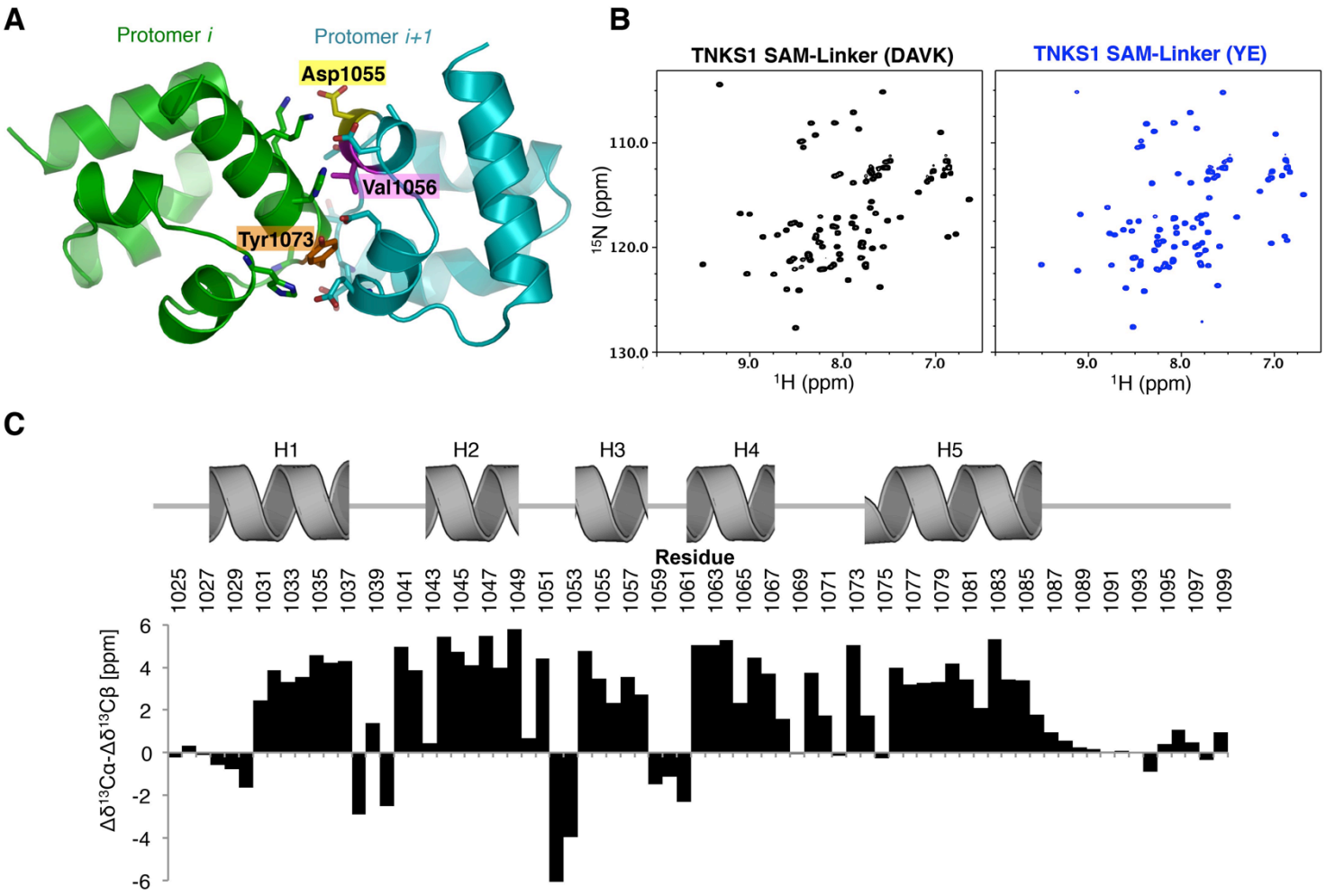

Figure 2| SAM mutants retain a folded structure. (**A**) Residues at the interface of two protomers in the predicted oligomer interface of TNKS1. Residues that were mutated to disrupt oligomerization are highlighted. (**B**) $^{1}H^{15}N$-HSQC NMR analysis of the TNKS1 SAM-Linker(DAVK) mutant (*left),* and the TNKS1 SAM-Linker(YE) mutant (*right)*. DAVK, D1055A/V1056K; YE, Y1073E. Both spectra are well dispersed and highly similar, consistent with folded, monomeric domains. (**C**) Chemical shift differences between random coil and experimentally determined Cα and Cβ atoms ($\Delta\delta^{13}C\alpha$-$\Delta\delta^{13}C\beta$ [ppm]). High values are predictive of helical structure.

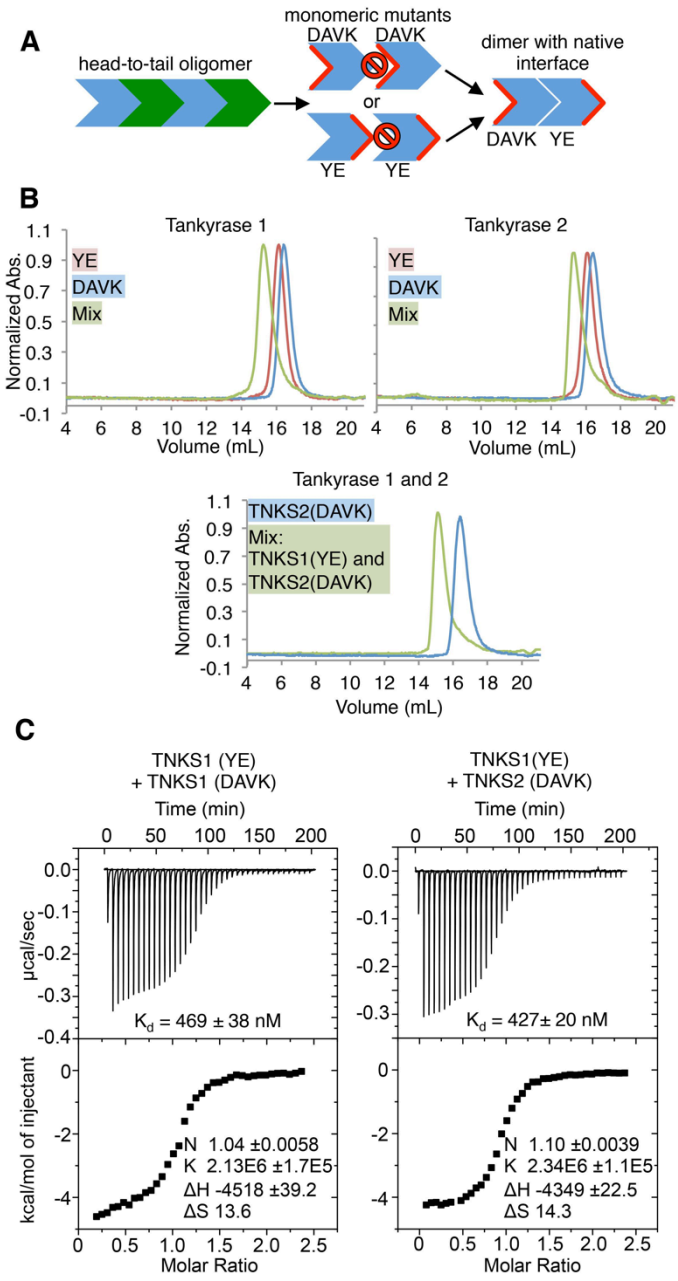

Figure 3| Tankyrase 1/2 SAM form strong homo and hetero-oligomers. (**A**) Conceptual schematic of experiments in Fig. 3. Residues are mutated on one face of the oligomeric interface to generate monomers (*center*). Complementary monomers can be mixed to generate dimers (*right*). Red indicates mutated surface. Prohibition signs indicate no-binding. YE, TNKS1 Y1073E or TNKS2 Y920E; DAVK, TNKS1 D1055A/V1056K or TNKS2 D902A/V903K. (**B**) Size exclusion chromatography (SEC) chromatograms of tankyrase 1 (*top left*) and tankyrase 2 (*top right*) SAM-PARP YE and DAVK mutants. (*Bottom*) SEC trace of a 1:1 mixture of SAM-PARP TNKS1 YE and TNKS2 DAVK, with TNKS2 DAVK elution profile shown as a reference. The maximum absorbance at 280 nm (y-axis) is normalized to 1 for each trace. (**C**) Isothermal titration calorimetry (ITC) of TNKS1 SAM-Linker YE with DAVK mutants *(left;* K_d of 469 ± 38 nM), and TNKS1 SAM-Linker(YE) with TNKS2 SAM-Linker(DAVK) (*right*; K_d of 427 ± 20 nM). K_d, dissociation constants.

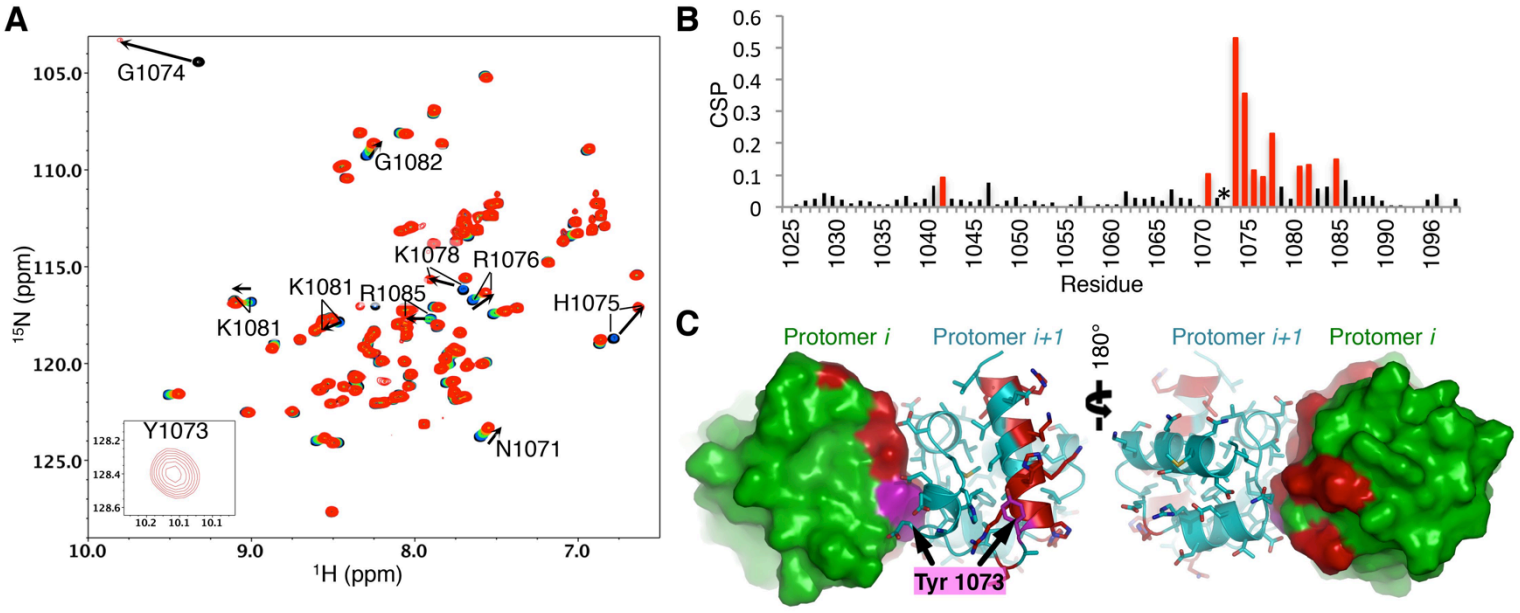

Figure 4| NMR mapping of the oligomeric interface supports model. (**A**) $^{1}H^{15}N$-HSQC of 150 µM TNKS1 SAM-Linker(D1055A/V1056K) (black) with increasing quantities of TNKS1 SAM-Linker(Y1073E): 0.25 molar equivalence (mol. eq.) (blue), 0.5 mol. eq. (green), 0.75 mol. eq. (orange), and 1.1 mol. eq. (red). A weak peak is seen for Y1073 at 1.1 mol. eq. when a spectrum was obtained at 250 uM TNKS1 SAM-Linker(D1055A/V1056K), but not in the unbound spectrum in matching conditions (*inset).* (**B**) Chemical shift perturbations (CSPs) determined between the 0 mol. eq. (black) and 1.1 mol. eq. (red) spectra shown in (A) plotted against residue number. Red bars indicate the top 15 percent most perturbed residues. Asterisk (*) indicates Y1073, which only has a detectable peak in the dimeric form. (**C**) Residues shown in (B) are plotted (red) on the surface/cartoon representation of two neighboring protomers (cyan and green) of the oligomer. The residue highlight in magenta is Y1073. The binding surface recapitulates the predicted interface between protomers.

Materials and Methods

Generation of the SAM oligomer model

The TNKS1 oligomer model was generated using a combination of structural homology and computational efforts. Rosetta *ab initio*[45] design was performed on TNKS1 SAM domain (residues 1018-1092) producing 62200 models. Models were trimmed to include only the core SAM domain (residues 1026-1088) for further modeling. The top model was used to search the PDB using TM-align[46] for structurally similar SAM domains that appear in deposited structures with multiple SAM folds. The top structural homologs identified by TM-align with SAM-SAM interfaces were used to generate starting positions for the oligomer model; these deposited structures were structurally aligned with our isolated SAM model, then used to model and refine the TNKS1 SAM oligomer in helical symmetry with RosettaCM.[49] During sampling, the side-chains, backbone, and symmetric definition were allowed to change and fragment insertion was allowed at all positions. No restraints were used, allowing for full degrees of motion. The final oligomer models converged on the same mode of interaction (SAM-SAM angle) most resembling the interface present in the PDB entry 1PK1. Therefore, while the SAM domain fold was predicted, this initial model was compared to homologous SAM structures to find clues about potential oligomeric interfaces. Hence the final model is a combination of fold prediction and homology assisted modeling.

Protein Expression and Purification

Mouse TNKS1 and human TNKS2 fragments or full-length protein were cloned into a pET-28a expression plasmid (Novagen, Madison, Wisconsin) with an N-terminal His_6 tag and tobacco etch virus (TEV) cleavage site and/or a pAL-SUMO plasmid (Zheng Lab, University of Washington) with N-terminal His_6, SUMO tag, and TEV protease site upstream of the TNKS

sequences. Site directed mutagenesis in the SAM domain was used to generate soluble TNKS fragments. All tags were removed before protein use unless otherwise noted. All regions in mouse TNKS1 used have 100 percent sequence identity to the human sequence at the protein level.

All proteins were expressed in *Escherichia coli* (BL-21) by induction with 0.10-0.20 mM isopropyl β-D-1-thiogalactopyranoside (IPTG; Research Products International, Mt. Prospect, Illinois) at an *attenuance* (D) of 0.6-1.2 at 600 nm in either LB media or $^{15}N/^{13}C$ minimal mops media and grown over night at 16 °C. TNKS1 SAM-PARP (residues 1024-1314) and TNKS1 SAM-Linker (residues 1024-1102) construct mutants (Y1073E and D1055A/V1056K) and TNKS2 SAM-Linker (residues 871-952) mutants (D902A/V903K and Y920E) were purified by Ni-NTA resin (Qiagen, Hilden, Germany), followed by dialysis in the presence of His-tagged TEV protease to remove imidazole. TEV was captured on Ni-NTA column and the eluates containing TNKS proteins were concentrated and further purified by SEC. TNKS2 SAM-PARP (residues 871-1166) mutants (D902A/V903K and Y920E) were purified by Talon resin (Clonetech, Mountain view, California), followed by a TEV cleavage to remove tags, and dialyzed overnight at 4 °C. After capturing TEV on a Talon resin, protein was then diluted in 30 mM MES pH 6.0 buffer to a salt concentration of <50 mM and purified using an SP column (GE Healthcare, Pittsburgh, Pennsylvania). Protein eluted from the SP column near 350 mM NaCl, was concentrated, and further purified by SEC into appropriate buffers.

Size Exclusion Chromatography and SEC-MALS

Size exclusion chromatography (SEC) and SEC-multi-angle light scattering (SEC-MALS) was performed at room temperature on a Superdex 200 10/300 GL (GE Healthcare) and a Superdex 200 Increase 3.2/300 (GE Healthcare), respectively, in running buffer (20 mM Tris-

HCl pH 7.5, 150 mM NaCl). For SEC, ~80-100 μg of samples was protein was injected in a 100 μL volume and elution profiles were monitored at 280 nm on an AtkaPurifier (GE Healthcare). Fifteen microliters of SEC-MALS samples were injected at 2 mg/mL onto a AktaPure purification system (GE Healthcare) equipped with a MiniDawn TREOS and a Optilab T-rEX detectors (Wyatt, Santa Barbara, California). SEC-MALS data was processed in the Astra (Wyatt) software. Reported molecular weights are average values over the length of the peak.

ITC

ITC was performed on a VP-ITC MicroCal colorimeter (Malvern Instruments Ltd., Worcestershire, United Kingdom) at 20 °C. Proteins were dialyzed into 25 mM sodium phosphate pH 7.0, 150 mM NaCl buffer overnight before use. For TNKS1-TNKS1 SAM binding, TNKS1 SAM-Linker(D1055A/V1056K) was concentrated to 400 μM (titrant) and TNKS1 SAM-Linker(Y1073E) was used at 20 μM (titrand). For TNKS1-TNKS2 binding, TNKS1 SAM-Linker(Y1073E) protein was concentrated to 400 μM (titrant) and the TNKS2 SAM-Linker(D902A/V903K) mutant (residues 871-952) was concentrated to 20 μM (titrand). Proteins were degassed before use. Titrant was added in 5 μL injections with a delay between each addition of 300 sec. A total of 40 injections were performed for each titration. Data was analyzed with the Origin 7.0 software (OriginLab Corp, Wellesley Hills, Massachusetts); curves were fit to a 1-site model.

NMR Spectroscopy

NMR data was collected on a Bruker Avance 600 mHz spectrometer fitted with a TCI CryoProbe (Bruker, Billerica, Massachusetts). All NMR data sets were obtained at 25 °C in 25 mM sodium phosphate pH 7.0, 150 mM NaCl. A standard set of triple resonance NMR experiments (CBCACONH, HNCACB, HNCOCA, HNCA)[52,53] were used for assignments of the

TNKS1 SAM-Linker(D1055A/V1056K) protein (assigned residues: 1025-1099) were acquired with 250 μM ^{15}N-^{13}C-labeled TNKS1 SAM-Linker(D1055A/V1056K), in the absence and presence of 322 μM unlabeled TNKS1 SAM-Linker(Y1073E) (bound spectrum). For the bound spectrum, assignments were guided by the unbound spectrum and were confirmed by triple resonance experiments. Assignments can be found in the supplementary material. ^{15}N-HSQC experiments were performed with 150 μM ^{15}N-labeled TNKS1 SAM-Linker(D1055A/V1056K) in the absence or presence of 38 μM, 75 μM, 94μM and 165 μM unlabeled TNKS1 SAM-Linker(Y1073E). All NMR data was processed with NMRPipe.[54] Peak intensity, chemical shift analysis, and NMR assignments were determined using NMRViewJ.[55] Predicted chemical shifts for the disordered sequence of TNKS1 SAM-Linker(D1055A/V1056K) were generated using a SBiNLab java script coded by Alex Maltsev using published calculations.[56–58] Deviations from predicted intrinsically disordered chemical shifts were calculated by the formula $\Delta\delta^{13}C\alpha$-$\Delta\delta^{13}C\beta$ [ppm], where $\Delta\delta^{13}C\alpha$ and $\Delta\delta^{13}C\beta$ are the difference between the disordered values and experimental values for Cα chemical shifts and Cβ chemical shifts, respectively. Chemical shift perturbations were determined using the formula $\Delta\delta j = [(^{15}N\Delta\delta j/5)^2 + (^{1}H\Delta\delta j)^2]^{1/2}$ where $^{15}N\Delta\delta j$ and $^{1}H\Delta\delta j$ are the difference in chemical shift between the bound and unbound states of TNKS1 SAM-Linker(D1055A/V1056K), respectively. The top 15 percent most perturbed residues were mapped onto the surface/cartoon of two SAM domain protomers within the oligomeric model of TNKS1.

Supplemental materials

There are two supplementary figures in the supporting information document included with this manuscript, and an excel spreadsheet containing NMR assignments for the TNKS1 SAM-Linker(D1055A/V1056K) mutant (see below).

Acknowledgements

We thank David Baker for computational resources used to generate our model. This work was supported by the National Institutes of Health (NIH) grant R01 GM099766 to W.X. and R.E.K., NIH T32 GM007270 to P.A.D., and NIH R01 GM092802 to David Baker (University of Washington).

Conflicts of Interest

The authors declare no conflicts of interest.

References

1. Huang SM a, Mishina YM, Liu S, Cheung A, Stegmeier F, Michaud GA, Charlat O, Wiellette E, Zhang Y, Wiessner S, et al. (2009) Tankyrase inhibition stabilizes axin and antagonizes Wnt signalling. Nature 461:614–620.

2. Levaot N, Voytyuk O, Dimitriou I, Sircoulomb F, Chandrakumar A, Deckert M, Krzyzanowski PM, Scotter A, Gu S, Janmohamed S, et al. (2011) Loss of Tankyrase-mediated destruction of 3BP2 is the underlying pathogenic mechanism of cherubism. Cell 147:1324–1339.

3. Wang W, Li N, Li X, Tran MK, Han X, Chen J (2015) Tankyrase Inhibitors Target YAP by Stabilizing Angiomotin Family Proteins. Cell Rep. 13:524–532.

4. Smith S, De Lange T (2000) Tankyrase promotes telomere elongation in human cells. Curr. Biol. 10:1299–1302.

5. Yeh T-YJ, Sbodio JI, Tsun ZY, Luo B, Chi NW (2007) Insulin-stimulated exocytosis of GLUT4 is enhanced by IRAP and its partner tankyrase. Biochem. J. 402:279–290.

6. Guo HL, Zhang C, Liu Q, Li Q, Lian G, Wu D, Li X, Zhang W, Shen Y, Ye Z, et al. (2012) The Axin/TNKS complex interacts with KIF3A and is required for insulin-stimulated GLUT4 translocation. Cell Res 22:1246–1257.

7. Dynek JN, Smith S (2004) Resolution of sister telomere association is required for progression

through mitosis. Science 304:97–100.

8. Chang P, Coughlin M, Mitchison TJ (2005) Tankyrase-1 polymerization of poly(ADP-ribose) is required for spindle structure and function. Nat. Cell Biol. 7:1133–1139.

9. Kim MK, Dudognon C, Smith S (2012) Tankyrase 1 regulates centrosome function by controlling CPAP stability. EMBO Rep. 13:724–732.

10. Ozaki Y, Matsui H, Asou H, Nagamachi A, Aki D, Honda H, Yasunaga S, Takihara Y, Yamamoto T, Izumi S, et al. (2012) Poly-ADP Ribosylation of Miki by tankyrase-1 Promotes Centrosome Maturation. Mol. Cell 47:694–706.

11. Zhang Y, Liu S, Mickanin C, Feng Y, Charlat O, Michaud G a, Schirle M, Shi X, Hild M, Bauer A, et al. (2011) RNF146 is a poly(ADP-ribose)-directed E3 ligase that regulates axin degradation and Wnt signalling. Nat. Cell Biol. 13:623–9.

12. Callow MG, Tran H, Phu L, Lau T, Lee J, Sandoval WN, Liu PS, Bheddah S, Tao J, Lill JR, et al. (2011) Ubiquitin ligase RNF146 regulates tankyrase and Axin to promote Wnt signaling. PLoS One 6.

13. DaRosa PA, Wang Z, Jiang X, Pruneda JN, Cong F, Klevit RE, Xu W (2014) Allosteric activation of the RNF146 ubiquitin ligase by a poly(ADP-ribosyl)ation signal. Nature 517:223–226.

14. Li N, Zhang Y, Han X, Liang K, Wang J, Feng L, Wang W, Songyang Z, Lin C, Yang L, et al. (2015) Poly-ADP ribosylation of PTEN by tankyrases promotes PTEN degradation and tumor growth. Genes Dev. 29:157–170.

15. Haikarainen T, Krauss S, Lehtio L (2014) Tankyrases: structure, function and therapeutic implications in cancer. Curr. Pharm. Des. 20:6472–88.

16. Lehtio L, Chi NW, Krauss S (2013) Tankyrases as drug targets. FEBS J. 280:3576–3593.

17. Riffell JL, Lord CJ, Ashworth A (2012) Tankyrase-targeted therapeutics: expanding opportunities in the PARP family. Nat. Rev. Drug Discov. 11:923–36.

18. Hatsugai K, Ohishi T, Sugimoto Y, Seimiya H (2010) Tankyrase-1 assembly to large protein complexes blocks its telomeric function. FEBS Lett. 584:3885–3890.

19. Langelier MF, Planck JL, Roy S, Pascal JM (2012) Structural basis for DNA damage-dependent poly(ADP-ribosyl)ation by human PARP-1. Science 336:728–32.

20. Qiao F, Bowie JU (2005) The Many Faces of SAM. Sci. Signal. 2005:re7–re7.

21. Kim CA, Bowie JU (2003) SAM domains: Uniform structure, diversity of function. Trends Biochem. Sci. 28:625–628.

22. Johnson PE, Donaldson LW (2006) RNA recognition by the Vts1p SAM domain. Nat. Struct. Mol. Biol. 13:177–178.

23. Oberstrass FC, Lee A, Stefl R, Janis M, Chanfreau G, Allain FHT (2006) Shape-specific

recognition in the structure of the Vts1p SAM domain with RNA. Nat. Struct. Mol. Biol. 13:160–167.

24. Aviv T, Lin Z, Lau S, Rendl LM, Sicheri F, Smibert CA (2003) The RNA-binding SAM domain of Smaug defines a new family of post-transcriptional regulators. Nat Struct Mol Biol 10:614–621.

25. Bhunia A, Domadia PN, Mohanram H, Bhattacharjya S (2009) NMR structural studies of the Ste11 SAM domain in the dodecyl phosphocholine micelle. Proteins Struct. Funct. Bioinforma. 74:328–343.

26. Stapleton D, Balan I, Pawson T, Sicheri F (1999) The crystal structure of an Eph receptor SAM domain reveals a mechanism for modular dimerization. Nat. Struct. Mol. Biol. 6:44–49.

27. Mercurio FA, Marasco D, Pirone L, Pedone EM, Pellecchia M, Leone M (2012) Solution structure of the first Sam domain of Odin and binding studies with the EphA2 receptor. Biochemistry 51:2136–2145.

28. Leone M, Cellitti J, Pellecchia M (2008) NMR Studies of a Heterotypic Sam-Sam Domain Association: The Interaction between the Lipid Phosphatase Ship2 and the EphA2 Receptor. Biochemistry 47:12721–12728.

29. Kwan JJ, Warner N, Pawson T, Donaldson LW (2004) The solution structure of the S. cerevisiae Ste11 MAPKKK SAM domain and its partnership with Ste50. J. Mol. Biol. 342:681–693.

30. Kim CA, Phillips ML, Kim W, Gingery M, Tran HH, Robinson MA, Faham S, Bowie JU (2001) Polymerization of the SAM domain of TEL in leukemogenesis and transcriptional repression. EMBO J. 20:4173–4182.

31. Kim CA, Gingery M, Pilpa RM, Bowie JU (2002) The SAM domain of polyhomeotic forms a helical polymer. Nat. Struct. Biol. 9:453–457.

32. Kim CA, Sawaya MR, Cascio D, Kim W, Bowie JU (2005) Structural organization of a sex-comb-on-midleg/polyhomeotic copolymer. J. Biol. Chem. 280:27769–27775.

33. Baron MK, Boeckers TM, Vaida B, Faham S, Gingery M, Sawaya MR, Salyer D, Gundelfinger ED, Bowie JU (2006) An architectural framework that may lie at the core of the postsynaptic density. Science 311:531–535.

34. Harada BT, Knight MJ, Imai S, Qiao F, Ramachander R, Sawaya MR, Gingery M, Sakane F, Bowie JU (2008) Regulation of Enzyme Localization by Polymerization: Polymer Formation by the SAM Domain of Diacylglycerol Kinase delta1. Structure 16:380–387.

35. Leettola CN, Knight MJ, Cascio D, Hoffman S, Bowie JU (2014) Characterization of the SAM domain of the PKD-related protein ANKS6 and its interaction with ANKS3. BMC Struct. Biol. 14:17.

36. Sayou C, Nanao MH, Jamin M, Posé D, Thévenon E, Grégoire L, Tichtinsky G, Denay G, Ott F, Peirats Llobet M, et al. (2016) A SAM oligomerization domain shapes the genomic

binding landscape of the LEAFY transcription factor. Nat. Commun. 7:11222.

37. Nanyes DR, Junco SE, Taylor AB, Robinson AK, Patterson NL, Shivarajpur A, Halloran J, Hale SM, Kaur Y, Hart PJ (2014) Multiple polymer architectures of human polyhomeotic homolog 3 sterile alpha motif. Proteins Struct. Funct. Bioinforma. 82:2823–2830.

38. De Rycker M, Price CM (2004) Tankyrase polymerization is controlled by its sterile alpha motif and poly(ADP-ribose) polymerase domains. Mol. Cell. Biol. 24:9802–12.

39. De Rycker M, Venkatesan RN, Wei C, Price CM (2003) Vertebrate tankyrase domain structure and sterile alpha motif (SAM)-mediated multimerization. Biochem. J. 372:87–96.

40. Thanos CD, Goodwill KE, Bowie JU (1999) Oligomeric structure of the human EphB2 receptor SAM domain. Science 283:833–836.

41. Meruelo AD, Bowie JU (2009) Identifying polymer-forming SAM domains. Proteins Struct. Funct. Bioinforma. 74:1–5.

42. Sbodio JI, Lodish HF, Chi NW (2002) Tankyrase-2 oligomerizes with tankyrase-1 and binds to both TRF1 (telomere-repeat-binding factor 1) and IRAP (insulin-responsive aminopeptidase). Biochem. J. 361:451–459.

43. Morrone S, Cheng Z, Moon RT, Cong F, Xu W (2012) Crystal structure of a Tankyrase-Axin complex and its implications for Axin turnover and Tankyrase substrate recruitment. Proc. Natl. Acad. Sci. 109:1500–1505.

44. Knight MJ, Leettola C, Gingery M, Li H, Bowie JU (2011) A human sterile alpha motif domain polymerizome. Protein Sci. 20:1697–1706.

45. Simons KT, Ruczinski I, Kooperberg C, Fox BA, Bystroff C, Baker D (1999) Improved recognition of native‐like protein structures using a combination of sequence‐dependent and sequence‐independent features of proteins. Proteins Struct. Funct. Bioinforma. 34:82–95.

46. Zhang Y, Skolnick J (2005) TM-align: a protein structure alignment algorithm based on the TM-score. Nucleic Acids Res. 33 :2302–2309.

47. Stafford RL, Hinde E, Knight MJ, Pennella MA, Ear J, Digman MA, Gratton E, Bowie JU (2011) Tandem SAM Domain Structure of Human Caskin1: A Presynaptic, Self-Assembling Scaffold for CASK. Structure 19:1826–1836.

48. Wei Z, Zheng S, Spangler SA, Yu C, Hoogenraad CC, Zhang M (2011) Liprin-Mediated Large Signaling Complex Organization Revealed by the Liprin-α/CASK and Liprin-α/Liprin-β Complex Structures. Mol. Cell 43:586–598.

49. Song Y, DiMaio F, Wang RY-R, Kim D, Miles C, Brunette TJ, Thompson J, Baker D (2013) High-resolution comparative modeling with RosettaCM. Structure 21:1735–1742.

50. Narwal M, Koivunen J, Haikarainen T, Obaji E, Legala OE, Venkannagari H, Joensuu P, Pihlajaniemi T, Lehtiö L (2013) Discovery of tankyrase inhibiting flavones with increased potency and isoenzyme selectivity. J. Med. Chem. 56:7880–7889.

51. Narwal M, Haikarainen T, Fallarero A, Vuorela PM, Lehtiö L (2013) Screening and structural analysis of flavones inhibiting tankyrases. J. Med. Chem. 56:3507–3517.

52. Sattler M, Schleucher J, Griesinger C (1999) Heteronuclear multidimensional NMR experiments for the structure determination of proteins in solution. Prog. Nucl. Magn. Reson. Spectrosc. 34:93–158.

53. Muhandiram DR, Kay LE (1994) Gradient-Enhanced Triple-Resonance Three-Dimensional NMR Experiments with Improved Sensitivity. J. Magn. Reson. Ser. B 103:203–216.

54. Delaglio F, Grzesiek S, Vuister GW, Zhu G, Pfeifer J, Bax A (1995) NMRPipe: A multidimensional spectral processing system based on UNIX pipes. J. Biomol. NMR 6:277–293.

55. Johnson BA, Blevins RA (1994) NMR View: A computer program for the visualization and analysis of NMR data. J. Biomol. NMR 4:603–614.

56. Kjaergaard M, Poulsen FM (2011) Sequence correction of random coil chemical shifts: Correlation between neighbor correction factors and changes in the Ramachandran distribution. J. Biomol. NMR 50:157–165.

57. Kjaergaard M, Brander S, Poulsen FM (2011) Random coil chemical shift for intrinsically disordered proteins: Effects of temperature and pH. J. Biomol. NMR 49:139–149.

58. Schwarzinger S, Kroon GJA, Foss TR, Chung J, Wright PE, Dyson HJ (2001) Sequence-dependent correction of random coil NMR chemical shifts. J. Am. Chem. Soc. 123:2970–2978.

Supplemental Data

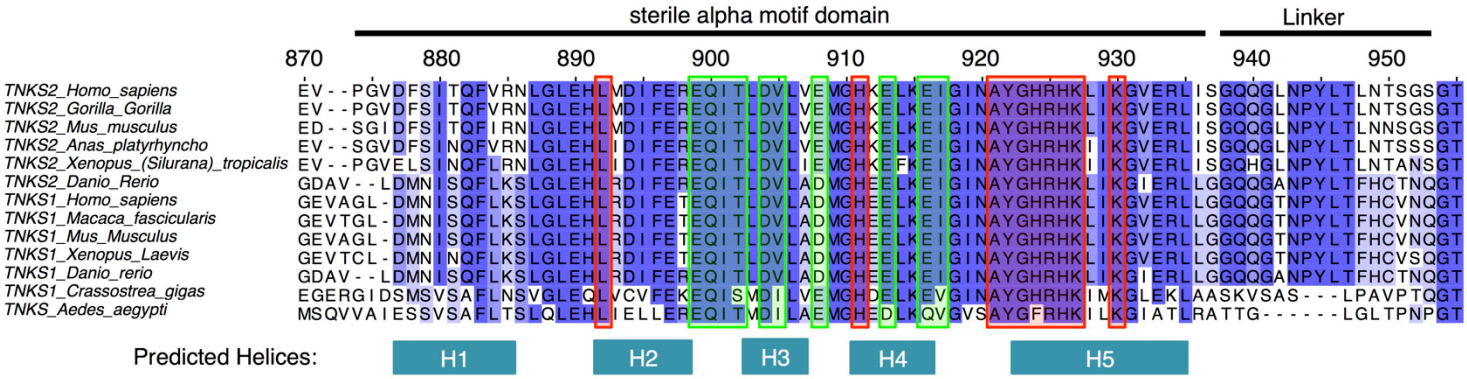

Supporting Information Figure S1| Sequence alignment of hTNKS1/2 SAM domains and orthologues. Sequence alignment showing the sterile alpha motif domain (SAM) and linker regions of TNKS1/2 and some of their orthologues. The SAM domain is well conserved. Human TNKS1 and TNKS2 SAM domains are 75 percent conserved. The positions of the five predicted helices (H1, H2, H3, H4, and H5) of the SAM domain are shown below the sequences (based on our model). Green boxes indicate residues on the surface generated between H2-H4 (mid-loop surface) that are at the predicted oligomeric interface; red boxes indicate residues on the H5 oligomeric interface (end-helix surface). Intensity of blue color indicates the degree of conservation at each position.

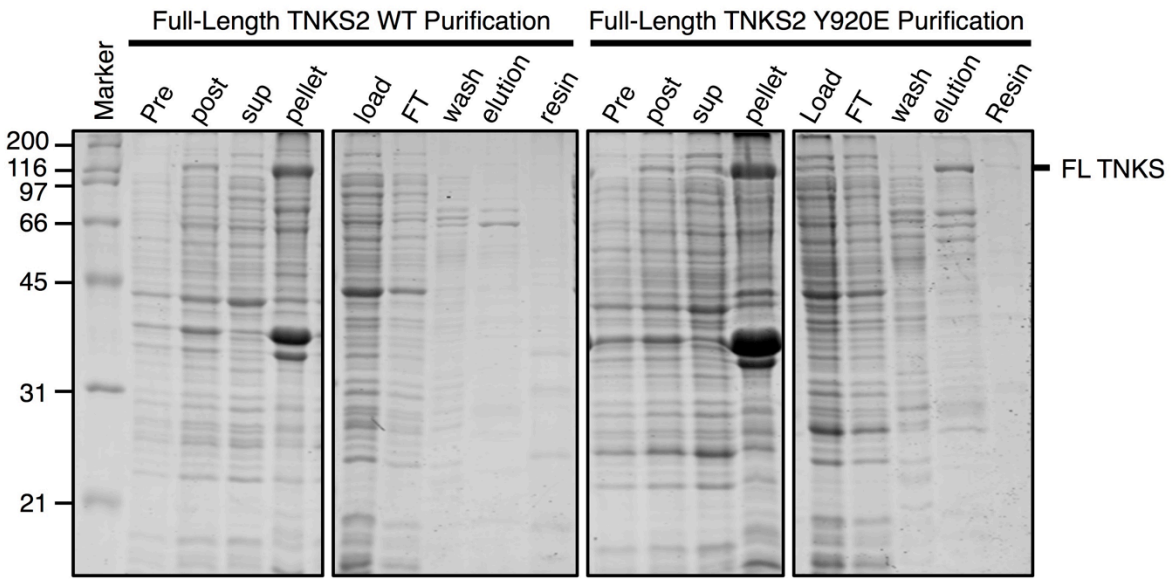

Supporting Information Figure S2| Mutant, but not wild-type TNKS2 can be purified from *Escherichia Coli*. Coomassie-stained SDS-PAGE gel of full-length TNKS2 purification. While both wild-type and mutants proteins were detectibly expressed, only mutant protein was retained in the soluble fraction. Whereas the wild-type protein could not be purified, the Y920E mutant protein could be purified using Ni-NTA resin in 20 mM Tris pH 7.6, 500 mM NaCl. Pre, cells before induction with IPTG; Post, after induction with 50 mg/L IPTG; sup, supernatant/soluble fraction after lysis and centrifugation; pellet, insoluble fraction after centrifugation; load, sample loaded onto Ni-NTA (same as "sup", but filtered through 0.22 μm filter); FT, flow-through/unbound material eluted from the Ni-NTA during protein binding in the presence of 5 mM imidazole; wash, wash step with 30 mM imidazole; elution, elution of protein with 500 mM imidazole, resin, boiled in SDS-PAGE sample loading buffer after elution. The Y920E mutant was eluted from the Ni-NTA in a soluble form and did not aggregate on the column resin.

Supporting Information Table 1: SAM mutant (DAVK) unbound assignments

Unbound Assignments

Sequence: GVAGLDMNIS QFLKSLGLEH LRDIFETEQI TLakLADMGH
EELKEIGINA YGHRHKLIKG VERLLGGQQG TNPYLTFHCV NQG

The following assignments are for TNKS1 SAM-Linker (D1055A/V1056K) at 250 uM

		Chemical Shift				
residue	ID	HN	N	C alpha	C beta	NOTE
1023	G					unassigned
1024	V			62.34	32.56	unassigned NH
1025	A	8.51	127.63	52.78	19.28	
1026	G	8.340	108.170	45.510	-	
1027	L	8.03	120.62	55.05	42.13	
1028	D	8.36	120.78	54.09	40.97	
1029	M	7.78	121.00	56.09	34.05	
1030	N	8.37	120.76	53.06	39.67	
1031	I	8.75	122.65	63.00	37.87	
1032	S	8.25	118.39	62.50	-	unassigned Cbeta
1033	Q	8.09	121.74	58.61	28.51	
1034	F	8.21	122.11	60.98	39.177	
1035	L	8.70	118.86	58.10	40.75	
1036	K	8.06	119.99	59.90	32.1	
1037	S	8.06	117.25	61.62	62.81	
1038	L	6.87	118.93	54.04	43.60	
1039	G	7.84	108.74	46.61	-	
1040	L	7.86	118.16	52.64	42.24	
1041	E	9.50	121.67	60.4	28.74	
1042	H	8.24	117.08	58.03	28.87	
1043	L	7.56	119.99	54.64	41.31	
1044	R	7.8	119.90	60.74	29.94	
1045	D	8.56	117.79	57.95	39.78	
1046	I	7.74	121.94	65.13	38.17	
1047	F	7.51	117.50	62.20	38.48	
1048	E	8.60	118.37	59.51	29.58	
1049	T	8.52	117.69	66.89	68.74	
1050	E	7.88	117.13	55.76	29.02	
1051	Q	7.69	115.66	56.54	25.73	
1052	I	8.30	119.12	61.26	45.32	
1053	T	6.64	115.48	59.10	71.06	
1054	L	9.02	122.58	58.42	41.18	
1055	a	8.12	118.06	55.01	18.080	
1056	k	7.38	117.18	58.62	33.120	
1057	L	8.35	121.32	57.41	aprox 41.1	

1058	A	7.72	118.49	54.51	18.25	
1059	D	7.18	114.78	53.91	42.130	
1060	M	7.68	120.17	57.35	35.330	
1061	G	8.42	110.48	43.160	-	
1062	H	8.85	119.04	62.67	32.02	
1063	E	9.10	116.82	60.24	28.54	
1064	E	8.28	118.88	60.85	29.01	
1065	L	8.07	118.09	57.08	41.900	
1066	K	8.57	121.35	60.110	32.360	
1067	E	7.77	119.60	59.250	29.470	
1068	I	6.95	109.06	61.72	37.680	
1069	G	7.57	105.19	45.15	-	
1070	I	8.02	121.21	59.47	33.190	
1071	N	7.60	123.84	55.76	39.24	
1072	A	8.47	124.15	51.71	18.09	
1073	Y			62.800	38.36	unassigned NH
1074	G	9.33	104.49	47.13	-	
1075	H	6.78	118.76	57.48	32.02	
1076	R	7.62	116.78	61.28	~31.88	
1077	H	9.00	116.85	60.42	31.58	
1078	K	7.70	116.26	59.95	33.46	
1079	L	7.80	119.55	58.65	42.54	
1080	I	8.22	119.98	65.28	39.08/38.8	
1081	K	8.46	117.92	57.08	30.460	
1082	G	8.30	109.280	47.280	-	
1083	V	8.60	124.05	66.25	31.35	
1084	E	7.74	121.64	59.74	29.9	
1085	R	7.90	117.76	58.81	30.15	
1086	L	7.78	120.04	57.47	42.74	
1087	L	8.06	117.26	56.02	41.85	
1088	G	7.88	107.14	45.95	-	
1089	G	8.08	108.16	45.59	-	
1090	Q	8.27	119.58	56.09	29.17	
1091	Q	8.53	121.16	56.29	29.200	
1092	G	8.44	109.93	45.43	-	
1093	T	8.040	113.080	61.960	69.960	
1094	N	8.46	121.89	51.33	39	
1095	P	-	-	63.840	31.930	
1096	Y	8.05	118.660	58.250	38.060	
1097	L	7.76	121.720	55.420	42.320	
1098	T	7.89	113.80	62.10	69.98	
1099	F	8.150	121.820	58.210	39.560	

Supporting Information Table 2: SAM mutant (DAVK) bound assignments

Bound Assignments

Sequence: GVAGLDMNIS QFLKSLGLEH LRDIFETEQI TLakLADMGH EELKEIGINA YGHRHKLIKG VERLLGGQQG TNPYLTFHCV NQG

The following assignments are for TNKS1 SAM-Linker (D1055A/V1056K) at 250 uM bound to TNKS1 SAM-Linker (Y1073E) at 322 uM

		Chemical Shift				
residue	ID	HN	N	C alpha	C beta	NOTE
1023	G				-	unassigned
1024	V			62.32	32.69	unassigned NH
1025	A	8.51	127.58	52.81	19.22	
1026	G	8.34	108.01	45.51	-	
1027	L	8.02	120.46	55.06	42.12	
1028	D	8.35	120.63	54.13	40.97	
1029	M	7.75	120.83	56.05	34.1	
1030	N	8.37	120.65	52.99	39.69	
1031	I	8.76	122.41	62.95	38.04	
1032	S	8.25	118.32	62.50	-	unassigned Cbeta
1033	Q	8.07	121.64	58.60	28.65	
1034	F	8.19	121.94	60.99	39.41	
1035	L	8.70	118.71	58.08	40.67	
1036	K	8.06	119.82	59.94	32.07	
1037	S	8.06	117.21	61.67	62.92	
1038	L	6.86	118.71	54.09	43.93	
1039	G	7.83	108.56	46.57	-	
1040	L	7.86	117.92	52.63	42.2	
1041	E	9.43	121.50	60.36	28.9	
1042	H	8.34	116.96	57.97	28.85	
1043	L	7.58	119.95	54.71	41.38	
1044	R	7.81	119.66	60.72	29.9	
1045	D	8.56	117.72	57.91	40.01	
1046	I	7.72	121.76	65.13	38.39	
1047	F	7.43	117.24	62.32	38.48	
1048	E	8.61	118.20	59.51	29.59	
1049	T	8.50	117.63	66.92	68.97	
1050	E	7.85	117.05	55.76	29.02	
1051	Q	7.68	115.49	56.53	25.73	
1052	I	8.31	119.08	61.22	37.28	
1053	T	6.64	115.40	59.13	71.45	
1054	L	9.01	122.48	58.43	41.20	
1055	a	8.11	117.93	55.00	18.01	
1056	k	7.37	117.08	58.61	33.07	

1057	L	8.36	121.38	57.43	41.45	
1058	A	7.72	118.36	54.46	18.23	
1059	D	7.17	114.72	53.93	42.13	
1060	M	7.68	120.08	57.35	35.43	
1061	G	8.42	110.39	43.16	-	
1062	H	8.87	119.18	62.65	32	
1063	E	9.09	116.83	60.41	28.78	
1064	E	8.27	118.58	60.84	28.91	
1065	L	8.05	118.10	57.06	38.19	
1066	K	8.59	121.29	60.33	32.49	
1067	E	7.72	119.26	59.33	29.54	
1068	I	6.93	108.83	61.65	37.99	
1069	G	7.55	105.19	45.21	-	
1070	I	8.04	121.10	59.18	32.91	
1071	N	7.54	123.21	55.82	39.34	
1072	A	8.50	124.05	51.72	18.45	
1073	Y	10.16	128.40	63.25	39.5	
1074	G	9.81	103.13	47.45	-	
1075	H	6.62	116.92	57.44	32.32	
1076	R	7.55	116.24	61.28	32.31	
1077	H	9.09	116.83	60.6	32.19	
1078	K	7.92	115.55	60.25	33.8	
1079	L	7.76	119.17	58.63	42.7	
1080	I	8.20	119.81	65.22	39.25	
1081	K	8.59	118.10	57.13	30.69	
1082	G	8.25	108.49	47.31	-	
1083	V	8.55	123.78	66.25	31.29	
1084	E	7.68	121.67	59.81	29.87	
1085	R	8.04	117.67	59.04	30.28	
1086	L	7.83	120.19	57.56	42.7	
1087	L	8.04	117.14	56.1	41.82	
1088	G	7.88	106.90	45.92	-	
1089	G	8.05	108.08	45.64	-	
1090	Q	8.27	119.39	56.05	29.2	
1091	Q	8.53	120.98	56.24	29.32	
1092	G	8.44	109.74	45.44	-	
1093	T	8.09	113.10	61.89	69.97	
1094	N	8.45	121.80	51.29	38.89	
1095	P	-	-	63.87	31.83	
1096	Y	8.05	118.47	58.32	38.15	
1097	L	7.76	121.40	55.42	42.43	
1098	T	7.89	113.71	62.14	70.01	
1099	F	8.15	121.66	58.27	39.62	

CHAPTER 4 ADDENDUM

The following is a short commentary on the work of Mariotti et al.[2] and Roccio et al.[3] relating to the role of SAM-mediate TNKS oligomerization in Wnt signaling and Axin turnover published shortly after the work presented in Chapter 4 was published in Protein Science.

Shortly after the publication of the manuscript presented in Chapter 4 (ref. 1) two papers reporting the structures of tankyrase (TNKS) SAM domains were published from Mariotti *et al.*[2] and Roccio *et al.*[3] in the journals Molecular Cell and Structure respectively. Mariottie et al. present multiple crystal structures of tankyrase mutants, including TNKS1 SAM D1055R in two crystal forms (although the same space group, $P2_1$) and TNKS2 SAM D902H/R924E. Roccio *et al.* were surprisingly able to crystalize the wild type (WT) SAM domain oligomer by setting trays with heterogeneous, aggregated SAM domain material. While our TNKS1 SAM model was generated using Rosetta *ab initio*/Rosetta CM, when superimposed, this model is visibly highly similar to the TNKS1 SAM crystal structures with C_α RMSDs of less then 1.4 Å (Figure 1A). Each of these studies generated models of the TNKS1/TNKS2 polymer that is formed via a large head-to-tail helical oligomer (Figure 1B). While the helical pitch of these polymers differ slightly, the surface used at the interface between protomers is the same. Both groups make similar mutations to the SAM domains as those given in Chapter 4 to disrupt the oligomeric state of tankyrase.

In the preparation of our manuscript[1] mutations were made to the SAM domain of tankyrase (tankyrase-2 in our case) to assess the physiological role of tankyrase oligomerization. Both Mariotti *et al.*[2] and Roccio *et al.*[3] performed the same experiments. Because RNF146 and tankyrase work together to degrade Axin they are positive regulators of Wnt signaling (Figure 2A). When WT tankyrase-2 is overexpressed in HEK293T cells in a

TOP Flash luciferase reporter assay for Wnt, luciferase activity is increases (Figure 2B). However, when oligomer disrupting mutants are overexpressed, an increase in luciferase activity is not observed (Figure 2B). This phenomenon was also observed by both Mariotti *et al.* and Roccio *et al.* The conclusion made from both groups is that oligomerization is important for Wnt signaling; the primary assumption being that tankyrase overexperession leads to more Axin turnover (see Figure 2A). While it is likely true that the SAM domains in tankyrases are indeed important for Wnt signaling, the reasons for this are hereto unclear. For instance, when a variant of tankyrase-1 lacking the catalytic domain (but including the SAM domain and ankyrin repeat region) is overexpressed the increase in Wnt signaling is still observed.[4] In fact, the apparent increase in Wnt signaling with this fragment is higher than simply overexpressing wild-type protein. Furthermore, when WT or oligomer disrupting TNKS2 SAM mutants are overexpressed in HEK293T cells, Axin levels reproducibly increase (Figure 2C). Therefore, both oligomer deficient and WT TNKS can both increase levels of Axin, but only WT TNKS can promote Wnt signaling. Interestingly, neither Mariotti *et al.* nor Roccio *et al.* reported levels of Axin when they overexpressed tankyrase.

At this stage it is difficult to know if the overexpression of tankyrase represents a physiological state for Wnt signaling. It has been reported extensively that tankyrase will form Axin-containing aggregates or puncta when overexpressed in cells, especially in the presence of PARP inhibitors.[2-9] Our data suggests that TNKS increases the amount of Axin when overexpressed (see Figure 2C), which may mean that TNKS is sequestering Axin through its tight interaction. It is also worth noting that endogenous TNKS oligomers may be disrupted by TNKS SAM mutants that “cap” the ends of endogenous TNKS polymers in

these overexpression experiments. This could explain the lack Wnt activation seen for mutant proteins. However, there is also a further complication of the varied roles that TNKS may play in Wnt signaling. For instance, in drosophila, TNKS enhances the recruitment of Axin to the membrane upon Wnt activation where it can then bind phospho-LRP6.[10,11] This role of tankyrase is dependent on its PARP activity; only PARylated Axin has enhanced LRP6 binding. However, SAM domain mediated oligomerization could also be important for the association of tankyrases with Axin at the membrane. Further work is needed to clarify the rolls of tankyrases, Axin PARylation, and the relevance of tankyrase overexpression. Hence, we did not feel it was appropriate to publish the data presented in Figure 2 as, we felt, it may give readers the wrong impression of tankyrase function and the role of the SAM domain in Wnt signaling.

Figures:

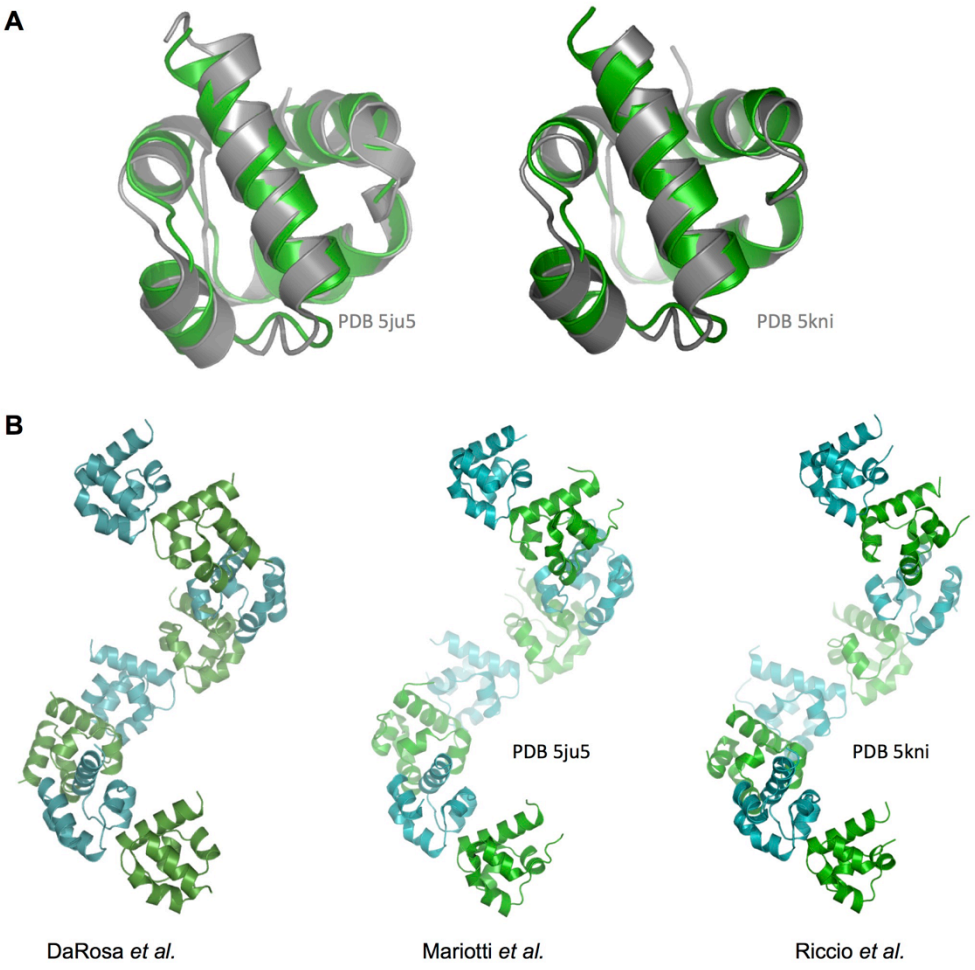

Figure 1 | Comparison of tankyrase SAM crystal structures with the computational model **(A)** Comparison of Rosetta CM model of the Tankyrase 1 SAM domain (green) with two crystal structures published shortly our work showing a very close structural match. Structural alignment of the Rosetta CM generated model with (*left*) the D1055R tankyrase-1 SAM domain mutant crystal structure (RMSD: 1.4 Å; pdb 5ju5)[2] and (*right)* the wild type tankyrase-1 SAM domain (RMSD: 1.3 Å; PDB 5kni).[3] **(B)** Comparison of the oligomerization models generated by Da Rosa *et al,.*[1] Mariotti *et al.*,[2] and Riccio *et al.*[3] The helical pitches differ slightly from model to model. Mariootti *et al.* report a helical pitch of 83 Å and 79 Å for TNKS1 SAM domain in crystal form 1 and 2 respectively, while the wild type oligomer reported by Riccio *et al.* has a helical pitch of 95.5 Å. Our computational model has a helical pitch of 81.4 Å.

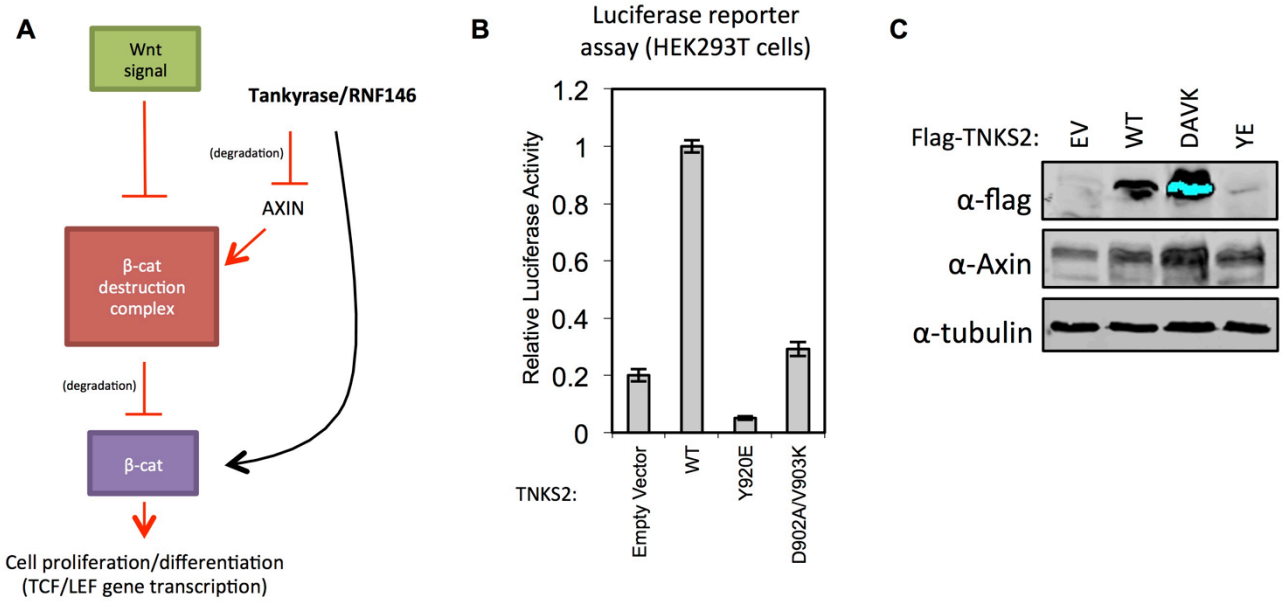

Figure 2 | Overexpression of tankyrase SAM mutants do not promote Wnt signaling
(A) Schematic of tankyrase/RNF146 regulation of Wnt signaling. Tankyrases PARylate Axin, the concentration-limiting component of the β-catenin (β-cat) destruction complex, and RNF146 ubiquitylates Axin. A Wnt signal serves to disrupt the β-cat destruction complex. "Degradation" indicates proteasomal degradation. **(B)** TCF/LEF TOPflash luciferase reporter assay for Wnt signaling. Error bars indicate standard deviation for two independent experiments. **(C)** Axin levels upon overexpression of flag-TNKS2 and oligomer disrupting mutants in HEK293T cells. EV, empty vector; WT, wild type; DAVK, D902A/V903K; YE, Y920E.

Materials and Methods:

TOPflash reporter assay and western blot

Dual luciferase reporter assays were performed per the manufactures instructures (Promega) HEK293T cells were transfected with empty pflag-CMV-2 vector or the indicated flag-TNKS2 construct, with a SuperTOPflash luciferase plasmid, and a Renilla luciferase control. Twenty-four hours after transfection samples were analyzed for reporter activity as indicated by the manufacturer. Values for luciferase activity are relative values to Renilla. For western blots, only the empty vector or flag-TNKS2 constructs were transfected and cells were lysed and analyzed by western blot 48 hours post transfection with anti-Axin, anti-tubulin, and anti-flag antibodies.

References:

1. DaRosa PA, Ovchinnikov S, Xu W, Klevit RE (2016) Structural insights into SAM domain-mediated tankyrase oligomerization. Protein Sci. 25:1744–1752.

2. Mariotti L, Templeton CM, Ranes M, Paracuellos P, Cronin N, Beuron F, Morris E, Guettler S (2016) Tankyrase Requires SAM Domain-Dependent Polymerization to Support Wnt-β-Catenin Signaling. Mol. Cell 63:498–513.

3. Riccio AA, McCauley M, Langelier M-F, Pascal JM (2016) Tankyrase Sterile α Motif Domain Polymerization Is Required for Its Role in Wnt Signaling. Structure 24:1573–1581.

4. Huang S-M a, Mishina YM, Liu S, Cheung A, Stegmeier F, Michaud G a, Charlat O, Wiellette E, Zhang Y, Wiessner S, et al. (2009) Tankyrase inhibition stabilizes axin and antagonizes Wnt signalling. Nature 461:614–620.

5. Callow MG, Tran H, Phu L, Lau T, Lee J, Sandoval WN, Liu PS, Bheddah S, Tao J, Lill JR, et al. (2011) Ubiquitin ligase RNF146 regulates tankyrase and Axin to promote Wnt signaling. PLoS One 6.

6. Thorvaldsen TE, Pedersen NM, Wenzel EM, Schultz SW, Brech A, Liestol K, Waaler J, Krauss S, Stenmark H (2015) Structure, Dynamics, and Functionality of Tankyrase Inhibitor-Induced Degradasomes. Mol. Cancer Res. 13:1487–1501.

7. Martino-Echarri E, Brocardo MG, Mills KM, Henderson BR (2016) Tankyrase Inhibitors Stimulate the Ability of Tankyrases to Bind Axin and Drive Assembly of beta-Catenin Degradation-Competent Axin Puncta. PLoS One 11:e0150484.

8. Hatsugai K, Ohishi T, Sugimoto Y, Seimiya H (2010) Tankyrase-1 assembly to large protein complexes blocks its telomeric function. FEBS Lett. 584:3885–3890.

9. De Rycker M, Price CM (2004) Tankyrase polymerization is controlled by its sterile alpha motif and poly(ADP-ribose) polymerase domains. Mol. Cell. Biol. 24:9802–12.

10. Yang E, Tacchelly-Benites O, Wang Z, Randall MP, Tian A, Benchabane H, Freemantle S, Pikielny C, Tolwinski NS, Lee E, et al. (2016) Wnt pathway activation by ADP-ribosylation. Nat. Commun. 7:11430.2.

11. Wang Z, Tacchelly-Benites O, Yang E, Ahmed Y (2016) Dual Roles for Membrane Association of Drosophila Axin in Wnt Signaling. PLoS Genet. 12:e1006494.

Appendix

Contributions to UHRF1 Biophysical Studies

In an ongoing collaboration with Joseph Harrison and Brian Kuhlman at the University of North Caroline Chapel Hill, I have been working to elucidate mechanism of activation of the E3 ubiquitin ligase UHRF1. Joseph Harrison recently discovered that UHRF1 is activated by binding to Hemi-methylated DNA (HeDNA). When UHRF1 binds HeDNA, but not unmethylated DNA this RING E3 is activated for histone H3 (primarily) K18 and K23 ubiquitylation. In a highly collaborative study,[1] I worked closely with Joseph Harrison to begin the characterization of the UHRF1 mechanism. I acted primarily as an advisor, but also performed a host of NMR and biochemical experiments on UHRF1 and fragments thereof that helped to bolster the most novel aspects of the UHRF1 paper indicated; namely, the activation of the ligase. I am a co-second author on the referenced paper. Joseph and I continue to work on UHRF1 and have recently made very significant strides on the functioning of this unique enzyme that promises to produce yet another publication. On this work, we have agreed, that I will be co-first author with Joseph.

Reference

1. Harrison, J. S. *et al.* Hemi-methylated DNA regulates DNA methylation inheritance through allosteric activation of H3 ubiquitylation by UHRF1. *Elife* **5,** e17101 (2016).

Copyright Permissions

Copyright Clearance Center RightsLink®

Home | Account Info | Help

nature publishing group

Title: Allosteric activation of the RNF146 ubiquitin ligase by a poly(ADP-ribosyl)ation signal

Author: Paul A. DaRosa, Zhizhi Wang, Xiaomo Jiang, Jonathan N. Pruneda, Feng Cong et al.

Publication: Nature

Publisher: Nature Publishing Group

Date: Oct 19, 2014

Logged in as:
Paul DaRosa
Account #:
3001119438
LOGOUT

Author Request

If you are the author of this content (or his/her designated agent) please read the following. If you are not the author of this content, please click the Back button and select an alternative Requestor Type to obtain a quick price or to place an order.

Ownership of copyright in the article remains with the Authors, and provided that, when reproducing the Contribution or extracts from it, the Authors acknowledge first and reference publication in the Journal, the Authors retain the following non-exclusive rights:

a) To reproduce the Contribution in whole or in part in any printed volume (book or thesis) of which they are the author(s).

b) They and any academic institution where they work at the time may reproduce the Contribution for the purpose of course teaching.

c) To reuse figures or tables created by them and contained in the Contribution in other works created by them.

d) To post a copy of the Contribution as accepted for publication after peer review (in Word or Text format) on the Author's own web site, or the Author's institutional repository, or the Author's funding body's archive, six months after publication of the printed or online edition of the Journal, provided that they also link to the Journal article on NPG's web site (eg through the DOI).

NPG encourages the self-archiving of the accepted version of your manuscript in your funding agency's or institution's repository, six months after publication. This policy complements the recently announced policies of the US National Institutes of Health, Wellcome Trust and other research funding bodies around the world. NPG recognises the efforts of funding bodies to increase access to the research they fund, and we strongly encourage authors to participate in such efforts.

Authors wishing to use the published version of their article for promotional use or on a web site must request in the normal way.

If you require further assistance please read NPG's online author reuse guidelines.

For full paper portion: Authors of original research papers published by NPG are encouraged to submit the author's version of the accepted, peer-reviewed manuscript to their relevant funding body's archive, for release six months after publication. In addition, authors are encouraged to archive their version of the manuscript in their institution's repositories (as well as their personal Web sites), also six months after original publication.

v2.0

BACK CLOSE WINDOW

JOHN WILEY AND SONS LICENSE TERMS AND CONDITIONS

May 15, 2017

This Agreement between Paul A DaRosa ("You") and John Wiley and Sons ("John Wiley and Sons") consists of your license details and the terms and conditions provided by John Wiley and Sons and Copyright Clearance Center.

License Number	4110410806862
License date	May 15, 2017
Licensed Content Publisher	John Wiley and Sons
Licensed Content Publication	Protein Science
Licensed Content Title	Structural insights into SAM domain-mediated tankyrase oligomerization
Licensed Content Author	Paul A. DaRosa,Sergey Ovchinnikov,Wenqing Xu,Rachel E. Klevit
Licensed Content Date	Jul 4, 2016
Licensed Content Pages	9
Type of use	Dissertation/Thesis
Requestor type	Author of this Wiley article
Format	Print and electronic
Portion	Full article
Will you be translating?	No
Title of your thesis / dissertation	Structural Studies of RNF146-Mediated PARylation-Dependent Ubiquitylation
Expected completion date	Jun 2017
Expected size (number of pages)	130
Requestor Location	Paul A DaRosa 13216 3RD AVE NW SEATTLE, WA 98177 United States Attn: Paul A DaRosa
Publisher Tax ID	EU826007151
Billing Type	Invoice
Billing Address	Paul A DaRosa 13216 3RD AVE NW SEATTLE, WA 98177 United States Attn: Paul A DaRosa

Total 0.00 USD

Terms and Conditions

TERMS AND CONDITIONS

This copyrighted material is owned by or exclusively licensed to John Wiley & Sons, Inc. or one of its group companies (each a"Wiley Company") or handled on behalf of a society with which a Wiley Company has exclusive publishing rights in relation to a particular work (collectively "WILEY"). By clicking "accept" in connection with completing this licensing transaction, you agree that the following terms and conditions apply to this transaction (along with the billing and payment terms and conditions established by the Copyright Clearance Center Inc., ("CCC's Billing and Payment terms and conditions"), at the time that you opened your RightsLink account (these are available at any time at http://myaccount.copyright.com).

Terms and Conditions

- The materials you have requested permission to reproduce or reuse (the "Wiley Materials") are protected by copyright.

- You are hereby granted a personal, non-exclusive, non-sub licensable (on a stand-alone basis), non-transferable, worldwide, limited license to reproduce the Wiley Materials for the purpose specified in the licensing process. This license, **and any CONTENT (PDF or image file) purchased as part of your order,** is for a one-time use only and limited to any maximum distribution number specified in the license. The first instance of republication or reuse granted by this license must be completed within two years of the date of the grant of this license (although copies prepared before the end date may be distributed thereafter). The Wiley Materials shall not be used in any other manner or for any other purpose, beyond what is granted in the license. Permission is granted subject to an appropriate acknowledgement given to the author, title of the material/book/journal and the publisher. You shall also duplicate the copyright notice that appears in the Wiley publication in your use of the Wiley Material. Permission is also granted on the understanding that nowhere in the text is a previously published source acknowledged for all or part of this Wiley Material. Any third party content is expressly excluded from this permission.

- With respect to the Wiley Materials, all rights are reserved. Except as expressly granted by the terms of the license, no part of the Wiley Materials may be copied, modified, adapted (except for minor reformatting required by the new Publication), translated, reproduced, transferred or distributed, in any form or by any means, and no derivative works may be made based on the Wiley Materials without the prior permission of the respective copyright owner.**For STM Signatory Publishers clearing permission under the terms of the STM Permissions Guidelines only, the terms of the license are extended to include subsequent editions and for editions in other languages, provided such editions are for the work as a whole in situ and does not involve the separate exploitation of the permitted figures or extracts,** You may not alter, remove or suppress in any manner any copyright, trademark or other notices displayed by the Wiley Materials. You may not license, rent, sell, loan, lease, pledge, offer as security, transfer or assign the Wiley Materials on a stand-alone

basis, or any of the rights granted to you hereunder to any other person.

- The Wiley Materials and all of the intellectual property rights therein shall at all times remain the exclusive property of John Wiley & Sons Inc, the Wiley Companies, or their respective licensors, and your interest therein is only that of having possession of and the right to reproduce the Wiley Materials pursuant to Section 2 herein during the continuance of this Agreement. You agree that you own no right, title or interest in or to the Wiley Materials or any of the intellectual property rights therein. You shall have no rights hereunder other than the license as provided for above in Section 2. No right, license or interest to any trademark, trade name, service mark or other branding ("Marks") of WILEY or its licensors is granted hereunder, and you agree that you shall not assert any such right, license or interest with respect thereto

- NEITHER WILEY NOR ITS LICENSORS MAKES ANY WARRANTY OR REPRESENTATION OF ANY KIND TO YOU OR ANY THIRD PARTY, EXPRESS, IMPLIED OR STATUTORY, WITH RESPECT TO THE MATERIALS OR THE ACCURACY OF ANY INFORMATION CONTAINED IN THE MATERIALS, INCLUDING, WITHOUT LIMITATION, ANY IMPLIED WARRANTY OF MERCHANTABILITY, ACCURACY, SATISFACTORY QUALITY, FITNESS FOR A PARTICULAR PURPOSE, USABILITY, INTEGRATION OR NON-INFRINGEMENT AND ALL SUCH WARRANTIES ARE HEREBY EXCLUDED BY WILEY AND ITS LICENSORS AND WAIVED BY YOU.

- WILEY shall have the right to terminate this Agreement immediately upon breach of this Agreement by you.

- You shall indemnify, defend and hold harmless WILEY, its Licensors and their respective directors, officers, agents and employees, from and against any actual or threatened claims, demands, causes of action or proceedings arising from any breach of this Agreement by you.

- IN NO EVENT SHALL WILEY OR ITS LICENSORS BE LIABLE TO YOU OR ANY OTHER PARTY OR ANY OTHER PERSON OR ENTITY FOR ANY SPECIAL, CONSEQUENTIAL, INCIDENTAL, INDIRECT, EXEMPLARY OR PUNITIVE DAMAGES, HOWEVER CAUSED, ARISING OUT OF OR IN CONNECTION WITH THE DOWNLOADING, PROVISIONING, VIEWING OR USE OF THE MATERIALS REGARDLESS OF THE FORM OF ACTION, WHETHER FOR BREACH OF CONTRACT, BREACH OF WARRANTY, TORT, NEGLIGENCE, INFRINGEMENT OR OTHERWISE (INCLUDING, WITHOUT LIMITATION, DAMAGES BASED ON LOSS OF PROFITS, DATA, FILES, USE, BUSINESS OPPORTUNITY OR CLAIMS OF THIRD PARTIES), AND WHETHER OR NOT THE PARTY HAS BEEN ADVISED OF THE POSSIBILITY OF SUCH DAMAGES. THIS LIMITATION SHALL APPLY NOTWITHSTANDING ANY FAILURE OF ESSENTIAL PURPOSE OF ANY LIMITED REMEDY PROVIDED HEREIN.

- Should any provision of this Agreement be held by a court of competent jurisdiction to

be illegal, invalid, or unenforceable, that provision shall be deemed amended to achieve as nearly as possible the same economic effect as the original provision, and the legality, validity and enforceability of the remaining provisions of this Agreement shall not be affected or impaired thereby.

- The failure of either party to enforce any term or condition of this Agreement shall not constitute a waiver of either party's right to enforce each and every term and condition of this Agreement. No breach under this agreement shall be deemed waived or excused by either party unless such waiver or consent is in writing signed by the party granting such waiver or consent. The waiver by or consent of a party to a breach of any provision of this Agreement shall not operate or be construed as a waiver of or consent to any other or subsequent breach by such other party.

- This Agreement may not be assigned (including by operation of law or otherwise) by you without WILEY's prior written consent.

- Any fee required for this permission shall be non-refundable after thirty (30) days from receipt by the CCC.

- These terms and conditions together with CCC's Billing and Payment terms and conditions (which are incorporated herein) form the entire agreement between you and WILEY concerning this licensing transaction and (in the absence of fraud) supersedes all prior agreements and representations of the parties, oral or written. This Agreement may not be amended except in writing signed by both parties. This Agreement shall be binding upon and inure to the benefit of the parties' successors, legal representatives, and authorized assigns.

- In the event of any conflict between your obligations established by these terms and conditions and those established by CCC's Billing and Payment terms and conditions, these terms and conditions shall prevail.

- WILEY expressly reserves all rights not specifically granted in the combination of (i) the license details provided by you and accepted in the course of this licensing transaction, (ii) these terms and conditions and (iii) CCC's Billing and Payment terms and conditions.

- This Agreement will be void if the Type of Use, Format, Circulation, or Requestor Type was misrepresented during the licensing process.

- This Agreement shall be governed by and construed in accordance with the laws of the State of New York, USA, without regards to such state's conflict of law rules. Any legal action, suit or proceeding arising out of or relating to these Terms and Conditions or the breach thereof shall be instituted in a court of competent jurisdiction in New York County in the State of New York in the United States of America and each party hereby consents and submits to the personal jurisdiction of such court, waives any objection to venue in such court and consents to service of process by registered or certified mail, return receipt requested, at the last known address of such party.

WILEY OPEN ACCESS TERMS AND CONDITIONS

Wiley Publishes Open Access Articles in fully Open Access Journals and in Subscription journals offering Online Open. Although most of the fully Open Access journals publish open access articles under the terms of the Creative Commons Attribution (CC BY) License only, the subscription journals and a few of the Open Access Journals offer a choice of Creative Commons Licenses. The license type is clearly identified on the article.

The Creative Commons Attribution License

The Creative Commons Attribution License (CC-BY) allows users to copy, distribute and transmit an article, adapt the article and make commercial use of the article. The CC-BY license permits commercial and non-

Creative Commons Attribution Non-Commercial License

The Creative Commons Attribution Non-Commercial (CC-BY-NC)License permits use, distribution and reproduction in any medium, provided the original work is properly cited and is not used for commercial purposes.(see below)

Creative Commons Attribution-Non-Commercial-NoDerivs License

The Creative Commons Attribution Non-Commercial-NoDerivs License (CC-BY-NC-ND) permits use, distribution and reproduction in any medium, provided the original work is properly cited, is not used for commercial purposes and no modifications or adaptations are made. (see below)

Use by commercial "for-profit" organizations

Use of Wiley Open Access articles for commercial, promotional, or marketing purposes requires further explicit permission from Wiley and will be subject to a fee.

Further details can be found on Wiley Online Library http://olabout.wiley.com/WileyCDA/Section/id-410895.html

Other Terms and Conditions:

v1.10 Last updated September 2015

Questions? customercare@copyright.com or +1-855-239-3415 (toll free in the US) or +1-978-646-2777.